Durham E-Theses

Electrical conductivity and luminescence in Cadmium Sulphide

Marlor, G. A.

How to cite:

Use policy

ABSTRACT

The work is conveniently divided into two sections:-
(i) the electrical properties of cadmium sulphide and (ii)
the optical properties of cadmium sulphide.

(i) Measurements have been made on thin pure
platelets of cadmium sulphide from which it is clear that
electrical conduction in these samples is governed by two
complex defect centres with associated levels within the
forbidden gap (0.41 eV - 0.61 eV; 0.25 eV - 0.83). This
has been deduced from measurements of the static current-
voltage curves made over a wide range of temperatures
coupled with an investigation of thermally stimulated curre
curves obtained after electron injection and optical
excitation. The measurements also demonstrate that Lampert
theory of Space Charge Limited Current Flow in an insulator
with traps is applicable at low current densities but that
trap emptying occurs when high current densities are passed
through a crystal.

(ii) Measurements of the spectral distribution of
ultra-violet stimulated fluorescence at $77^{O}K$ and $300^{O}K$,
demonstrate the existance of electronic energy levels within
the forbidden gap which can be correlated with those deter-
mined from the electrical experiments. The spectral distri-
bution of luminescent emission has been measured in pure

and doped samples from which it is concluded that edge emission is associated with both sulphur vacancies and interstitials (0.13 eV below the conduction band and 0.16 eV above the valence band respectively.). The two emission series can be separate in suitable crystals. Further work, with better resolution of the emission bands should clarify the position further. Electro-luminescence, due to the recombination of injected electrons and holes, is attribute to bulk processes which produce the edge emission series, surface and impurity recombination.

Electrical Conductivity and Luminescence in

Cadmium Sulphide

by

G. A. Marlor. M.Sc.

Presented in candidature for the degree of Doctor
of Philosophy of the University of Durham,

September 1964

INTRODUCTION

The electrical and optical properties of cadmium sulphide
have been studied by several workers over a period of many
years. Progress in the understanding of these properties has
been inhibited by the difficulty of growing large, pure single
crystals with good homogeneity and controlled stoichiometry.
Stoichiometric single crystals are insulators and consequently
many experimental techniques which have been applied to semi-
conductors cannot be used in the investigation of cadmium
sulphide. The development of new techniques, and the inter-
pretation of established ones in the context of semi-insulators,
have further retarded progress in the understanding of the
electrical and optical properties of II-VI compounds.

Potentially, cadmium sulphide has important uses in the
detection of electromagnetic radiation with wavelengths extending
from those of Gamma rays to light in the visible and infra-red
region of the spectrum. There are many possible uses in purely
electronic devices. The most serious problems experienced
with the use of cadmium sulphide as a detector in the visible
region today are the long response time at low light levels,
together with the problem of preparing detectors with controlled

and reproducible properties. The present difficulties may be overcome, and the full potential of the material realised once the basic electronic properties are more fully understood. In particular, an understanding of the type of crystal now available should lead to the production of better crystals or crystals more suited to a particular purpose. The work reported here is directed towards that end.

The first three chapters of this thesis are devoted to a discussion of the electrical and optical properties of semiconductors and insulators. The electrical and optical properties of cadmium sulphide are discussed in the next two chapters. The growth of single crystals of cadmium sulphide in our laboratory is described in chapter six. The remaining chapters deal with the experiments carried out, their analysis and the conclusions that can be drawn. Measurements of space charge limited currents and thermally stimulated currents are reported. In particular, photochemical changes are shown to take place and a voltage threshold is confirmed for the injection of excess charge into these crystals. The variations in spectral distribution of the luminescent emission at 77^OK from several different crystals, excited by ultra-violet radiation, are presented. The spectral distribution of luminescence, excited by the simultaneous electrical injection of electrons and holes, is compared with the photoluminescent spectrum. Additional measurements include the sensitivity of cadmium sulphide to Gamma rays, and visible and infra-red

light at different temperatures.

ACKNOWLEDGMENTS

CONTENTS

Electrical Conduction in Crystalline Solids

1.1. Band Theory.

The band theory of solids is described in many texts
on solid state physics (1). This theory explains satisfactorily
the differences between insulators, semiconductors and metals.
The quantum mechanically allowed states for electrons in
crystalline solids are divided into bands of energy. The
bands which determine the electrical conductivity of a solid
are the highest filled band and the next highest allowed band.
The former band derives from the valence electrons and is
termed the valence band while the latter is called the con-
duction band. An insulator has a band structure as shown in
fig. 1.1.(a). The separation between the conduction band
and the valence band is usually more than about 2eV, the lower
limit being chosen such that there is negligible thermal
excitation of electrons across the forbidden gap at room
temperature. A semiconductor has a smaller gap which allows
thermal excitation at ordinary temperatures and hence conduction,
fig. 1.1.(b). Metals are characterised by either a partially
filled valence band or over-lapping conduction and valence
bands. In both instances conduction is possible as there are
higher energy states available to the electrons, and an electron
can gain energy from an applied field. Metallic types of
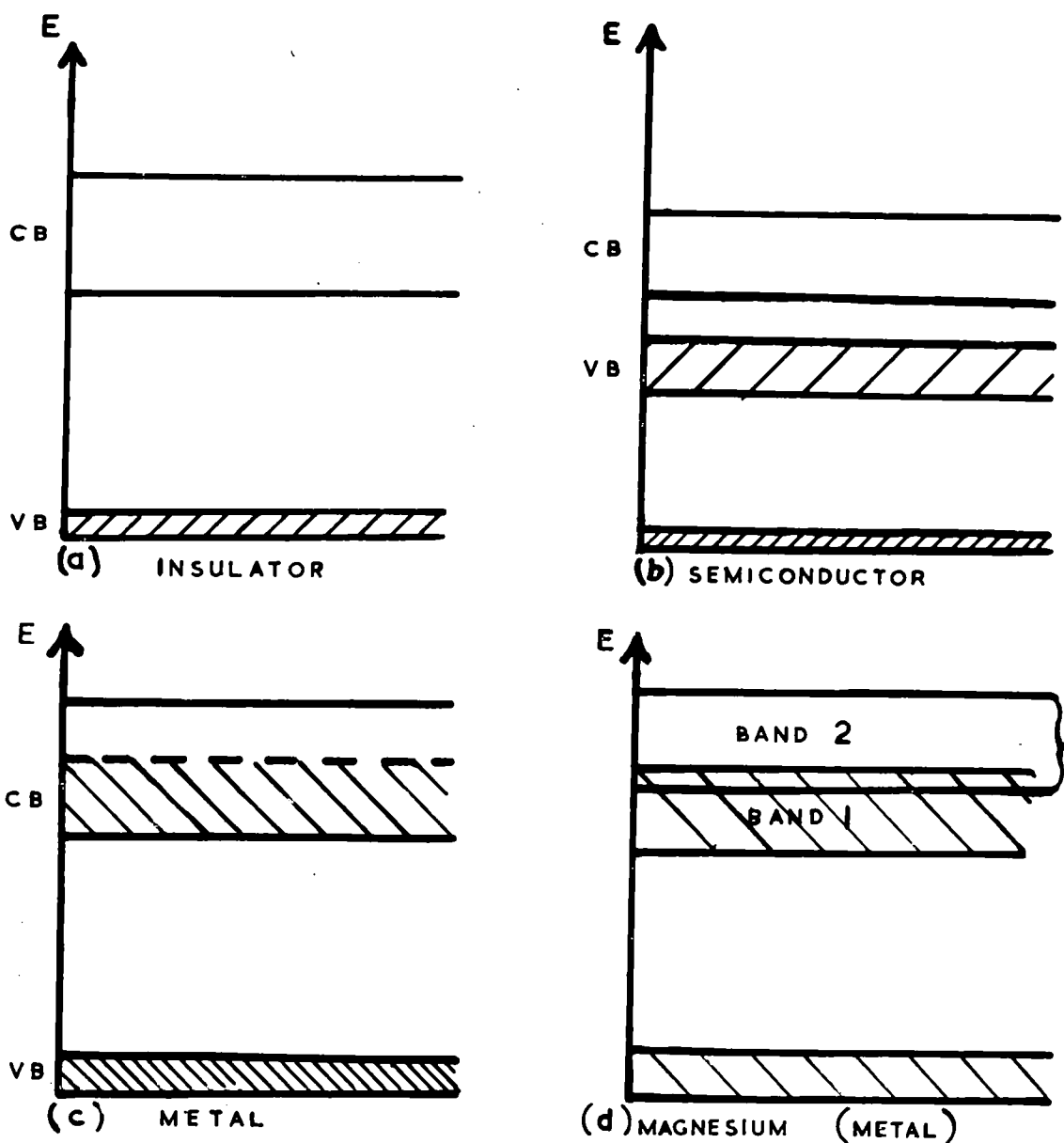
FIGURE 1.1

ELECTRON DISTRIBUTIONS IN SOLIDS

(SHADING INDICATES STATES FULL AT 0°K)

band structure are illustrated in fig. 1.1.(c).(d).

The solution of the Schrodinger equation for an electron in a one dimensional periodic potential, $V_x = V(x + a\, n)$ with period a, yields an electron wave equation

$$\Psi_k(x) = U_k(x)\, \exp\,(ikx) \qquad\qquad 1.1.$$

where $U_k(x)$ is periodic with period a, and k is the wave number vector. If the potential were known it would, in principle, be possible to calculate all the electron states and hence the band structure of a solid. In practice the potential experienced by an electron, and the electron correlation effects, are not accurately known. Further the magnitude and complexity of the calculations necessitate drastic simplifying assumptions (2). At present, band structure calculations are in qualitative agreement with experiment.

The one dimensional model does not predict the over-lapping band scheme of metals. The solution of the three dimensional problem however, satisfactorily includes this case, and also indicates the possibility of different band structures for different directions of the k-vector.

1.2. Effective Mass.

A localised electron in a solid may be described by a group of functions similar to that given in equation 1.1. The

electron velocity can then be shown to equal the group velocity of the wave packet $\frac{d\omega}{dk}$. The angular frequency ω is related to the energy, E, by $\omega = 2\pi\nu = \frac{E}{\hbar}$. Thus we have

$$\text{Electron velocity } v = \frac{d\omega}{dk} = \hbar^{-1} \cdot \frac{dE}{dk} \qquad \text{1.2.1.}$$

In the case of an electron moving in a periodic potential, the energy E is related to the wave vector k by a function of the form plotted in fig. 1.2. All values of E can be included if values of k are restricted to the range $0 < k < \frac{\pi}{a}$. The exact dependence of E on k is determined by the potential V_x.

Consider an electric field, F, applied to the crystal, then the rate of increase of energy is

$$\frac{dE}{dt} = e.F.\ v \qquad \text{1.2.2.}$$

By substituting for v from equation 1.2.1., we have

$$\frac{dk}{dt} = \frac{e.F.}{\hbar} \qquad \text{1.2.3.}$$

Differentiation of equation 1.2.1. gives for the acceleration

$$\frac{dv}{dt} = \hbar^{-1} \left(\frac{d^2E}{dk^2} \right) \frac{dk}{dt} \qquad \text{1.2.4.}$$

Using 1.2.3. for $\frac{dk}{dt}$ the acceleration becomes

$$\frac{dv}{dt} = \left(\frac{1}{\hbar} \right)^2 \cdot \left(\frac{d^2E}{dk^2} \right) \cdot e.F. \qquad \text{1.2.5.}$$
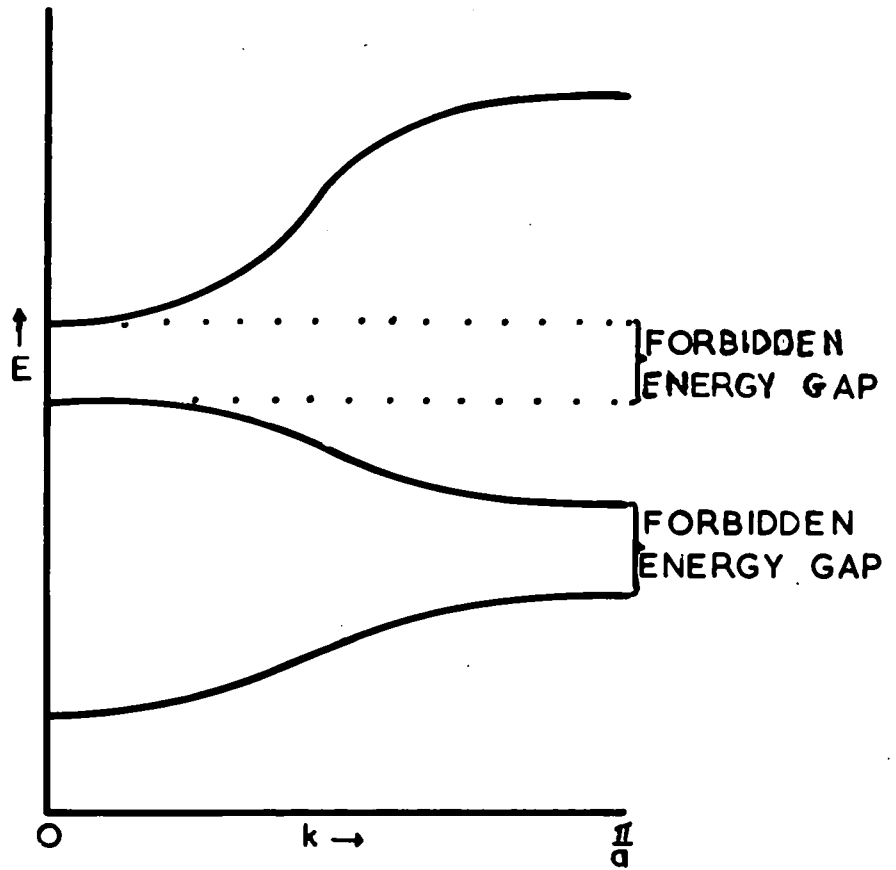
FIGURE 1.2

REDUCED REPRESENTATION OF

ENERGY BANDS

The acceleration produced by the force acting on a free electron is

$$\frac{dv}{dt} = \frac{e.F.}{m} \qquad \qquad 1.2.6.$$

Comparison of equations 1.2.5. and 1.2.6. shows that by defining an effective mass

$$m^* = \hbar^2 \left(\frac{d^2E}{dk^2}\right)^{-1} \qquad \qquad 1.2.7.$$

the motion of an electron in a solid can be considered to be the same as that of a free electron with mass m^* in an applied field F.

The three situations of particular interest are those in which:-

(i)   Electrons lie near the bottom of the conduction band only.

(ii) A relatively small number of electrons are absent from the top of the valence band.

(iii) Two bands overlap, or a band is partially filled.

Situation (i) corresponds to electron or n-type semi-conductivity. The motion of the electrons may be described by assigning an appropriate positive effective mass to each electron in the conduction band.

Case (ii) corresponds to hole, or p-type conductivity which arises from the collective behaviour of the remaining electrons in the valence band in an applied field. The effective mass now becomes negative. It is common practice to consider

the collective motion of the electrons as equivalent to that of holes which have a positive mass and positive charge.

(iii) Half full or overlapping bands are characteristic of metals. The valence electrons available fill the band to some energy E_1. Electrons within kT of this energy are principally responsible for the electrical properties of the metal. If this energy is above the point of inflexion in the E versus k curve all the electrons within kT of E_1 will behave like holes and the metal will be a p-type conductor (1.a p.318). Thus a metal with a positive Hall coefficient has a nearly filled band. A metal in which the band is filled to a point E_1 below the point of inflexion behaves as an n-type conductor.

1.3. Equivalent Number of Carriers.

The acceleration produced by an external electric field is inversely proportional to the effective mass of the carrier concerned. A carrier with an effective mass of one half the free electron mass has a response to an external electric field equivalent to two carriers with the free electron mass. Therefore, the equivalent number of carriers is

$$N_E = \Sigma \frac{m}{m*}$$

where the summation is taken over all the occupied states in the band. For a band filled to some energy, E_1, N_E can be

shown to be given by

$$N_E = \frac{2am}{\hbar^2} \left(\frac{dE}{dk}\right)_{E_1}$$

The equivalent number of carriers therefore increases from zero at the bottom of a band, passes through a maximum at the point of inflexion in the E versus k curve and finally decreases to zero at the top of a band.

1.4. Total Current.

The current flowing in a semiconductor comprises two components, due to the motion of electrons and holes. The conductivity, σ , can be expressed as

$$\sigma = n.e.\mu_e + p.e.\mu_p \qquad\qquad 1.4.$$

where n and p are the densities of electrons and holes in the conduction and valence bands respectively. The symbols μ_e and μ_p are the corresponding mobilities, i.e. the drift velocities of the carriers per unit field. Carrier mobilities are discussed later in this chapter.

1.5. Density of Carriers.

At any temperature above absolute zero, thermal excitation processes raise a finite number of electrons to the conduction band. The number of current carriers available in the conduction and valence bands can be derived in a simple form.

The concentration of electrons n(E)dE with energies lying between E and /dE must equal the product of the concentration of available energy levels in this range and the probability that an electron will possess an energy E.

Thus $n(E)dE = g(E)f(E)dE$ 1.5.1.

Integration of equation 1.5.1. over the appropriate band yields the number of carriers available in that band. The function g(E) is the density of states per unit volume.

In the simplest case, with spherical constant energy surfaces in k-space, where the conduction band minimum occurs at k = 0, and the E versus k relation is parabolic near this point, we have for electrons

$$g(E) = \frac{1}{2\pi^2} \left(\frac{2 m_e^*}{\hbar^2} \right)^{3/2} E^{1/2}$$ 1.5.2.

E is measured from the bottom of the conduction band. The function f(E) is the Fermi-Dirac distribution function

$$f_e(E) = \frac{1}{e^{\frac{(E - E_F)}{kT}} + 1}$$ 1.5.3.

E_F is that energy at which the probability of a state being occupied is one half. For a non-degenerate semiconductor or insulator, where carriers only occupy states near the band edges, $E - E_F \gg kT$ and equation 1.5.3. reduces to

$$f_e(E) = \exp \frac{E_F - E}{kT} \qquad 1.5.4.$$

The corresponding functions for the valence band are found by replacing E by $- E_G - E$ (where E_G is the energy gap) and the effective mass m_e^* by m_p^* in equation 1.5.2. With holes equation 1.5.3. is replaced by

$$f_h(E) = 1 - f_e(E)$$

This equation states that the probability of finding a hole is equivalent to the probability of finding an empty electron state.

The concentration of free electrons, n, can be found by substituting equations 1.5.2. and 1.5.4. in equation 1.5.1. and integrating over the conduction band.

Thus

$$n = 2 \left(\frac{m_e^* kT}{2\pi \hbar^2} \right)^{3/2} \exp \left(\frac{E_F}{kT} \right) \qquad 1.5.5.$$

The concentration of free holes, p, is

$$p = 2 \left(\frac{m_p^* kT}{2\pi \hbar^2} \right)^{3/2} \exp \frac{-(E_F + E_G)}{kT} \qquad 1.5.6.$$

The factors multiplying the exponential terms on the right hand side of the above equations are commonly written N_c and N_v respectively. N_c and N_v are called the effective densities of states.

In intrinsic semiconductors n = p and equations 1.5.5. and

1.5.6. can be equated to give

$$E_F = -\frac{E_G}{2} + \frac{3kT}{4} \ln \frac{m_p^*}{m_e^*} \qquad 1.5.7.$$

In an extrinsic n-type semiconductor, where there are N_d donors near the conduction band, equation 1.5.5. is valid provided $E - E_F \gg kT$. Thus the position of the Fermi level can be found from equation 1.5.5. if n is known. Equation 1.5.6. can also be used for the equivalent situation of acceptor levels near the valence band. Multiplying equations 1.5.5. and 1.5.6. yields

$$n\,p = N_c\,N_v \exp\left(\frac{-E_G}{kT}\right) \qquad 1.5.8.$$

This product is independent of the addition of impurities. There are a wide variety of situations which can arise when donors and acceptors are present in the same crystal (1).

1.6. Injection of Excess Carriers.

An alternative way in which carriers can be supplied to the conduction bands of semiconductors and insulators is by injection from metal contacts. In such an event the density of carriers is determined by the capacitance of the crystals. When an electric field is applied, the current is limited by the space charge of the carriers. This is important in insulators because only small applied voltages are required for the injected current to become large compared to that

carried by the equilibrium density of carriers. Space charge limited conduction is discussed in a later chapter.

1.7. Carrier Mobility.

The equation of motion of an electron or hole in an applied external field F is

$$\frac{dv}{dt} = \frac{eF}{m^*} \qquad \text{see equation 1.2.5.}$$

In the absence of any scattering mechanism an isolated electron would gain energy from the field and consequently move up the E versus k curve of fig. 1.2. As it did so the effective mass would increase at first, become discontinuous, change sign and then continue to become less negative. At the top of the E versus k curve the electron would suffer Bragg reflection with a reversal in sign of its momentum. Finally it would complete the remaining half of the cycle. This is illustrated in fig. 1.7. where plots of energy, velocity and effective mass are shown as functions of momentum. Thus, if there are no scattering mechanisms the electron could not contribute to a current. In the absence of scattering mechanisms, the electron distribution cannot be made asymetrical In the instance of a full band, scattering cannot occur as there are no states available for scattered electrons to take up. Thus the electrons execute this cycle with no resultant current.
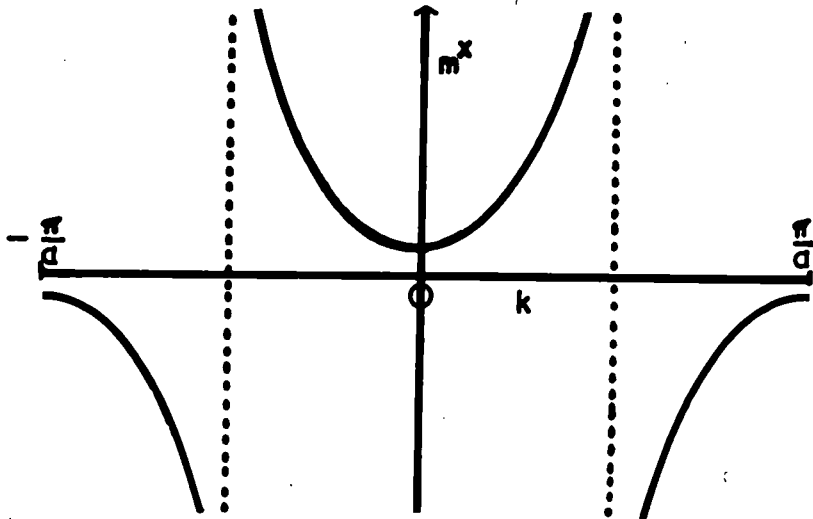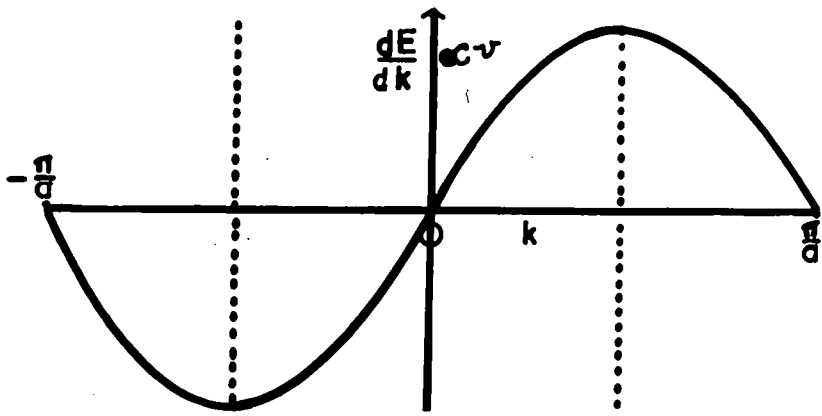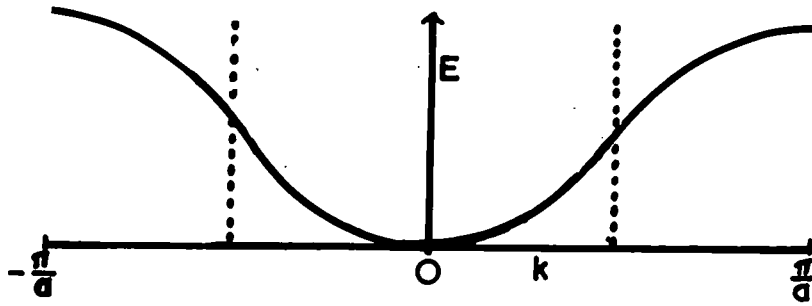
FIGURE 1·7
TYPICAL E, dE/dk and m^x versus k CURVES

In real crystals, there can be several scattering mechanisms. When external electric or magnetic fields are applied a non-equilibrium distribution is produced. A relaxation time can then be defined as the characteristic time for a non-equilibrium distribution of velocities to return to thermal equilibrium.

Thus

$$v_D(t) \;=\; v_D(0) \, \exp \frac{-t}{\tau} \qquad\qquad 1.7.1.$$

where $v_D(0)$ represents the initial non-equilibrium velocity distribution and $v_D(t)$ is the distribution after time t. From equation 1.7.1. the deceleration of the electron can be written as $v_D(t)$ divided by τ. The equation of motion may now be written

$$\frac{d \, v_D(t)}{dt} \;+\; \frac{v_D(t)}{\tau} \;=\; \frac{eF}{m^*} \qquad\qquad 1.7.2.$$

In equilibrium, the drift velocity is constant and $\dfrac{d \, v_D(t)}{dt}$ in equation 1.7.2. is zero. Thus

$$v_D(t) \;=\; \frac{eF.\tau}{m^*}$$

and the mobility, which is the drift velocity per unit field is

$$\mu_e \;=\; \frac{e\,\tau}{m^*_e} \qquad\qquad 1.7.3.$$

A mobility can similarly be defined for holes. In

non-degenerate semiconductors it is necessary to consider
the mean relaxation time $\langle\tau\rangle$ averaged over all electron
energies. In metals and degenerate semiconductors τ is
the relaxation time of electrons with the Fermi energy.
The scattering mechanism allows an asymetrical electron
distribution to be established so that the crystal can
support a current. If the scattering mechanism is isotropic,
then the relaxation time is equal to the mean free time
between collisions and the mean free path is $v_D(t).\tau$.

1.8. <u>Scattering Mechanisms</u>.

There are two main types of scattering mechanism in
semiconductors, (a) those associated with the thermal
vibrations of the structure and (b) those caused by various
imperfections. (3)(4). Other intrinsic scattering mechanisms
which may be significant are (c) carrier-carrier scattering
and (d) inter valley scattering in semiconductors with com-
plicated band structures. The expressions for various forms
of scattering are in general complex and it is more appro-
priate in this discussion to consider the temperature vari-
ation of mobility which might be expected in the more
important cases.

Above absolute zero, the thermal oscillations in a
solid with two atoms per unit cell can be divided into two
classes. In the first class both atoms in a unit cell

oscillate in the same direction. Such oscillations form the acoustical branches of the lattice vibrational spectrum. The waves have small wave number and correspond to sound waves in the crystal. The second class of vibrations are those in which the atoms in a unit cell move in opposite directions. The dipole produced can couple strongly to electromagnetic waves. These oscillations form the optical modes of the vibrational spectrum. There are three components, two transverse, and one longitudinal, for each type of oscillation. The quantum mechanical solution of the equation of motion of a set of linear oscillators is well known.(1). Only certain energies are allowed, which for a lattice are given by

$$E_i = (n + \frac{1}{2}) \hbar \omega_i$$

where $\omega_i = 2\pi\nu_i$ is the frequency of the ith allowed oscillation. The state in which each atom is at rest at its position of equilibrium is not allowed. The lattice can exchange quanta of energy $\hbar\omega$, which by analogy with photons are termed phonons.

Scattering introduced by the longitudinal acoustical modes leads to a carrier mobility which is proportional to $T^{-3/2}$. Scattering by other modes produces more complex variations. Electron-electron scattering and electron-hole scattering usually have only small effects on the mobility. The former depends on the velocity dependence of the

relaxation time, and the latter is similar to ionised impurity scattering discussed below. Inter valley scattering arises when a sophisticated band model is considered. The E versus k curve can have several minima which depend not only on the magnitude but also on the direction of the k vector. Electrons conduct in these various minima, which are called valleys, and can be scattered between them. Momentum is conserved either by the emission or absorption of a phonon. This scattering process is unlikely at low temperatures but increases with increasing temperature as more phonons become available. The evaluation of intrinsic scattering mechanisms at low temperatures can be complicated if the non-equilibrium phonon distribution has a long relaxation time. The lattice has difficulty in returning to equilibrium after receiving energy from a scattered electron and it becomes necessary to consider the effect of this non-equilibrium distribution on subsequent scattering events.

Scattering by ionised impurities is dependent upon the concentration of impurities and the temperature. At ordinary temperatures and small impurity concentrations the mobility varies approximately as $T^{3/2}$. At low temperatures and high concentrations of impurity the mobility varies as $T^{-1/2}$. Scattering by neutral impurities is independent of temperature.

Scattering by grain boundaries, dislocations and the deformed potential due to the crystal surface are likely to

be small in reasonable quality crystals, and overshadowed
by a more prominent mechanism.

The mobility is independent of electric field if the
electrons are in equilibrium with the lattice. This is
only true for small applied fields. With large fields the
electron temperature may become considerably higher than that
of the lattice. The mobility of the hot electrons as they
are called is inversely dependent upon some power of the
field between one half and one. At very high fields, electrons
may lose energy in exciting optical phonons and the current
saturates.

A critical review of scattering processes in germanium,
and the calculated mobilities can be found in reference (4).
This review contains a comprehensive list of references to
original work.

1.9. Contacts.

In the preceding sections it has been shown how
electrical currents can flow in crystalline solids. The
supply of electrons and holes to semiconductors depends
upon the relative magnitude of the work functions of the
semiconductor and metal contact. This is illustrated in
fig. 1.9. The respective work functions are $\emptyset_S$ and $\emptyset_M$.
The electron affinity of the semiconductor is $\chi_S = \emptyset_S - E_F$.
The contact between metal and semiconductor for $\emptyset_M > \emptyset_S$ has
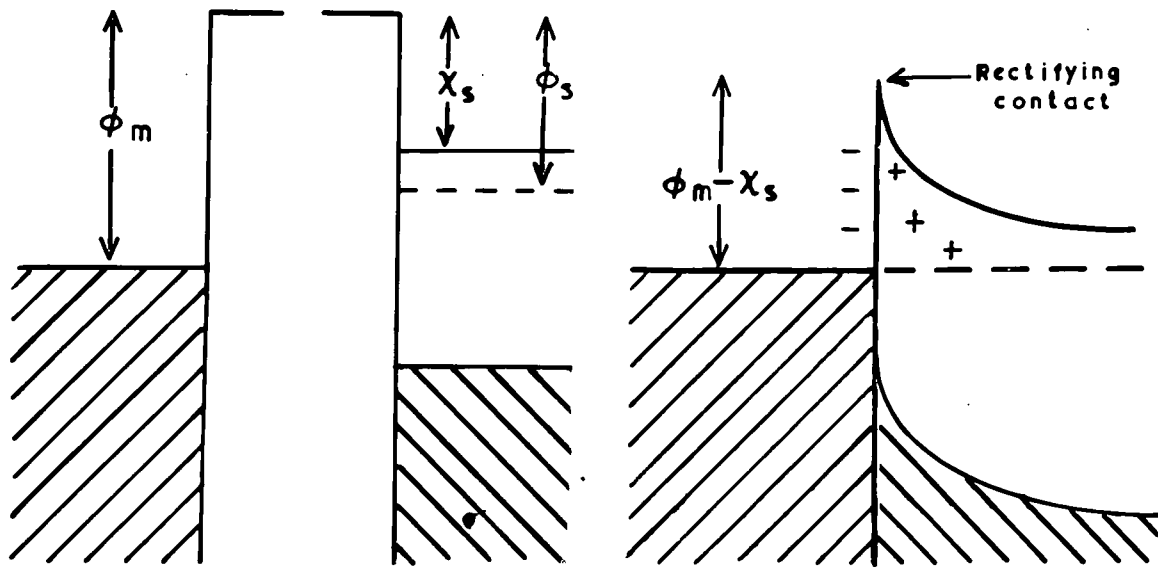
HIGH WORK FUNCTION METAL $\phi_m > \phi_s$
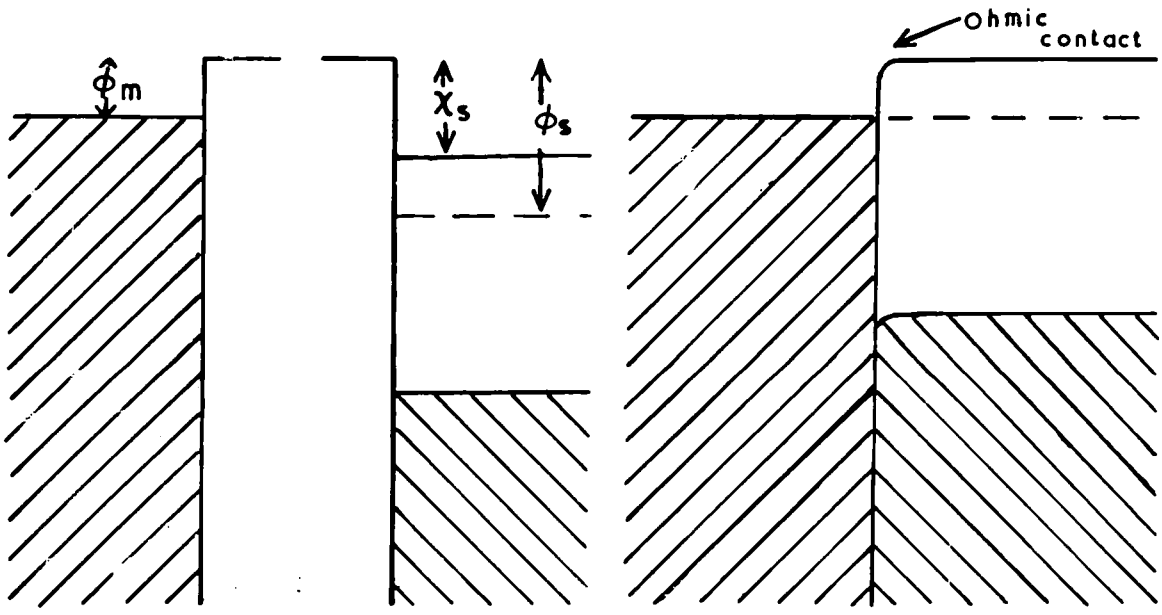
LOW WORK FUNCTION METAL $\phi_m < \phi_s$

FIGURE 1.9

n-TYPE SEMICONDUCTOR – METAL CONTACTS

rectifying properties.   On making contact there is a flow of electrons from the semiconductor to the metal and a depletion layer is established in the semiconductor. Electrons flowing into the conduction band have to surmount the potential barrier formed by this layer.   This is the reverse direction of the rectifying contact.   Electrons flowing out of the valence band do not have this barrier to cross.   Such a contact, therefore, has a poor electron injection efficiency but good hole injecting properties. (The electrons moving out of the valence band are raised to the Fermi level in the metal by the applied field).

Similar reasoning applied to a contact where $\emptyset_M < \emptyset_S$ leads to a conclusion that this type of contact is very efficient for electron injection but poor for hole injection. The limitations of metal contacts are discussed in reference (5).

CHAPTER II

Optical Properties of Semiconductors

2.1. Introduction

The interaction of light with semiconductors, where the word light is used to include ultra-violet and infra-red radiation, provides a powerful basis for the investigation of the properties of solids. Two of the most important measurements are those of the transmission and reflection of unpolarised and plane polarised light. The measurements can be made at different temperatures and with the crystal in electric and magnetic fields or under physical stress if required. The interpretation of the results of the numerous possible experiments helps to clarify the details of the band structure of semiconductors.

The investigation of photoconductivity enables information to be gained about the internal electronic processes. The property of photoconductivity arises from the increase in the number of carriers available for conduction when light is absorbed. Suitable contacts to the crystal surfaces are required in order that a field may be applied to induce a photocurrent to flow.

2.2. Optical Constants

The propagation of an electromagnetic wave through

a solid may be described by solving Maxwell's equations assuming there is no permanent charge density. The electrical component of the wave can be shown to be (6)

$$E_x = E_o \exp \frac{-\omega k x}{c} \exp i\omega(t - \frac{nx}{c}) \qquad 2.2.1.$$

This equation represents a wave of frequency $\omega/2\pi$ travelling with velocity c/n, the amplitude of which is damped by the first exponential term. The refractive index, N, is complex and expressed as

$$N = n - i k \qquad 2.2.2.$$

The real and imaginary parts of N are sometimes referred to as the refractive index, n, and the coefficient of extinction, k

$$2 n^2 = \epsilon \left[1 + (1 + \frac{\sigma^2}{\omega^2 \epsilon^2 \epsilon_o^2})^{1/2} \right] \qquad 2.2.3.$$

$$\text{and} \quad 2 k^2 = \epsilon \left[1 - (1 + \frac{\sigma^2}{\omega^2 \epsilon^2 \epsilon_o^2})^{1/2} \right] \qquad 2.2.4.$$

The symbols ϵ and ϵ_o are the dielectric constants of the crystal and free space and σ is the conductivity at the optical frequency $\omega/2\pi$. Equations 2.2.1. to 2.2.4. describe the general behaviour of a crystal in an electromagnetic field. It is convenient for our purpose to distinguish between three situations. (i) absorption by free electrons

(ii) absorption across the energy gap, (iii) absorption due to levels within the forbidden energy gap. Lattice absorption will not be discussed in detail.

2.3. Absorption by Free Carriers

Free electron absorption is predominant in metals, but only becomes important in semiconductors at wavelengths above one micron. In a semiconductor the absorption is limited by the width of the band concerned. Five phenomena have been widely exploited in determining details of the band structure of some solids.

(i) Cyclotron Resonance is a technique which can be used to determine the effective mass m^* (7). Apparatus is set up to observe microwave absorption in a semiconductor placed in a magnetic field. The radiation field is polarised with its electric vector perpendicular to the magnetic field. When $\omega = \dfrac{eH}{m^* C}$ the electrons absorb energy continuously from the incident radiation and execute a spiral motion about the magnetic field. A measure of the frequency at which the resonance occurs provides an estimate of m^*. The sharpness of the line absorption depends upon the quantity of energy the electron can gain from the field before it suffers a scattering event. Thus the absorption depends upon the relaxation time. (Section 1.7.). Cyclotron resonance can only be observed when $\omega\tau \gg 1$. Cyclotron resonance has been measured at infra-red frequencies, where ω is large, in

indium antimonide. (8). A steady magnetic field of 60,000 gauss was used and resonance observed at 41 microns. Pulsed magnetic fields have been used to study infra-red cyclotron resonance in indium arsenide. (7).

(ii) The Plasma Effect is associated with the large decrease in the reflection of infra-red radiation which occurs at a certain frequency ωp, the plasma frequency. The magnitude of ωp can be obtained from the expression for the refractive index using equations (2.2.2.), (2.2.3.), (2.2.4.). We have

$$N^2 = (n - ik)^2 = \epsilon - \frac{i\sigma}{\omega\epsilon_o} \qquad 2.3.1.$$

The conductivity at a frequency ω is given by equations 1.7.3. and 1.4. with $\tau = 1/i\omega$, if losses are neglected.

Equation 2.3.1. can then be expressed as

$$(n - ik)^2 = \epsilon \left[1 - \frac{Ne^2}{\omega^2 \epsilon \epsilon_o m^*} \right] = \epsilon \left[1 - \frac{\omega p^2}{\omega^2} \right] \qquad 2.3.2.$$

where N is the density of carriers.

The plasma frequency, $\omega p^2 = Ne^2/m^*\epsilon\epsilon_o$, corresponds to a large change in reflection of a semiconductor. This frequency corresponds to the lower limit for propagation of an electromagnetic wave through a semiconductor. Incident radiation of frequency $\omega < \omega p$ is totally reflected. From equation 2.3.2. the refractive index n is zero. At a

frequency above ωp given by $\omega_{min}^2 = \omega p^2 \left[1 - \epsilon^{-1} \right]^{-1}$,
the refractive index is unity and the semiconductor is matched
into free space. The reflectivity is zero and the semi-
conductor transmits the radiation. At frequencies higher than
this minimum, the reflectivity rises and $n^2 \rightarrow \epsilon$ (equation 2.3.2.
The inclusion of absorption losses shows that the reflectivity
for $\omega < \omega p$ is slightly less than unity and the reflectivity
minimum is not quite zero. The effective mass can be deter-
mined from this change in reflectivity if the dielectric
constant is measured at high frequency and N, the density of
carriers, is determined from a Hall effect measurement.

(iii) The magneto-Plasma effect is similar to that
just described. A magnetic field is applied parallel to
the direction of propagation of the incident light. The
magnetic field results in a splitting of the plasma edge
into two. The amount of splitting is equal to the cyclotron
resonance frequency. This permits a direct determination
of the effective mass m^*.

(iv) Faraday Rotation is observed at frequencies
above the plasma frequency in magnetic fields well below the
cyclotron frequency. The experiment is carried out by pro-
pagating a linearly polarised wave parallel to the magnetic
field. The plane of polarisation is rotated due to the
different indices of refraction of the two circularly
polarised components. Typical values of the rotation for

indium antimonide are $H = 10^4$ gauss, $N = 10^{17}$ cm^{-3} and λ = 15 microns, $\Theta = 250^o$/mm. The angle of rotation in c.g.s. units is given by

$$\Theta = \frac{Ne^3 H \lambda^2}{8\pi^2 \sqrt{K} C^4 m^{*2}} \qquad 2.3.3.$$

where K is the dielectric constant.

(v)   The Voigt Effect is observed under similar conditions to Faraday rotation. A plane polarised beam is perpendicularly incident on a semiconducting slab with the plane of polarisation at 45° to the magnetic field. The magnetic field is parallel to the plane of the slab. Since the two components of the incident light have different indices of refraction they emerge with a phase difference after passing through the specimen. The transmitted wave is elliptically polarised. The magnetic field can be varied to obtain circularly polarised light which is then detected. The phase difference is given by

$$\delta = \frac{1}{16\pi^3 \sqrt{K}} \frac{Ne^4 \lambda^3 H^2}{c^6 m^{*3}} \qquad 2.3.4.$$

The effective mass can be determined directly by combined measurements of Faraday rotation and Voigt effect.

More detail of the effects (i) - (v) can be found in references (7 - 14).

An important consequence of the variation of effects

(ii) to (v) with the density of carriers is that the band structure may be explored. Crystals with different doping levels are measured. The variation of m* is then a measure of the curvature of the band. Cyclotron resonance requires $\omega > \omega p$ and for semiconductors with a high density of carriers impossibly large magnetic fields would be required to achieve resonance (7).

Absorption within a band is only possible by indirect transitions. This will be discussed in the next section. The effects (i) - (v) are also observed for holes, and separate measurements are made for holes of different masses in a split valence band.

2.4. Absorption Across the Energy Gap

An electron in the valence band of a semiconductor can be considered as a bound electron. When the electron suffers a disturbing force, the restoring force can be taken to be proportional to the displacement, and the damping proportional to the velocity. Thus according to classical mechanics

$$m \frac{d^2 x}{dt^2} + mg \frac{dx}{dt} + m \omega_o^2 x = eE \exp i\omega t \qquad 2.4.1.$$

where g is the damping term. This is the equation of motion for an electron in an applied electric field E exp $i\omega t$. Solution of this equation in terms of x enables the polari-

zability to be obtained. This is related to the dielectric constant and hence an expression for the optical constants may be obtained. This gives the relations between n, k and frequency shown in fig. 2.4.1. Although this is the classical approach (11) there is good qualitative agreement with the detailed quantum-mechanical result. The classical method neglects four main points. (i) The electrons are subject to the periodic field of the lattice. (ii) The distribution of electrons over a number of states is ignored. (iii) The existence of a constant relaxation time $\tau = 1/g$ is assumed. (iv) No provision is made for transitions between states.

A more detailed quantum-mechanical treatment (6) gives expressions for the optical constants

$$n^2 - k^2 - 1 = \sum_j \frac{ne^2 f_j/m\epsilon_0 (\omega_j^2 - \omega^2)}{(\omega_j^2 - \omega^2)^2 + \omega^2 g_j^2} \qquad 2.4.2.$$

$$2nk = \sum_j \frac{(ne^2 f_j/m\epsilon_0)\omega g_j}{(\omega_j^2 - \omega^2)^2 + \omega^2 g_j^2} \qquad 2.4.3.$$

The interaction of the field is the sum of the interactions of linear oscillators. The contribution from each oscillator depends on the oscillator strength f. Each of the resonance frequencies corresponds to an allowed transition between electronic states.

Absorption by electrons lying in bands below the valence band occurs only with wavelengths in the x-ray region of the
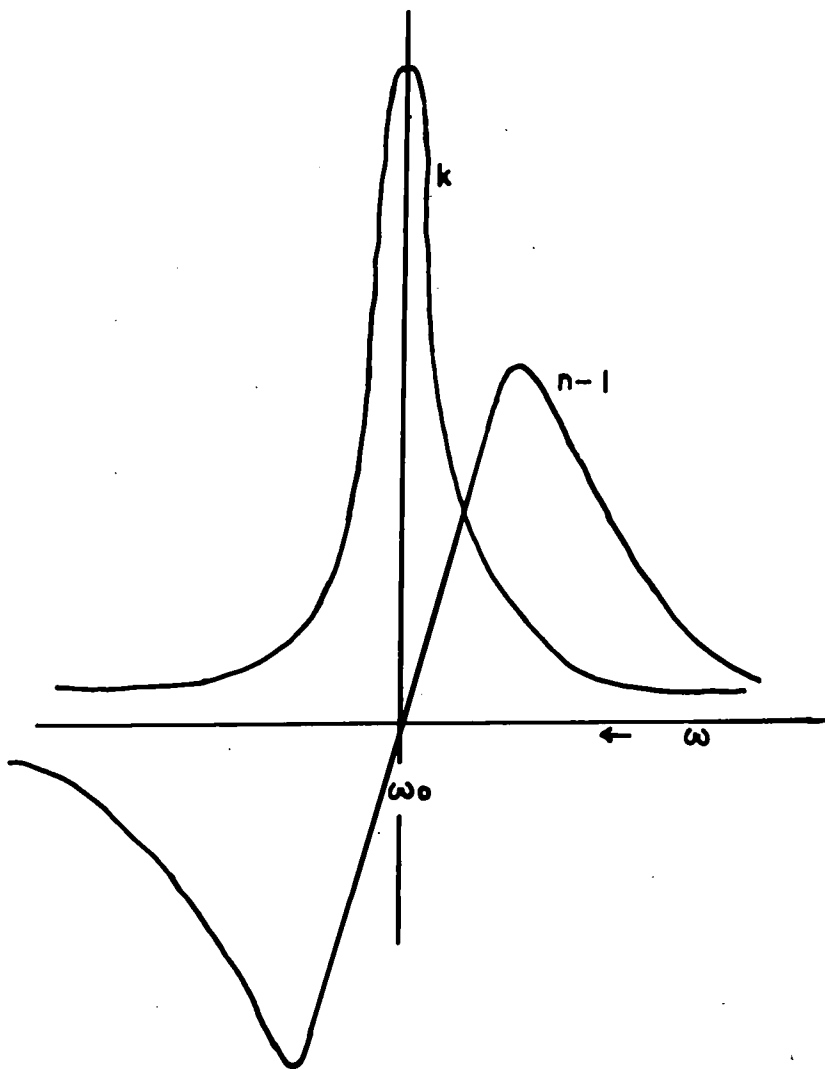
n . k   VERSUS   ω

FIG   2.4.1

spectrum.   This range is beyond the scope of this discussion.

Photons incident upon a semiconductor with energy sufficient to raise a valence electron to the conduction band are absorbed.   Photons with energy less than that of the forbidden gap are not absorbed.   Mathematically, very many more oscillators are available to contribute to the absorption when the photon energy exceeds the forbidden gap.

The quantum mechanical selection rule states that the difference in wave number of the initial and final state of the electron shall be equal to the wave vector of the radiation. The wave vector of the radiation is small compared with that of the electron.   Thus the transition is vertical between the bands on the E versus k diagram for the transition to be highly probable, fig. 2.4.2.   Non-vertical transitions are very much less likely.   The momentum in such transitions is conserved by the absorption or emission of a phonon (s).   Germanium and silicon have indirect gaps so that non-vertical, as well as vertical transitions occur.   Direct transitions only are obtained in semiconductors with simple energy surfaces with minima at k = 0.   This is discussed later with particular regard to cadmium sulphide which has energy band structure of the latter type. As stated in the last section direct transitions within a band are not allowed, since energy and momentum cannot both be conserved in such circumstances.   As the energy of an electron increases within a band its wave vector must change.   ~~Free~~

INDIRECT GAP

DIRECT GAP
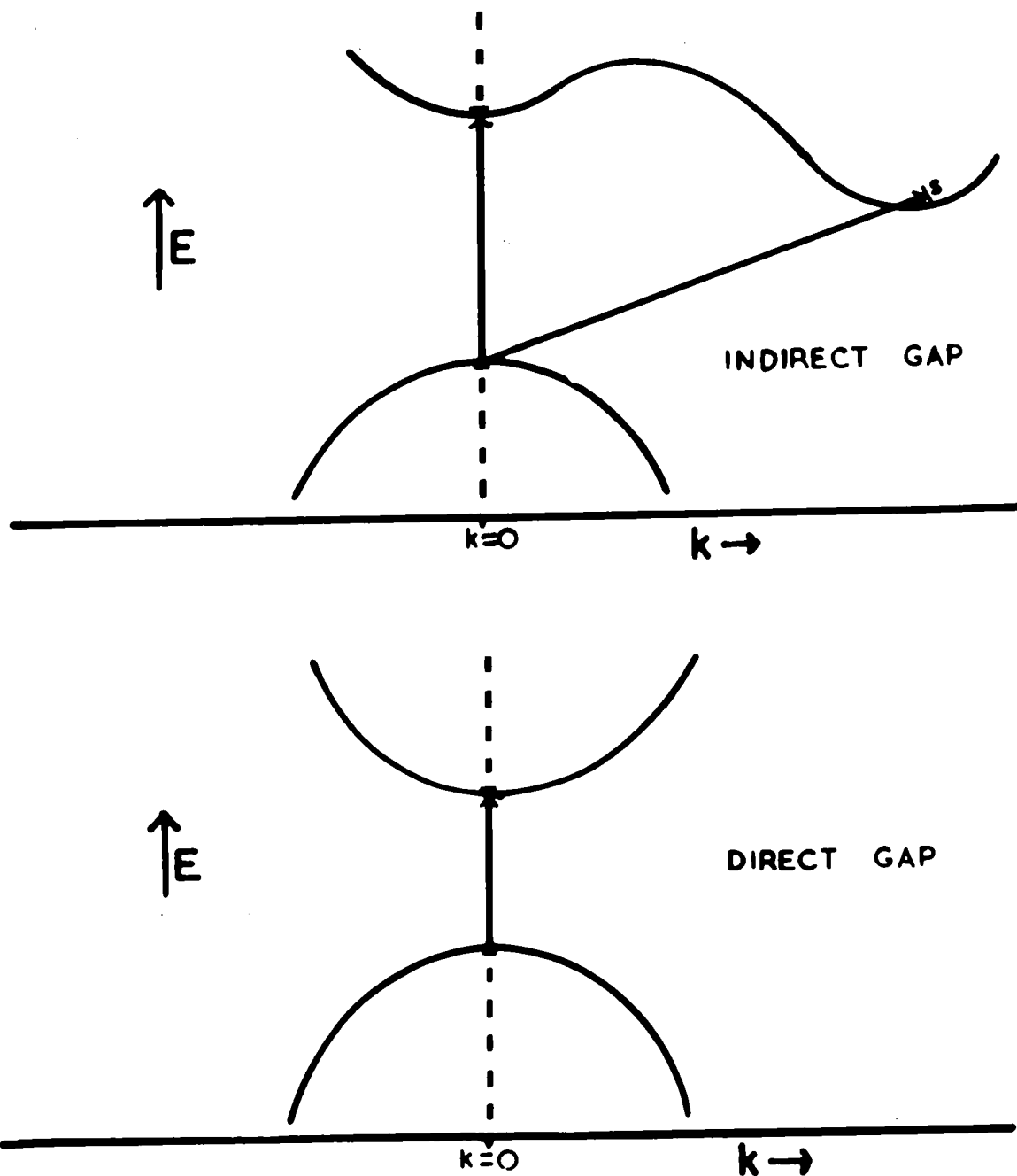
FIGURE 2.4.2.
TYPICAL ENERGY BANDS

Free carrier absorption is due to transitions of the indirect type, and the nature of the absorption is therefore dependent on the type of scattering which is operative.

Electrons excited to the conduction band and the accompanying holes can contribute to a current through the crystal. A typical absorption curve for a semiconductor is shown in Fig. 2.4.3. The absorption on the long wavelength side of the main band may be due to an indirect transition or to levels close to the band edges.

Lax and Zwerdling (14) have reviewed magneto-optical phenomena in semiconductors. Effects corresponding to (i) - (v) section 2.3., have been measured which are associated with interband transitions.

2.5.   Absorption due to Levels within the Gap.

Absorption by electrons bound to impurity centres or native defects, or excitation to these levels in the forbidden gap from the valence band can also contribute to an increase in free carrier concentration. The identification and source of these levels is perhaps the most important, outstanding problem in an investigation of wide band gap crystals. An important series of energy states are associated with excitons. An exciton is a region of localised excitation energy, in which an excited electron interacts with a hole in the valence band. An exciton has no charge and cannot contribute directly to conduction processes. The interaction between hole and
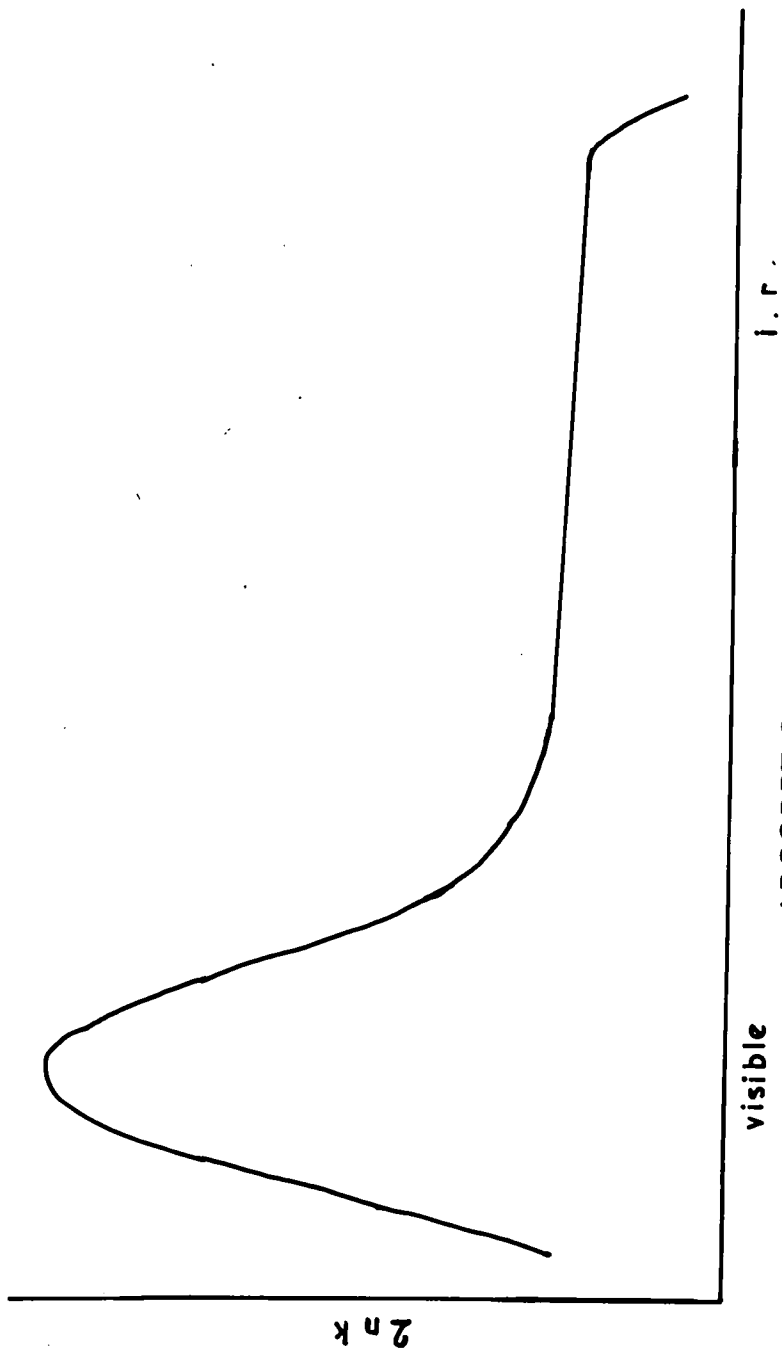
ABSORPTION SPECTRUM

FIG 2.4.3

electron introduces a series of hydrogen-like levels below the conduction band with the conduction band as the series limit. Excitons have been extensively investigated in cadmium sulphide. Further details can be found in chapter five.

Absorption by optical modes of the lattice, mentioned in section 1.8., is a prominent effect. This usually occurs in the wavelength range from 10 to 50 microns and provides information concerning the crystal bonding. The absorption spectrum contains the 'Reststrahlen' or residual ray bands a name which originates from early measurements of reflection spectra. The term arises from the use of this effect in selection of specific wavelengths by reflection from crystals.

2.6. Determination of Optical Constants.

The reflectivity of a surface is related to the optical constants as follows

$$R = \frac{(n-1)^2 + k^2}{(n+1)^2 + k^2} \qquad 2.6.1.$$

With many semiconductors the transmission is high for wavelengths in the infra-red shorter than those corresponding to the plasma frequency. In this event k in equation 2.6.1. may be neglected. The reflectivity then gives a direct measure of the refractive index.

If the absorption is not negligible two independent reflectivity measurements are required to determine n and k.

Further details can be found in reference (15).

2.7. Luminescent Emission from Semiconductors.

Luminescent emission from semiconductors may be stimulated by the production of excited electronic states. The excitation can be produced by electromagnetic radiation, electron bombardment or by the injection of minority carriers from the contacts. Internal excitation is also possible by impact ionisation or field ionisation. The internal heating of a crystal during dielectric breakdown is another mechanism which can lead to the emission of light. Electro-luminescence effects in powders are probably due to impact or field ionisation(16).

It is usual to distinguish somewhat arbitrarily between phosphorescence and fluorescence by the length of the decay time of the emission. Phosphorescence has a long decay and is the light emitted after a time $> 10^{-8}$ secs of the excitation event. Phosphorescence is associated with the excited electrons spending some time in a trapping centre. Fluorescence has a decay time $< 10^{-8}$ secs which is characteristic of the lifetime of an isolated excited atom(17). The actual decay time is not a good measure of which process is predominant. Where doubt arises as to the mechanism, the variation of the decay time with temperature may enable the distinction to be made. In this work, emission stimulated

by ultra-violet radiation will simply be termed luminescence, and that stimulated by injection of electrons and holes electroluminescence.

The photon energy of the emitted light is always less than that of the excitation. This arises because, according to the Franck-Condon principle, the absorption process is so rapid that the excited electron immediately afterwards is not in thermal equilibrium with its surroundings. This is the result of a change in electrostatic polarisation with the excited atom. After the excitation transition the system relaxes, and vibrational energy is dissipated in the lattice. There is a similar loss of energy to the lattice on emission which takes place when the electron returns to the ground state. The whole process explains the Stoke's shift, which requires the energy of the absorbed photon to be greater than that of the emitted quantum.

The quantum mechanical selection rule for emission is similar to that for absorption, and the transitions are essentially vertical unless crystal momentum is conserved by the emission or absorption of a phonon(s).

2.8. Photoconductivity

Photoconductivity is a consequence of the production of free carriers by absorbed electromagnetic radiation. The additional carriers contribute to the current flow in an

applied field. (18). Free electrons and holes can be created by exciting an electron across the band gap. A free electron can also be produced by excitation from a filled level within the gap, and a hole by excitation of an electron from the valence band to an acceptor level. In each case carriers are made available to enhance those already present in thermal equilibrium. The sensitivity or gain of a photoconductor is determined by the free carrier lifetime τ. The gain will be high if τ is large so that many electrons can enter and leave the crystal before recombination occurs. The gain will be reduced if the carrier spends some fraction of its total free lifetime in a trapping level. Trapping levels may enhance photoconductivity by trapping a carrier of one type and reducing the probability of recombination. The distinction between trapping and recombination centres is made by comparing the relative probabilities of thermal ejection of the trapped electron to the conduction band and recombination with a free hole. Levels near the band edge generally behave as trapping centres. Levels near the centre of the forbidden gap, once they have captured a carrier have a high probability of capturing a carrier of the opposite kind and behave as recombination centres. A particular centre may act in both capacities at different temperatures.

The response time of a photoconductor to a change in incident light flux is determined by the total lifetime of excited carriers. This time is the sum of the free

lifetime and the time spent in trapping levels. Either
mechanism may predominate in a particular semiconductor
under different conditions of temperature and illumination.
The response time is critically dependent on the electronically
active defect centres within the forbidden gap. The gain,
G, of a photoconductor is defined as

$$G = \frac{\Delta I}{eF} \qquad\qquad 2.8.1.$$

where ΔI is the photocurrent, and F the total number of
electron-hole pairs being created per second in the photo-
conductor. The gain can also be expressed as, the ratio of
the free lifetime of a charge carrier, to its transit time
between electrodes. For a majority carrier photoconductor
this becomes

$$G = \frac{\tau}{T} \qquad\qquad 2.8.2.$$

where T is the transit time. The transit time is $T = \frac{d^2}{\mu_e V}$.
Thus equation 2.8.2. can be written

$$G = \tau \mu_e \frac{V}{d^2} \qquad\qquad 2.8.3.$$

where d is the electrode separation. There is no limit to
the gain of a photoconductor according to equation 2.8.3.
It can be shown, however, that maximum gain is achieved at
the onset of space charge limited conduction (discussed in

the following chapter). The maximum gain is (5)

$$G_{max} = \frac{\tau_o}{\tau_{RC}} \quad M \qquad 2.8.4.$$

$$M = \frac{N_1}{N_2} \qquad 2.8.5.$$

where τ_o is the response time of the photoconductor and τ_{RC} is the dielectric relaxation time. M is the ratio of the positive charges on the anode, N_1, to the total increase in photoexcited carriers, N_2, accompanying an increase in the absorbed light flux. N_2 is only dependent on the electronic structure and the intensity of illumination. Space charge limited conduction begins when $N_1 = N_2$. This occurs when the injected carrier density equals the bulk carrier density at some voltage V. At higher voltages the number of charges on the anode increases with the number of injected carriers and M retains a value of unity. Recombination centres with levels in the forbidden gap may increase M to a value approaching 500. The net effect is that the space charge limited threshold is raised but the free electrons are not in thermal equilibrium with the recombination centres. From equation 2.8.4. with M restricted to a value $\leqslant 1$ the product of gain, G, and bandwidth, $1/\tau_o$, is constant. Thus a sensitive photoconductor must have a long response time.

The response time of the contact puts a further limit

on the gain-bandwidth product (19) if this is longer than the response time determined by the bulk of the photoconductivity. A more complete treatment of the gain-bandwidth product and the contact response time is given in reference 5 which includes many original references.

CHAPTER III

Space Charge Limited Conduction

3.1. Introduction

Conduction in a crystalline solid can usually be described in terms of the relation $\sigma = ne\mu_e + pe\mu_p$. The densities of electrons and holes are given by equations 1.5.5. and 1.5.6. or their equivalents for a solid with levels in the forbidden gap. Mott and Gurney [20] pointed out that under certain circumstances excess carriers could be supplied to an insulator at the contacts. These injected carriers would lead to a current in excess of that expected from the equilibrium concentration of carriers. The excess current is limited purely by its own space charge. To observe space charge limited (s.c.l.) currents three conditions must be satisfied. (i) The contacts must permit the injection of excess carriers. (ii) The carriers must remain in the appropriate band to contribute to the current. (iii) The injected carrier density must be high with respect to the residual carrier density. Under these circumstances the current is limited by the space charge of the injected carriers. By neglecting diffusion, Mott and Gurney showed that the current density is

$$J_c = \frac{9 \, \epsilon \, \mu \, V^2}{8d^3} \qquad\qquad 3.1.$$

where ϵ is the permittivity of the solid and d the electrode
separation. Equation 3.1. refers to a single carrier
conduction mechanism in a plane-parallel slab in one dimen-
sion. A thin crystal is necessary to observe s.c.l. currents
due to the third power dependence of current on electrode
separation. Single carrier, and two carrier, s.c.l. con-
duction have been described in a previous thesis (5). A
brief outline only will be given here for reference purposes
in describing the experimental results.

3.2. Lampert's Theory of Single Carrier Conduction

A simplified theory of s.c.l. conduction in the
presence of traps has been proposed by Lampert (21). He
considered an insulator with one discrete trapping level
and a single carrier conduction mechanism. The result of
his analysis can be explained with the aid of Fig. 3.2.1.
The current is confined within three limiting characteristics.
It cannot be below the Ohm's law value for the neutral
crystal, curve a, Fig. 3.2.1. It cannot be above curve b
which is a plot of equation 3.1. and represents the current
when all the injected carriers are free. The current cannot
be to the right of curve c which corresponds to the situation
where all the injected carriers are trapped. The line c
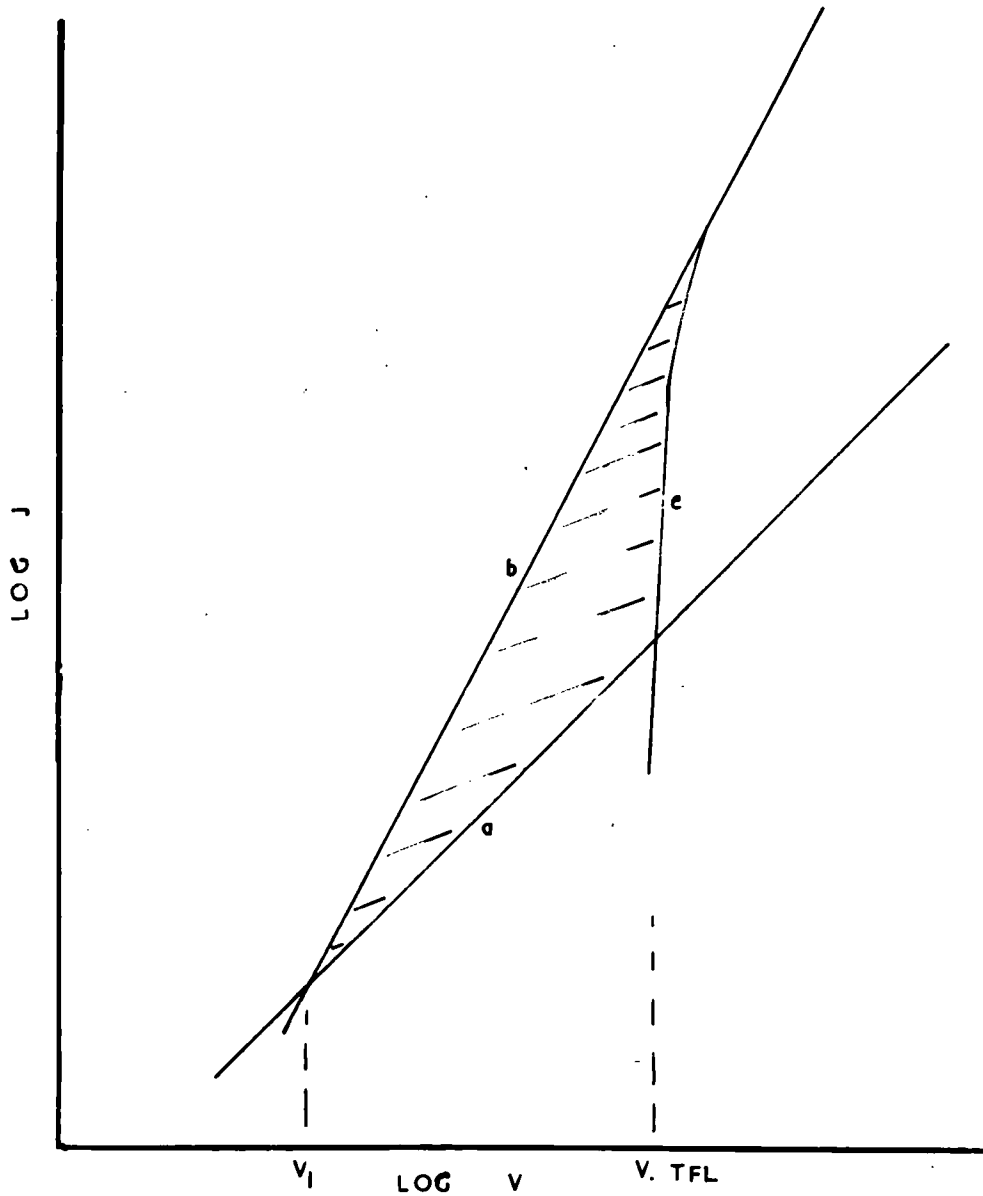
FIG   3.2.1

LIMITING   CURRENT - VOLTAGE CHARACTERISTICS

·AFTER   LAMPERT

is referred to as the traps-filled-limit. Lampert showed

that the actual current is given by a reduced square law

$$J = \frac{9 \, \Theta \, \epsilon \, \mu \, V^2}{8d^3} \qquad \text{3.2.1.}$$

where Θ is the ratio of free to trapped carriers and is

independent of voltage, provided the Fermi level at the

anode (for electrons) lies below the trap depth. He also

showed that the traps filled limit voltage is given by

$$V_{TFL} = \frac{ed^2 \, Nt}{2\epsilon} \qquad \text{3.2.2.}$$

where Nt is the density of traps, and the Ohmic to square

law transition takes place when the applied voltage reaches

a value

$$V = \frac{ed^2 \, \bar{n}}{2\epsilon\Theta} \qquad \text{3.2.3.}$$

where $\bar{n}$ is the thermal equilibrium carrier density. This

theory does not apply where the current is dominated by

carrier diffusion rather than drift in the electric field.

3.3. Two Carrier s.c.l. Conduction

Two carrier s.c.l. conduction has been treated by

several authors.(19.22-25). The current density is related

either to the square or cube of the voltage depending on

the mechanism of the recombination of the two carriers, the

lifetimes of the carriers and the possibility of neutralis-
ation of the injected charge by the carrier of opposite sign.
Lampert (19.25) has considered the variation of lifetime
of a carrier with increasing carrier injection. He pre-
dicted a negative resistance effect since at high injection
levels the crystal must remain electrically neutral.

Two carrier s.c.l. conduction affords a means of
obtaining low field electro-luminescence. The recombination
of carriers is accompanied by emission of photons with energy
corresponding to that released during the recombination.

CHAPTER IV

Electrical Conduction in Cadmium Sulphide

4.1. Introduction

Cadmium sulphide crystallizes in the hexagonal close packed (wurtzite) lattice (26). It can be thought of as two interlocking hexagonal arrays, of cadmium and sulphur. Each cadmium atom is bonded to four sulphur atoms with an interatomic distance of 2.52 Å. Pauling (27) established a criterion for expressing the percentage of ionic bonding in terms of the electronegativity difference of the atoms, i.e. the ability of the atoms to attract electrons. Cadmium sulphide has 22% ionic bonding according to this formalization. (14). This degree of ionic character in the bonding is the cause of the wide band gap in cadmium sulphide. The interaction of individual atomic orbitals when the atoms are brought together to form a crystal is not as great as that in a covalent crystal, such as germanium, where all valence electrons are shared between the atoms.

4.2. Crystal Growth

Single crystals of cadmium sulphide can be prepared by sublimation from powder in the temperature range $900^{\circ}C$ to $1200^{\circ}C$ using either an inert atmosphere or vacuum. In

many variations of the basic technique the sublimation is assisted by passing a carrier gas over the charge (28,29,30). Single crystals can also be prepared from the constituent elements, and by a transport technique which utilises iodine as a carrier (5). The crystals formed are generally small rods (1 cm by 1 mm diameter) or thin plates (0.1 mm by 0.5 cm square.). Large crystals can be grown by modifying the basic technique (31).

The comparatively high temperatures required make the stoichiometry and incorporation of unwanted impurities in cadmium sulphide difficult to control. Growth from the melt requires high pressures (of the order of 100 atmospheres) to prevent dissociation of the cadmium and sulphur. Temperatures needed are in the region of 1300°C. Good control of the growth parameters under these conditions would at the present time be even more difficult to achieve than in the vapour phase techniques.

4.3. Forbidden Energy Gap

The width of the forbidden gap at any particular temperature depends on the criteria chosen to define it. Sommers et al (32) from photoelectromagnetic (PEM) measurements give a value of 2.48eV at room temperature. Curie (17, p.81) quotes a value of 2.43eV at the same temperature from measurements of the fundamental optical absorption limit. It is usual to define the band gap as the energy at which

the absorption coefficient is 100 mm^{-1}. Using this criterion, the band gap for cadmium sulphide will be taken as 2.52 eV and 2.43 eV at liquid nitrogen and room temperature respectively (17.p.109).

4.4. Band Structure of Cadmium Sulphide

Elaborate calculations of the band structure of cadmium sulphide by Balkanski and des Cloizeaux (33) indicate that the valence band is split into three sub-bands. The suggested structure is shown in Fig. 4.4. The lowest band arises from the s-orbitals of the sulphur ions, the next band from the p-orbitals parallel to the c-axis of the crystal, and the upper band from the p-orbitals perpendicular to the hexagonal axis. The upper band is split by about 0.016 eV at 4.3^{O}K by spin-orbit coupling. A review of the evolution of this concept of the band structure is given in reference (17), along with a comprehensive list of references. Thomas and Hopfield (34,35), in particular, from a study of reflectance and luminescence in cadmium sulphide support this theory. Their work, and other optical work in support of this band structure, is discussed in more detail in the following chapter. It should be noted from Fig. 4.4. that the probability of interaction of an electromagnetic wave with electrons in the two uppermost levels of the valence band depends on the orientation of

C.B.

E // C
E ⊥ C

E ⊥ C

± 0.016eV

0.074eV

V.B.s

~1eV
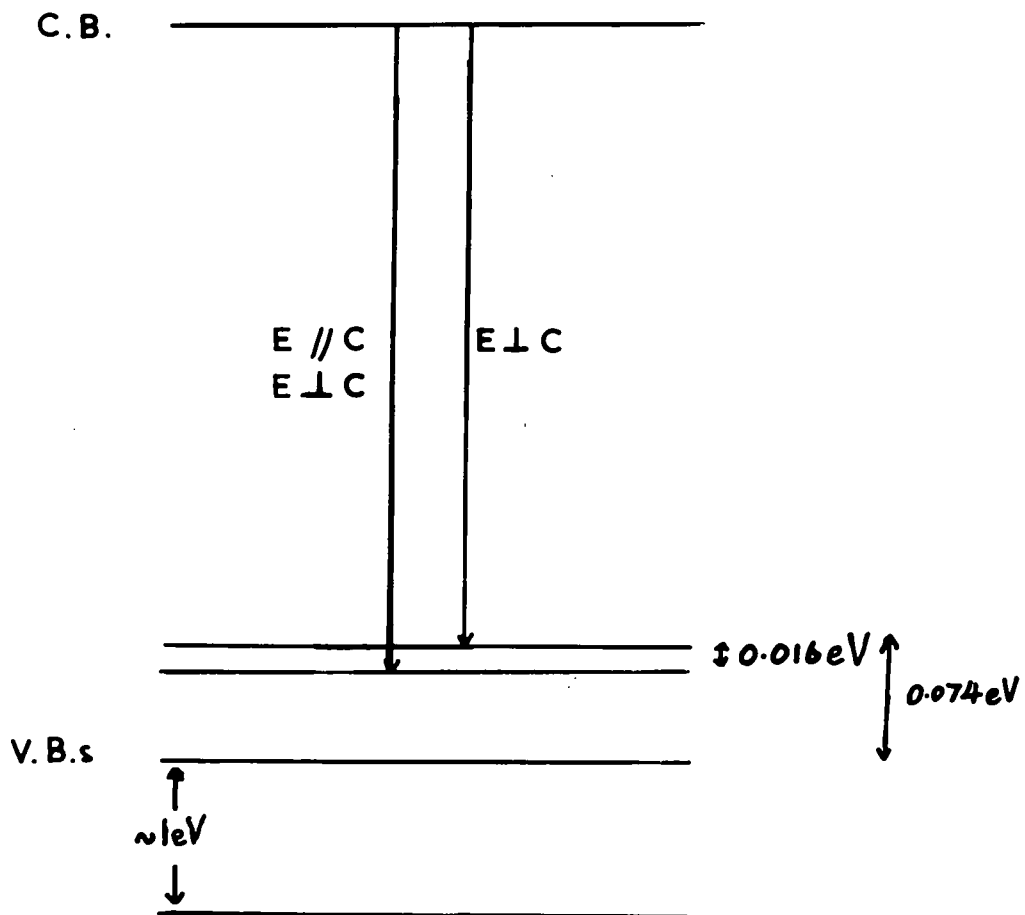
BAND STRUCTURE OF CdS

(BALKANSKI , des CLOIZEAUX)

FIG 4.4.

the plane of polarization of the wave with respect to the c-axis of the crystal.

4.5. The Effective Mass of Electrons and Holes

It has been shown earlier that the effective mass of a free carrier depends on the shape of the E vs k curve. The shapes of the energy surfaces are not well known for cadmium sulphide. An estimate of the electron effective mass has been given by Kröger et al (36) from Hall effect, resistivity and thermoelectric power measurements. To evaluate their results they assumed an electron mobility dependent upon acoustic and optical mode scattering which gave $0.20 \ m_e < m^* < 0.27 \ m_e$. Estimates from the temperature dependence of the Hall effect and the Zeeman effect of the reflectance and absorption spectra are summarized by Zook and Dexter (37). Their galvomagnetic measurements are in agreement with the values obtained by the earlier methods giving $m^* = 0.21 \ m_e$. Further agreement is provided by a study of the free electron absorption in doped cadmium sulphide. (38). All these experiments indicate that the conduction band minima occurs at k = 0 and that the effective electron mass is essentially isotropic.

The effective mass of holes is different in each of the valence bands. Values of $0.7 \ m_e$ and $5.0 \ m_e$ have been determined for the upper and lower level of the uppermost

valence band, by Thomas and Hopfield (35). They observed the change in exciton absorption of incident plane polarized light, on reversal of a magnetic field, for the two perpendicular directions of polarization.

Cyclotron resonance has been recently observed in cadmium sulphide using microwaves with a wavelength of six millimetres (39). An electron effective mass of 0.17 m_e and a hole effective mass of 0.81 m_e are reported. These values are in reasonable agreement with earlier work.

4.6. Carrier Mobility and Scattering Mechanisms.

The electron mobility in doped cadmium sulphide can be determined from resistivity and Hall effect measurements. It is of the order of 210 cm^2/V.sec. at room temperature and follows a $T^{-3/2}$ temperature variation in the range $150^{O}K$ to $700^{O}K$.(36). Below $150^{O}K$ ionized impurity scattering may predominate. Krüger et al fitted the high temperature variation of mobility to an expression involving the acoustical and optical modes. The acoustic scattering is responsible for the dominant $T^{-3/2}$ mobility variation at the higher temperatures.

Spear and Mort (40) have measured the electron and hole mobilities in undoped cadmium sulphide in the range $80^{O}K$ to $500^{O}K$ using a drift technique. It should be pointed out that the drift mobility will only be equal to the conductivity mobility if there is no trapping. This arises

because the mobility is defined as the drift velocity of free carriers per unit field. Spear and Mort interpreted the experimental variation of the electron mobility in terms of a transition from a lattice controlled to a trap controlled mobility as the temperature decreased below 250°K. They further suggested that the depth of the trapping level decreases with an increasing concentration of the impurities responsible for the traps. Above 250°K the mobility varied as $T^{-3/2}$.

The hole mobility was observed to decrease from a maximum of 15 cm^2/volt.sec. above and below room temperature. The high temperature variation may be interpreted in terms of lattice scattering, while the low temperature variation was explained in terms of transitions between the two upper levels of the valence band. Mort and Spear's measurements were carried out with the applied field perpendicular to the c-axis. The mobility they measured was consequently dependent upon the scattering in this direction of current flow.

Zook and Dexter (37), using measurements of Hall and magnetoresistance effects, concluded that mobility in cadmium sulphide can be satisfactorily attributed to a combination of optical mode and piezoelectric scattering. Piezoelectric scattering is brought about by the electric fields which are set up by the acoustic vibrations in a

polar crystal (41). Zook and Dexter point out that piezo-
electric scattering is anisotropic and for complete agreement
between theory and experiment they suggest anisotropic
impurity scattering is also important at low temperatures.
(77°K). The Hall mobility is not equal to the conductivity
mobility but related to it by a weighting factor which takes
account of the actual velocity distribution of carriers in
a particular crystal. Zook and Dexter's work was done on
low resistivity(of the order of 1 ohm.cm.) cadmium sulphide
and refers to electrons. The measurements were taken
parallel and perpendicular to the c-axis.

4.7. Defect Levels

Cadmium sulphide prepared as pure as possible is
a high resistivity n-type material. The resistivity is
10^{10} ohm.cm. or higher. Cadmium sulphide in this state could
be called a semi-insulator. It can be converted into a
low resistivity n-type semiconductor by the substitution
of chlorine bromine or iodine, all of which substitute for the
sulphur atoms producing shallow donor levels approximately
0.03 eV below the conduction band. Similarly substitution
of aluminium, gallium or indium for cadmium produces shallow
donor levels and low resistivity material.(42). A stoichio-
metric excess of cadmium has a similar effect (41). The
production of p-type cadmium sulphide is not yet possible

and this may be due to the high activation energy of acceptors which is generally put at the order of 1 eV above the conduction band (43,44). Copper or silver substituting for cadmium, or a cadmium vacancy are examples. The exception to this is the production of impurity band p-type conduction attained with a very high doping level of copper (45).

Defects with levels in the forbidden gap between the above extremes are very important in determining the photo-conductive properties of cadmium sulphide. A recent analysis by Nicholas (46) summarises the trapping levels found in this region for crystals grown under similar conditions to those used in this work. The levels were investigated using the thermally stimulated current method. With this technique the crystal is cooled and the levels filled with electrons by intense illumination. On heating the crystal, at a uniform rate, and monitoring the current passed by the crystal, various maxima are observed which correspond to the release of electrons from levels in the forbidden gap. A careful analysis of the thermally stimulated current curve provides values for the various levels. Using this technique Nicholas identified trapping levels at 0.05, 0.14, 0.25, 0.41, 0.63 and 0.83 eV below the conduction band. The 0.14, 0.41 and 0.83 eV traps are associated with a photochemical reaction. In particular it was suggested that the 0.83 eV level might in fact be the activation energy required to

destroy a trap complex. The 0.63 eV level has a high cross section for electron capture (i.e. high probability of capturing an electron) and has been separately identified as the compensating level which produces high resistivity, pure cadmium sulphide. (5). The possible origins of the various levels are as follows (i) 0.05 eV is a double negatively charged sulphur vacancy (ii) 0.14 eV is also associated with sulphur vacancies (iii) 0.25 eV is a singly charged sulphur vacancy (iv) 0.41 eV is an unidentified neutral level (v) 0.63 eV is a singly positive charged cadmium vacancy (vi) 0.83 eV is an activation energy for the destruction of a trap complex. These are merely tentative suggestions. Only certain levels are observed in a particular crystal under given conditions.

4.8. Contact to Cadmium Sulphide

The problem of making ohmic contact to cadmium sulphide has already been covered in some detail (5). Experimentally, it is found that evaporated indium on a surface of cadmium sulphide, which has previously been cleaned by electron or hydrogen ion bombardment, makes a satisfactory ohmic or injecting contact. Conversely, this type of contact is hole blocking. Silver, copper and graphite make good hole injecting contacts, and can be applied either by evaporation or in an air-drying suspension.

CHAPTER   V

Optical Properties of Cadmium Sulphide

5.1. Absorption in Cadmium Sulphide

The absorption spectrum of cadmium sulphide has been measured by Balkanski and Waldron (47), at the fundamental absorption edge, for light polarized perpendicular and parallel to the c-axis of the crystal. The absorption is shifted by 0.016 eV as expected due to the splitting of the upper valence band. Dutton (48) has observed two peaks in the reflectivity spectrum at the absorption edge and confirms this value. Bube (49) has observed two maxima in the photoconductivity excitation spectra. The splitting of the maxima is 0.018 eV. Kelly and Fredericks (68), from similar measurements, find a difference of 0.019 eV in the maxima for light polarized perpendicular and parallel to the c-axis. These photoconductivity measurements correspond to the same band structure.

Detailed information about the band structure has been obtained by Thomas and Hopfield (34,35,50,51). They have studied the exciton absorption close to the absorption edge by investigating the associated reflection spectra of polarized light. Thomas and Hopfield found three exciton series corresponding to the three valence bands.(34).

Further work (50) has led to the identification of numerous absorption lines due to impurities and the interaction of these impurities with excitons.

Exciton emission spectra have been studied in the ultra-violet stimulated fluorescence spectra of cadmium sulphide by Beil and Broser (52). They obtained estimates of the hole mobility, μ_h of 25 cm^2/volt.sec., and a hole lifetime $\tau_h < 10^{-6}$ secs. These values were deduced from measurements of the decay of the emission with time. Beil and Broser's values of μ_h and τ_h agree with Mort and Spear's estimates discussed in section 4.6.

Collins (53) has measured the reflection (Restrahlen) of unpolarized radiation from cadmium sulphide in the far infra-red. The reflection has a maximum near 38 microns due to the interaction of the incident radiation with the transverse optical modes of the lattice. Collins fitted the reflection data to the classical dispersion relations and Fresnel equations. (6). From this work, the wave number of the transverse optical mode frequency, νt, is 241 cm^{-1}. νt is related to the longitudinal optical frequency by the equation $\nu_L = \nu t (\frac{\varepsilon}{\varepsilon_o})^{1/2}$, (54), and gives a value of 305 cm^{-1} for the wave number of longitudinal vibrations.

Balkanski and Besson (69) have studied the absorption and reflection spectra of thin platelets of cadmium sulphide

in the wavelength range 15 to 30 microns. Seven

absorption maxima were observed which Balkanski and Besson

interpreted as combinations of four basic phonon frequencies

of 295 cm^{-1}, 276 cm^{-1}, 260 cm^{-1} and 199 cm^{-1}. Marshall

and Mitra (55) have extended this work by measuring the

transmission up to 40 microns. They observed thirty

absorption peaks which could be attributed to multiphonon

processes. Marshall and Mitra assign the maxima to com-

binations of basic frequencies viz (i) longitudinal optical

ν_{LO} = 295 cm^{-1} (ii) transverse optical ν_{TO_1} = 261 cm^{-1}

(iii) transverse optical ν_{TO_2} = 238 cm^{-1} (iv) longitudinal

acoustical ν_{LA} = 149 cm^{-1} (v) transverse acoustical ν_{TA_1} =

79 cm^{-1} (vi) transverse acoustical ν_{TA_2} = 70 cm^{-1}. Marshall

and Mitra also review earlier work in reference 55.

The refractive index of cadmium sulphide is 2.6

at 5000 Å (56) and the static dielectric constant 11.6 (36).

Dexter (57) and Sawamato (39) have measured cyclotron

resonance, and Piper and Marple have studied the infra-red

free carrier absorption, as mentioned earlier. Piper

and Marple measured the transmission and reflectance spectra

of gallium doped cadmium sulphide in the spectral range 1 to

35 microns. The effective mass, m^*, was calculated from

the free electron contribution to the refractive index to

be 0.22 m_e. The carrier concentration was determined from

a Hall effect measurement.

5.2. Photoconductivity

Cadmium sulphide is an extremely sensitive photo-conductor. The current flowing through a crystal can be increased, by a factor of about 10^6 under illumination with light of 1 ft. candle intensity. The high photoconductive gain is generally ascribed to the trapping of free holes in recombination centres with a small electron capture cross-section which leads to a long electron lifetime (58,59). Such recombination levels, which are called sensitisation centres, have a small probability of capturing an electron once a hole has been captured. Thus, this type of centre increases the free electron lifetime and hence the sensitivity (section 2.8.). Infra-red radiation can release these trapped holes which then recombine with electrons through fast recombination levels. This reduces the gain and results in the effect known as infra-red quenching. A summary of this effect, and a comprehensive list of references has been given by Lambe and Klick. (60). The correlation of the properties of the centres with levels in the forbidden gap with the response time and sensitivity of a photoconductor was discussed in section 2.8.

The variation in sensitivity of cadmium sulphide with increasing excitation intensity can be less than or greater than unity depending on the intensity of illumination and the temperature (18. p.335 ff.). The departures from

linearity arise from the opposing effects of temperature
and excitation level on the crystal. An increase in
temperature reduces the effect of the sensitising centres,
since holes, thermally freed from these levels, can then
recombine through fast recombination channels. This is
the mechanism of temperature quenching of photoconductivity.
An increase in the intensity of illumination leads to
a decrease in the free electron lifetime as trapping levels
become filled and begin to act as recombination centres.
Both these effects lead to a relationship $I \propto L^n$ between
the photocurrent, I, and the intensity of excitation L
where $\frac{1}{2} < n < 1$. In contrast with this type of behaviour,
super-linearity may occur, i.e. $n > 1$. On increasing the
intensity of illumination the distribution of trapped holes
between the two types of recombination centre can change.
This leads to a photosensitivity dependent upon a power
of the excitation of the order of 1.7, when the majority
of the holes remain in the sensitising centres. This
behaviour provides a further illustration of the importance
of levels within the forbidden gap in determining the
photoconductive properties.

5.3. Edge Emission

An important property of cadmium sulphide is associated

with the light emitted when a crystal is cooled to $77^O K$
or below and excited with radiation in the fundamental
absorption band. An example of the spectral emission
distribution of a pure single crystal is illustrated in
Fig. 5.3. It is called edge emission since it occurs
close to the optical absorption edge. The more recent
explanations of edge emission associate it with electron-
hole recombination via either a sulphur vacancy or a
sulphur interstitial (53. 61-63.70). It is not yet clear
whether the emission is due to the recombination of a
free electron with a trapped hole or a trapped electron
with a free hole. Hopfield (70) has shown that the heights
of the different peaks, I_n, follow a Poisson distribution

$$I_n = I_o \frac{N^n}{n!} \qquad\qquad 5.3.$$

The first emission line Io is attributed to electron-
hole recombination without the emission of a phonon. The
n th line is recombination with the emission of n phonons.
The mean number of emitted photons, N, is 0.87 to fit the
experimental data. The Poisson distribution indicates that
the multi-phonon interactions are a random process.

An emission at shorter wavelengths with a similar
structure is attributed to recombination via surface states.
(61). A third region of emission occurs at still shorter
wavelengths and is ascribed to exciton transitions (34,35,52).
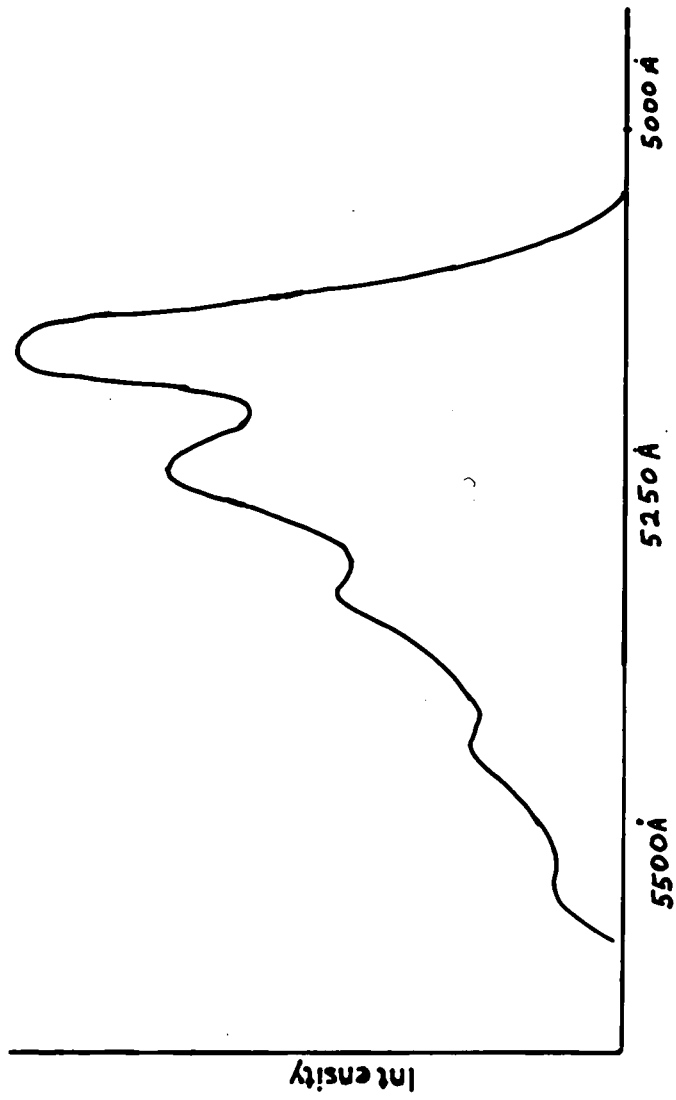
EDGE EMISSION AT 77°K (KLICK)

FIG 5.3

The main edge emission i.e. that at the longest wavelengths, exhibits fine structure which is attributed to the coupling of the emission with the longitudinal optical phonons of the lattice. Thus the spacing between adjacent maxima corresponds in wave number to the longitudinal optical phonon frequency of approximately 300 cm^{-1}, which agrees with Collins (53) estimation of ν_L of 305 cm^{-1}. The emission is polarized in accordance with the selection rules appropriate to the splitting of the upper valence band into two levels.(62). The emitted light is polarized perpendicular and parallel to the c-axis of the crystal in the intensity ratio of approximately ten to one at $77^O K$. From the temperature variation of this intensity ratio, Collins and Hopfield (62) deduced the separation of the two valence bands to be 0.014 eV. The experimental arrangement was insufficiently sensitive to determine this separation from the shift in the position of the peaks.

The surface emission shows multi-phonon structure in the same way as the edge emission. The exciton structure arises from electron-hole interaction and the accompanying series of hydrogen-like levels close to the conduction band. These levels have been studied in emission spectra by Beil and Broser (52) and Collins (53). The former excited the crystals with ultra-violet radiation, whereas

Collins used 1 MeV electrons. The study of these levels in reflection experiments has already been discussed in section 5.1. A study of the edge emission of a variety of differently doped cadmium sulphide crystals forms the subject matter of chapter eight of this thesis.

5.4. Injection Luminescence

Electro-luminescence at low fields has been observed in single crystals of cadmium sulphide (5.64). Smith investigated this emission at room temperature using crystals with indium contacts. In order to obtain a visible light emission the anode had to be formed electrically. Similar emission can be obtained without contact forming by using suitable anode materials. (65). The spectral distribution reported by Smith shows a maximum coincident with the optically stimulated edge emission of cadmium sulphide, together with a second maximum at shorter wavelengths. Further measurements of injection electro-luminescence are presented later in this thesis.

5.5. Photoconductive Spectral Response

The spectral sensitivity of highly photoconductive cadmium sulphide is illustrated in Fig. 5.5. The response is a maximum at the absorption edge. Bube (18) has inter-preted the shape of the curve in terms of a transition from
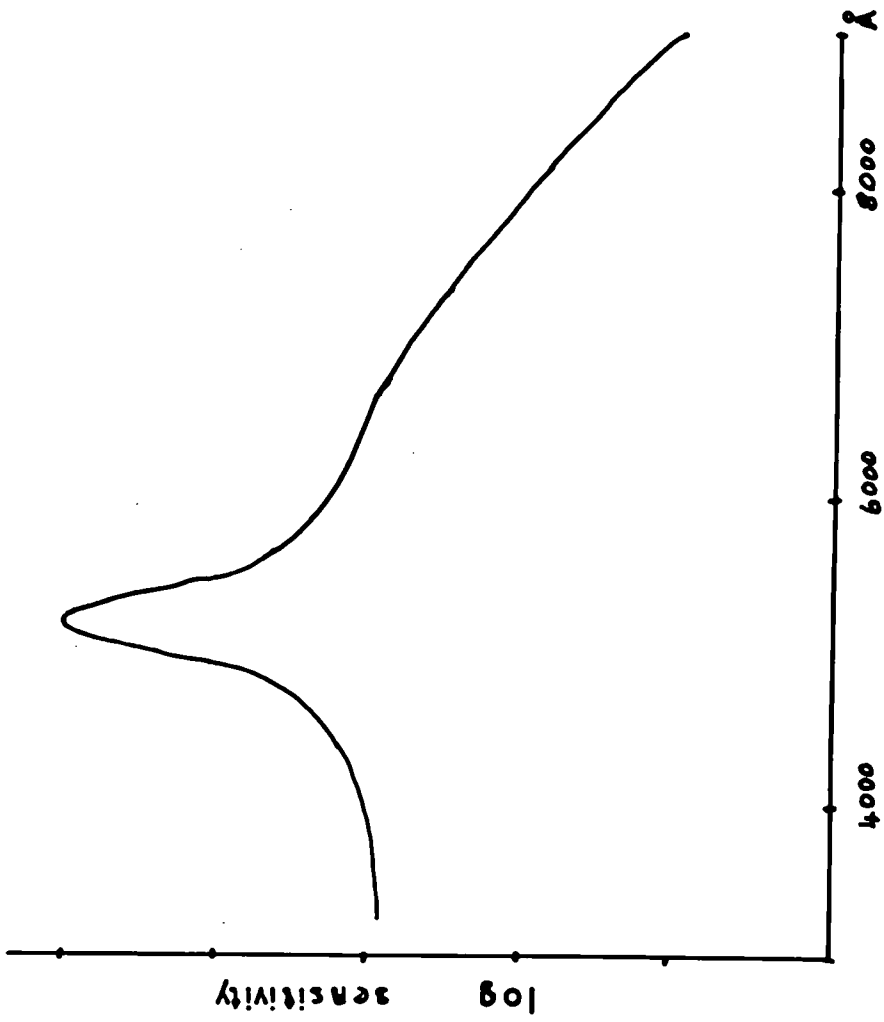
SPECTRAL SENSITIVITY OF CdS (BUBE)

FIG 5.5

volume to surface sensitivity as the wavelength decreases
beyond the absorption edge. At wavelengths shorter than
the absorption edge the incident radiation is absorbed at
the surface, and the rapid surface recombination limits the
sensitivity. At the absorption edge the radiation is
absorbed by the bulk of the crystal and the carriers
generated have a longer lifetime. At wavelengths longer
than the absorption edge, the photosensitivity decreases
due to the inability of the incident light to create
electron-hole pairs. This interpretation is supported by
the observation that the decay time of the photo-current
is a maximum at the absorption edge, and that it decreases
rapidly at shorter wavelengths becoming constant some 300 $\overset{o}{A}$
on the high energy side. Several workers have studied this
effect (66). The photoconductive response to light polarized
parallel and perpendicular to the c-axis has been mentioned
in section 5.1. Cadmium sulphide is more sensitive to
light polarised parallel to the c-axis (49). The photo-
conductive response can also be used to study exciton absorption
(67).

CHAPTER VI

Crystal Growth

6.1. Growth of Pure Crystals

The experimental arrangement used in this laboratory to grow single crystals of cadmium sulphide has previously been described in some detail. (5). Pure plate-like crystals were required for the electrical measurements described in the following chapter. Cadmium sulphide powder, supplied by Light and Company, was de-gassed for 3 to 5 hours at $500^{o}C$ under a high vacuum ($< 10^{-5}$ mms. Hg). The de-gassed powder was then sublimed at a temperature of $1175^{o}C$ in a silica tube placed in a tubular furnace. The sublimation was assisted by a flow of high purity argon (99.995% w/v) which passed over copper heated to $400^{o}C$ to remove traces of oxygen, and through a drying tower containing aluminium calcium silicate to remove water. Single crystals of cadmium sulphide were formed on the walls of the silica tube at temperatures in the range 850 to $950^{o}C$. This temperature region was displaced approximately 10 cms from the charge of powder which was situated in the hottest zone of the furnace. The argon flow rate was approximately 200 mL/min. Growth was maintained for 70 minutes. The temperature was controlled by an Ether Transitrol Type 991 controller to $\pm 6^{o}C$. All

the electrical measurements described in this work refer to crystals grown by this technique with no deliberately added impurity. Typical crystals are shown during initial growth in Fig. 6.1.1. and the experimental arrangement in Fig. 6.1.2.

6.2. Purity of Crystals.

The purity of the starting material and the effectiveness of the usual outgassing procedure were not known. The method of growth led to the removal of many impurities by differential sublimation. The technique of using previously grown crystals as a starting charge, which was often done, helped to provide crystals of higher purity. Powder x-ray photographs of crystals showed no impurity lines, but this method of analysis is relatively insensitive. Powder photographs of the residue near the cooler portion of the growth zone did show elemental cadmium. This suggests that dissociation of the charge was occurring, so that the crystals were probably deficient in sulphur. Sulphur was deposited further down the silica tube in the cooler regions. In some trials the starting powder was de-gassed at 950°C for two hours under high vacuum. This led to considerable dissocation and the appearance of green spots in the mass of yellow cadmium sulphide. No impurities were detected in this green powder by x-ray photographs. The green cadmium sulphide did not show edge emission at liquid nitrogen temperatures,
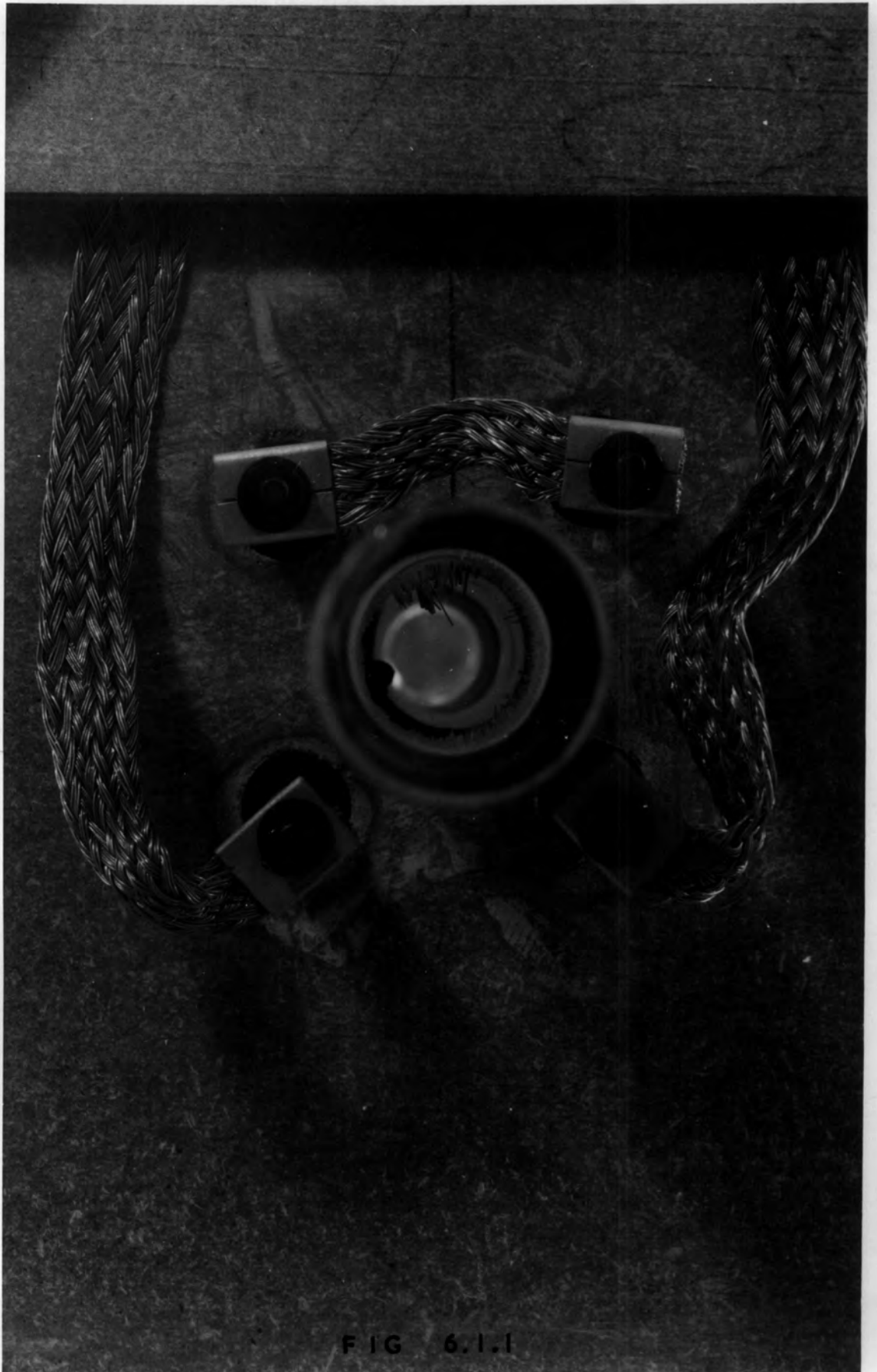
FIG 6.1.1

FIG 6.1.2

whereas the remainder of the de-gassed charge did. The
possibility exists that the appearance of a green spot
might have been due to an excess of cadmium at that particular
point. The mechanism of crystal growth was entirely different
when cadmium sulphide, which had been de-gassed at $950^{o}C$
instead of $500^{o}C$, was used as the starting charge. It was
found to be very difficult to grow good plate-like crystals,
presumably as a result of the excess preliminary dissociation
to cadmium and sulphur.

An attempt was made to correlate edge emission with
stoichiometry by observing the edge emission of crystals as
grown in the silica tube. The silica tube, when cooled to
room temperature after a growth run, was placed in a liquid
nitrogen bath. The tube was then irradiated with a high
pressure mercury vapour lamp which emitted preponderently at
3650 Å. The green edge emission was most intense in the
growth region. However, in the midst of the green emitting
region some red and orange emitting crystals were observed.
This suggested that edge emission, if it is due to non-
stoichiometry or impurities in the crystals, depends very
strongly upon the local growth conditions within the tube.

6.3. Impure Crystals

Seven types of impure crystal were grown principally

for optical measurement purposes. The crystals were pre-
pared with the following impurities (i) oxygen (ii) hydrogen
(iii) water (iv) iodine (v) chlorine (vi) silver and (vii)
indium.

Crystals (i) were grown by removing the heated copper
and mixing small quantities of oxygen with the argon flow.
To produce yellow plate-like crystals it was necessary
for the oxygen flow rate to be less than 10 mL/min.
If the flow rate was higher the resulting crystals became
brown in colour and the crystallinity deteriorated, moreover
the crystals were non-luminescent. A large brown crystal
of cadmium sulphide was grown by sublimation in air, using
a silica tube open to the atmosphere at both ends, without
the assistance of a carrier gas. This crystal did not
show edge emission. Cadmium oxide was also formed in the
cooler portions of the tube in the form of small irregular
crystals. The majority of crystals grown in oxygen contained
a strong red component in their luminescence. The presence
of oxygen could conceivably lead to crystals with an excess
of cadmium, since the sulphur can be oxidised to sulphur
dioxide. The presence of small quantities of oxygen led to
enhanced growth rates. (5). Care had to be taken to preserve
the luminescence, which was destroyed if the oxygen flow
was too great.

(ii) Crystals were also grown in hydrogen using a

similar gas mixing technique. With a hydrogen flow rate of 50 mL/min. good plates were obtained. A flow of 100 mL/min however led to the production of irregularly shaped brown crystals. This was similar to the residue produced when the high oxygen flow was used. The hydrogen may also preferentially remove sulphur in the form of hydrogen sulphide.

(iii) The argon was bubbled through de-ionised water to grow crystals in the presence of water vapour. The edge emission appeared to be intensified in these crystals compared with pure crystals.

(iv) Crystals doped with iodine were grown using the iodine transport method (5). These crystals were grown in a closed, evacuated, silica tube. A small quantity of iodine transported the cadmium sulphide down a temperature gradient maintained along the tube. Transport occurred in the form of cadmium iodide and sulphur. After the cadmium sulphide had been deposited, at the cooler end of the tube, the iodine diffused back to the charge and the cycle was repeated. Crystals grown in this way were hexagonal rods with coloration ranging from orange to deep red.

(v) Chlorine was incorporated by bubbling the argon through dilute hydrochloric acid. The crystals are also orange in colour.

(vi), (vii) Crystals with silver and indium were provided by J. Woods of this department. These were grown

at G.E.C. Ltd., by similar techniques. The impurities
were incorporated by passing the argon carrier gas over
molten silver and indium respectively.

6.4. Conclusions

High resistivity plate-like crystals can be conveniently
prepared by a sublimation technique. The stoichiometry and
impurity content of these crystals, however, is difficult
to determine and control. No sensitive analytical techniques
were available to determine the impurity content. Recent
work by L. Clark of this laboratory suggests that zinc is
present in similar highly de-gassed powder. This was
indicated by x-ray fluorescent spectra. The amount is of
the order of 10's of parts per million. Analysis of crystals
grown from this powder, by sublimation in an atmosphere of
sulphur, shows that the final zinc content is very much lower.
Crystals grown from a starting charge of known impurity
content would be more satisfactory, and an accurate analysis
of grown crystals is highly desirable. The possibility of
contamination of the crystals by the silica growth tube
must also be borne in mind.

The type of crystal on which the electrical measure-
ments were made is shown in Fig. 6.4.1. The dimensions
of the plates were of the order of 5 x 4 x 0.02 mms. The
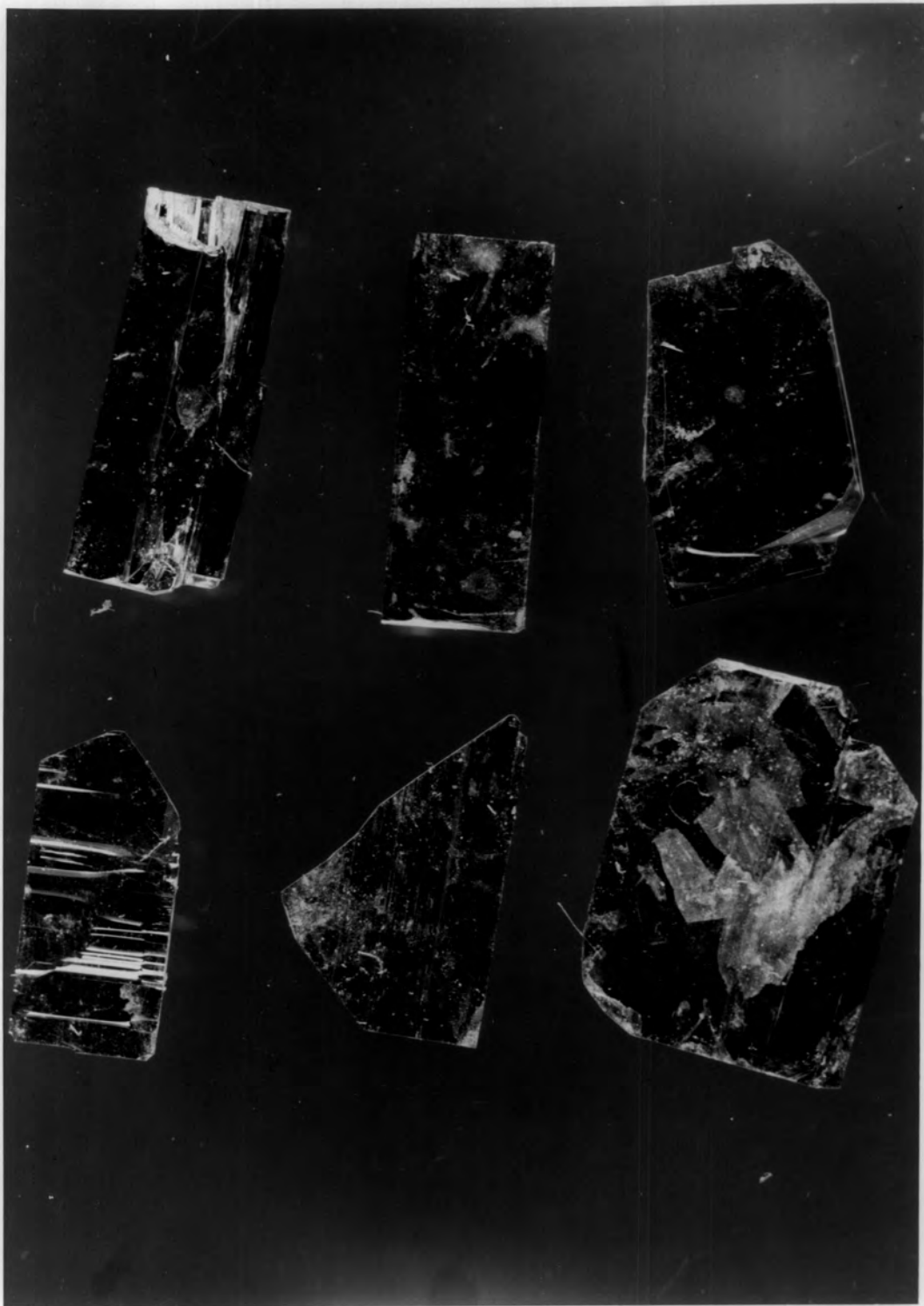
FIG   6.4.1

samples used were free from surface striations which are often apparent in many crystals.

Optical measurements were made on both plates and rods. Typical rods are shown in Fig. 6.4.2. For these measurements crystal dimensions are not critical and crystals were selected for maximum intensity of edge emission

The effect of various impurities and the stoichiometry of the crystals is discussed in the section concerned with the optical properties of the crystals.
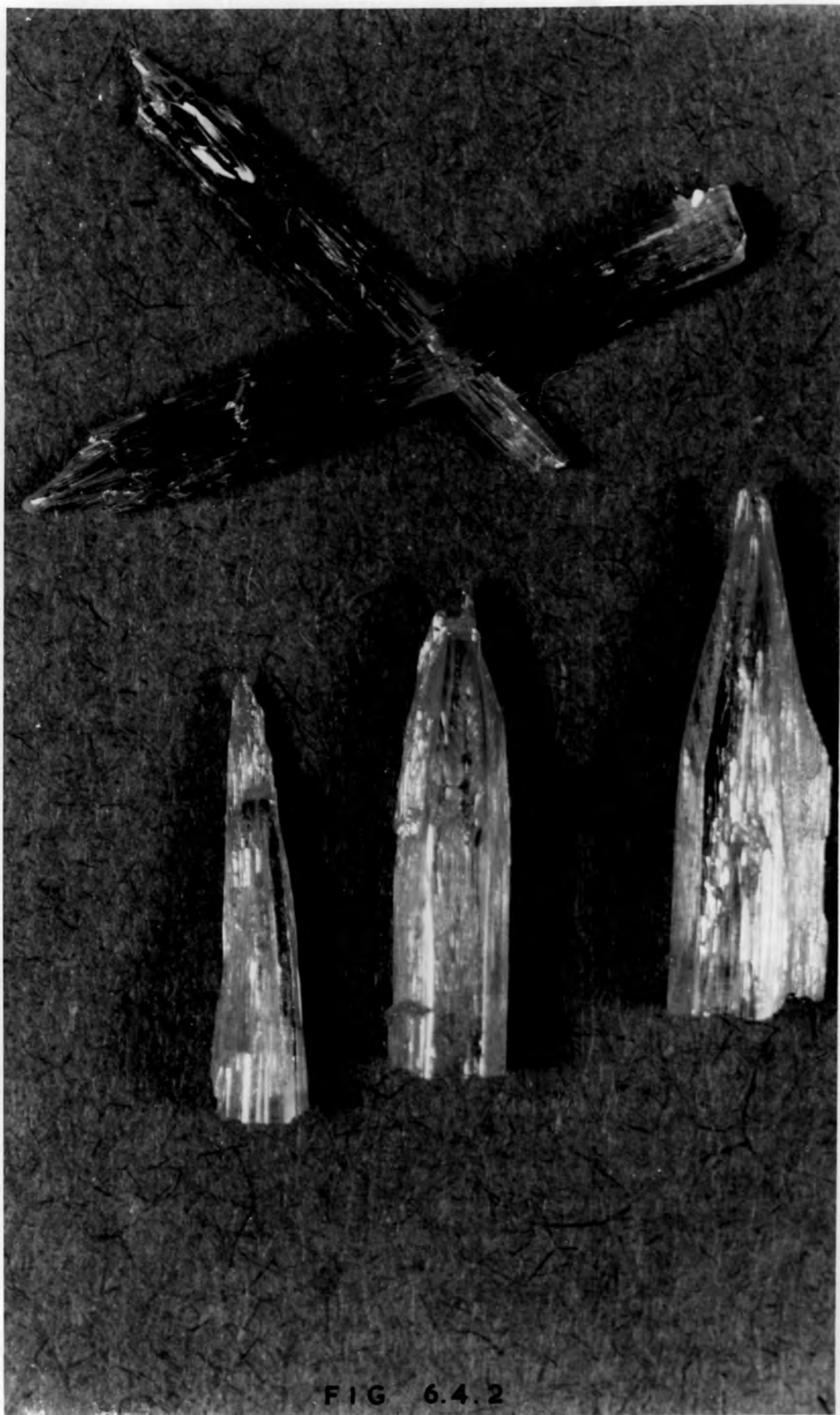
FIG 6.4.2

CHAPTER VII

Electrical Measurements

7.1. Introduction

The experiments described in this chapter are concerned entirely with single carrier ohmic and space charge limited currents. (Section 3.2.). The measurements were carried out in an attempt to extend the ideas and resolve some of the problems described in the earlier work (5). The apparatus used was essentially the same. The main aspects of the earlier work on single carrier space charge limited currents can be found in reference 65. A reprint of this paper is appended at the end of this thesis. Minor modifications were made to the apparatus. These are described below. The scope of the work was extended to include thermally stimulated current measurements (Section 4.7.), to obtain some direct information of the role of trapping processes. The electron traps were filled in two ways, either optically or electrically. In the latter case, traps were filled by the injection of carriers from the negative contact. Some measurements of the response of cadmium sulphide to visible, infra-red and gamma radiation are also presented.

7.2. Apparatus

Thin plate-like crystals only were used. They were

mounted in the copper cryostat which is shown in Fig. 7.2.1.
The crystals were soldered with indium on to a glass or silica
cover slip with dimensions of 22 x 22 x 0.18 mms. The cover
slip was held against the central copper block. The mounting
of the crystals is described in the next section. The outer
nickel-silver, vertical tube and the body of the cryostat
acted as a vacuum jacket. The inner nickel-silver, vertical
tube supported the central copper block, which was hollowed out
internally. The space between the two tubes was evacuated.
Nickel-silver was used for the vertical tubes to insulate the
crystal thermally from its surroundings. Two, four way
metal-glass seals, soldered into the bottom corners of the
cryostat, provided electrical access for current and thermo-
couple leads. These seals were not light tight, so that it
was necessary to shroud the whole of the cryostat in thick
black cloth. The side of the cryostat was covered by a
copper plate sealed to the body by an O-ring. The face of
the cryostat opposite the crystal had a similar O-ring seal.
This could be blanked off or used, with a suitable window,
to allow light to fall on to the crystal. The two current
leads entering the cryostat were terminated at two 6.B.A. bolts
supported near the central block by two copper strips. The
bolts were insulated electrically by P.T.F.E. washers. Two
phosphor bronze spring contacts, later tinned with indium,
led from these bolts to the cover slip. Freezing mixtures,
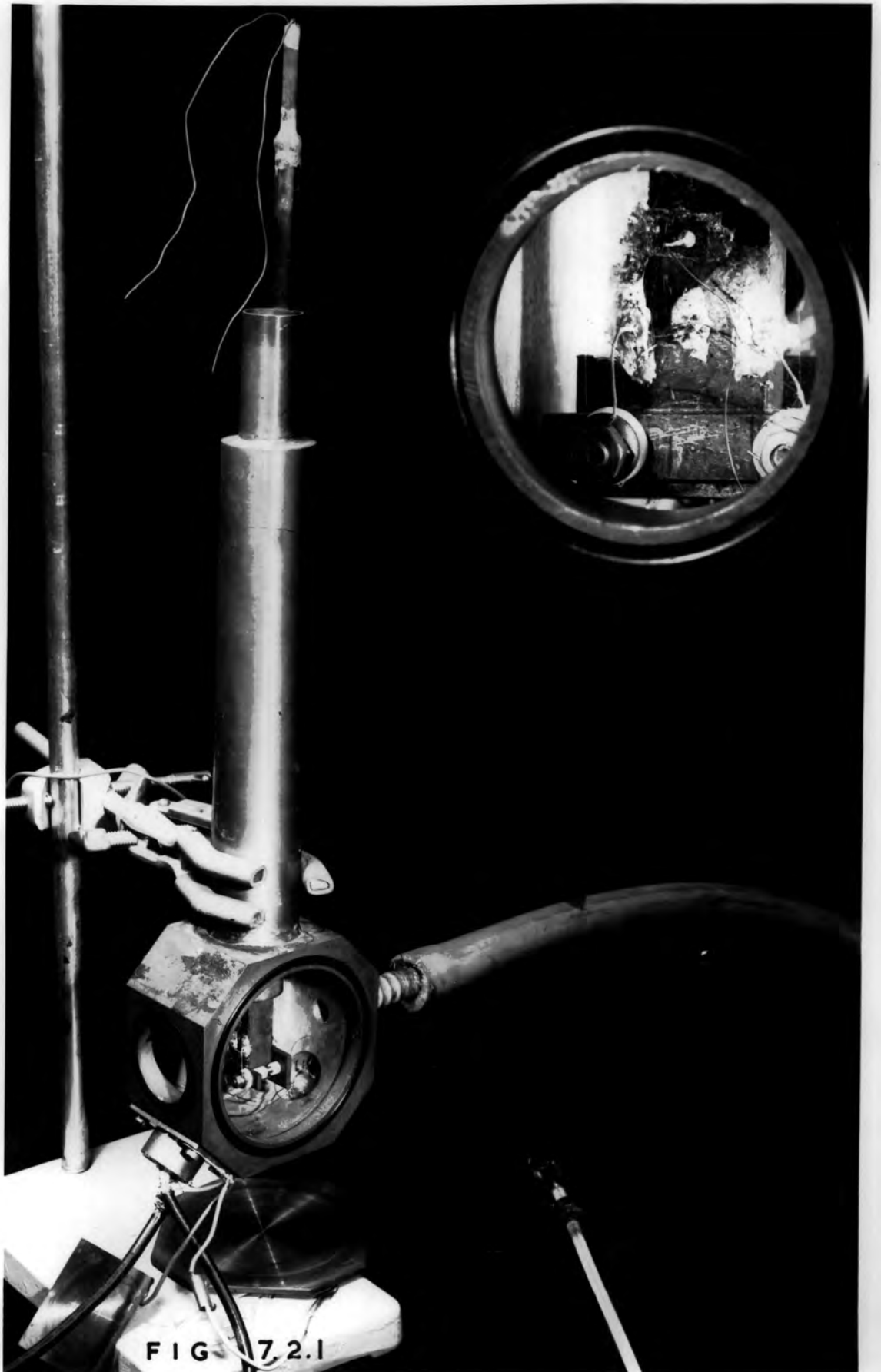
FIG 7.2.1

and a platinum heater, encased in a silica jacket, were
inserted into the copper block directly behind the crystal.
With liquid nitrogen and the heater, the temperature of the
crystal could be varied from 80°K to 453°K. The high
temperature limit was imposed by the possibility of melting
the soft solder holding the central copper block to the
inner nickel-silver tube.

Voltages up to 2 volts, with an accuracy of $\pm$ 0.05%
were derived from a Pye portable potentiometer. This is in
contrast to the earlier work where a high tension battery,
with a suitable potential divider circuit and voltmeter,
were used. The accuracy then was of the order $\pm$ 5%. Voltages
from 2 to 200 volts were obtained using the high tension
battery. The current through the crystals was measured with
a vibrating reed electrometer, Electronic Instruments Ltd.,
model 33B and current measuring unit model A33B. The current
was measured by determining the voltage developed across a
suitable resistance in series with the crystal. Values of
10^6, 10^8, 10^{10} ohms were available in the current measuring
unit. Resistors of from 10 to 10^5 ohms, in steps of x 10
were substituted to measure the higher currents. The input
impedance of the electrometer was 10^{13} ohms. The full scale
deflection could be changed by adjusting the gain, from 10
millivolts to 1 volt, in steps of x 3. The overall accuracy

of the system was of the order of $\pm$ 5%. The output of the

electrometer was fed to a pen recorder. The speed of this

recorder could be varied between 12 inches per minute and

2 inches per hour with interchangeable gears and drive. The

e.m.f. of the copper-constantan thermocouple in the cryostat

was measured with reference to a second junction in an oil

bath at room temperature. A second Pye portable potentiometer,

with a Scalamp galvanometer, were used to determine the

thermocouple e.m.f.'s.

7.3. Contacts and Mounting of Crystals

Throughout this work, the technique of mounting the

crystal has been improved. In the initial stages, the crystal

was supported on a glass cover slip. One phosphor bronze

wire made direct contact to the top of the crystal, whilst

the second wire made contact via indium melted on to the

cover slip. This arrangement was used in all the earlier work.

(5). Spurious voltages, discussed later in this chapter,

were observed which might have been due to any one of the

following effects. (i) Strain which could be introduced in

the crystal when the cover slip was inserted into the cryostat.

(ii) Strain introduced in the glass at different temperatures

by differential thermal expansion and contraction. (iii)

Strain caused by the pressure of the phosphor bronze contact

on top of the crystal (cadmium sulphide is piezoelectric).
(iv) The different metal junctions in the cryostat could
introduce thermal e.m.f.'s (v) Thomson e.m.f.'s could be
present in the leads from the glass-metal seal.

The mounting procedure which was finally evolved
was designed to reduce effects (i) - (v) to a minimum.
However, no significant reduction of the spurious voltages
was effected by these improvements. This negative result
indicates that the effects described later in this chapter
are genuine properties of cadmium sulphide.

The procedure adopted was as follows. A suitable,
clear, plate-like crystal was selected. The mean thickness
was measured on the vernier scale of a metallurgical micro-
scope. The microscope was focussed on to the bottom and
top surfaces of the crystal in several regions over the
crystal. A correction was applied to obtain real from
apparent depths using a value of refractive index of 2.6.(56).
This method of estimating the thickness agreed to within 5
microns with measurements made with a vernier travelling
microscope while viewing the edge of the crystal. Typical
thicknesses were of the order of 50 microns.

Indium contacts were evaporated on to both faces of the
cadmium sulphide crystal. The surfaces of the crystal were
cleaned by bombardment with hydrogen ions before evaporation.

This was done in an Edwards Model 6E coating unit equipped
with a 2keV direct current discharge head. Care was taken
during this, and subsequent, operations to ensure that the
crystal was at room temperature before exposure to the
atmosphere. The indium was evaporated through a hole in a
brass mask to provide a circular contact area of about
$2.5.10^{-2}$ sq. cms.

The silica cover slip used to support the sample was
thoroughly cleaned in acetone and de-ionised water. The
use of silica, instead of glass, minimised thermal strain (ii).
Secondary considerations for making the change were associated
with the higher resistivity of silica and the elimination
of possible electrolytic action in the glass. After cleaning
the silica, three strips of indium, isolated from each other,
were soldered to the surface. The crystal was placed on
one of the indium strips and heated to $300^{o}C$ for 3 minutes
in an atmosphere of high purity argon. This was carried out
with a small strip heated placed under a bell jar. The
contact, made in this way, was used as the cathode in the
experiments described later in this chapter. A small ball
of indium was next sweated, under argon, on to the exposed
upper, evaporated layer on the crystal. Care was taken to
ensure that the indium dot did not overlap the evaporated
layer and hence increase the possibility of hole injection

from this anode. A gold wire, tinned with indium, was then soldered into this top contact. The other end of the gold wire was soldered on to one of the two remaining indium strips on the cover slip. These operations were carried out under argon. This technique produced mechanically robust contacts. With this method strain caused by the pressure of a spring contact on the crystal was eliminated (iii). The gold wire was tinned with indium to reduce thermoelectric e.m.f.'s (iv) The strength of the whole construction is illustrated by the fact that attempts to remove the contacts by force led to the fracture of the crystal. At this stage the crystal and cover slip were ready for insertion in the cryostat.

A small quantity of silicon vacuum grease was smeared on to the central copper block of the cryostat. This served to improve the thermal contact between the crystal on its silica support and the copper block. The cover slip was then placed on the copper block and the springs adjusted to make contact with the appropriate indium strips while pressing the silica against the block. The phosphor bronze springs were also tinned with indium to reduce thermoelectric e.m.f.'s (iv) The thermocouple was soldered to the third indium surface on the cover slip, within a few millimetres of the crystal, but isolated electrically from it. Finally the cryostat was evacuated and the crystal and cover slip raised to a temperature of approximately $160^\circ C$, to melt the indium

contacts, and solder the indium-tinned, phosphor bronze contacts to the cover slip. This process also helped to reduce the strain set up within the crystal by the mounting procedure (i) The melting of the indium (155°C) was observed through a window on the side of the cryostat. Thermo-electric e.m.f.'s in the circuit from the glass-metal seal to the spring contacts (iv) (v) were reduced by making both leads identical in length and by ensuring that they were symmetrically placed in the cryostat.

A preliminary experiment indicated that the thermocouple temperature recorded was within 2°C of the crystal temperature over the whole range investigated. A subsidiary experiment was also carried out with no crystal on the cover slip to test for leakage currents. No measurable current was detected with applied voltages of up to 200 volts. The insulation impedance across the face of the cover slip was therefore greater than 2.10^{15} ohms. A final check with a 10^{12} ohm resistor in place of the crystal showed that the leakage impedance across the measuring resistor was greater than 5.10^{11} ohms. A crystal is shown in place on the central copper block in Fig. 7.2.1.

7.4. Temperature Variation of Direct Current-Voltage Characteristic

A typical room temperature, current-voltage character-

istic of a thin platelet of cadmium sulphide is shown in
Fig. 7.4.1. According to Lampert's single carrier space
charge limited (s.c.l.) current theory (section 3.2.) the
characteristic is split into four regions, shown in Fig.
7.4.1. as (a), (b), (c), (d). Region (a) is the result of
true ohmic conduction by carriers thermally present in the
conduction band of the crystal. Region (b) is a s.c.l.
conduction in the presence of traps, equation 3.2.1.
According to Lampert the steep rise in current, (c) is due
to the filling of all the traps as the voltage increases
beyond what he called the traps filled limit. The traps filled
limit occurs at a voltage V_{TFL}, given by equation 3.2.2.
Region (d) is the theoretical square law for an insulator,
equation 3.1. This region will not be observed if the wattage
dissipated leads to thermal breakdown of the crystal.

In the earlier work an estimate was made of the total
trap density from the variation with temperature of the voltage
at which the transition from (a) to (b) occurs. This was
compared with the total trap density deduced by applying equa-
tion 3.2.2. to the measured traps filled limit voltage. The
two estimates did not agree (see paper at end of thesis).
This type of measurement has now been carried out on a number
of other crystals. The results are reported below.

A series of preliminary experiments were conducted to
ensure that excess trapped charge was removed from the
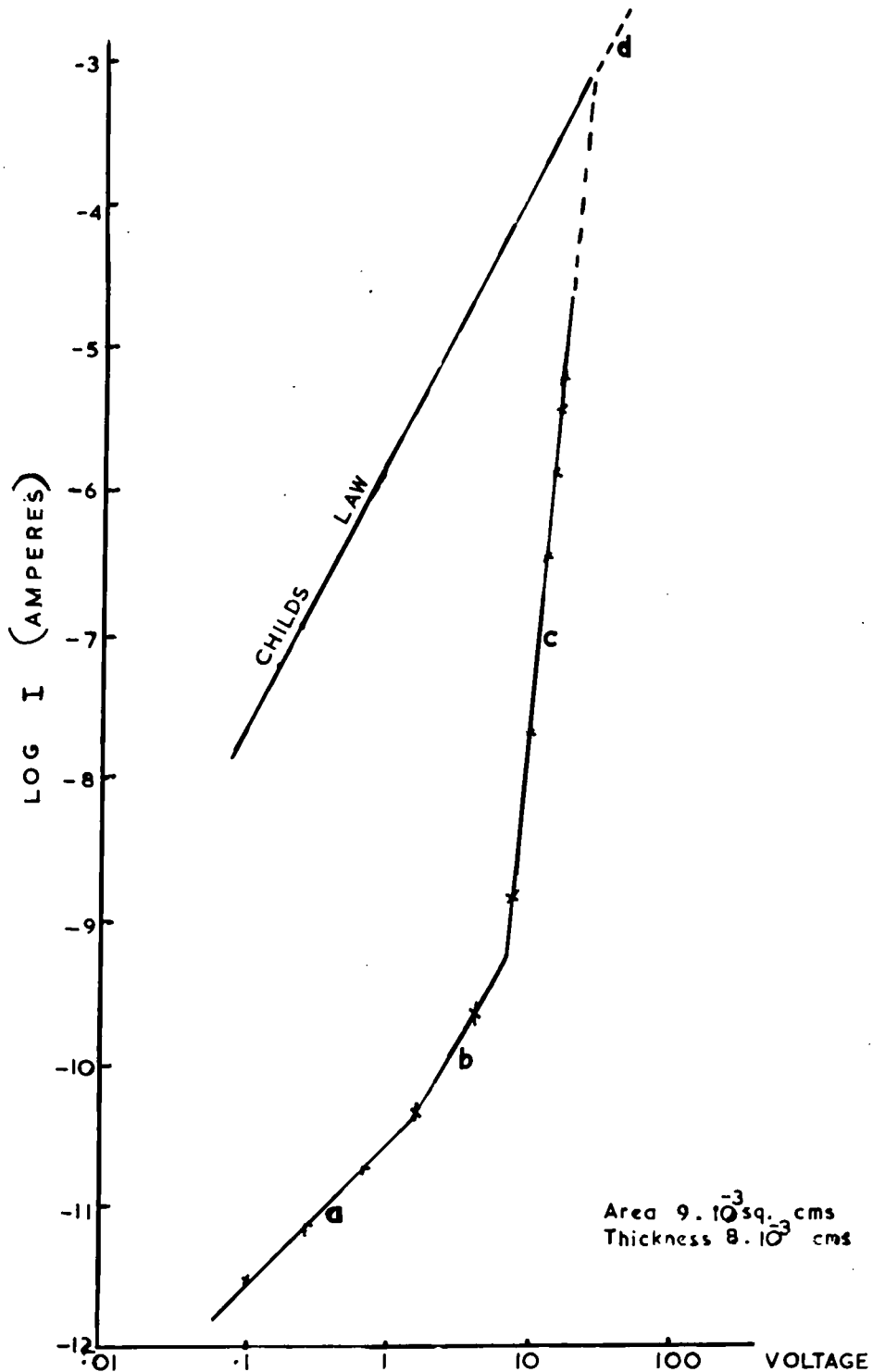
FIG. 7.4.1

CHARACTERISTIC OF A CRYSTAL

WITH TWO INDIUM

CONTACTS

mounted crystal. The crystal was heated to some temperature

T, above room temperature, for a time, t. During this time

the crystal was shorted to earth. The current-voltage

characteristic was measured after cooling to room temperature.

This cycle was then repeated for various combinations of

temperatures T and times t. Typical room temperature

characteristics obtained are shown in Fig. 7.4.2. As the

cycle progressed, the resistance of the crystal decreased

before it finally increased to a stable value. Before

measurements were made over the temperature range 77^OK to

373^OK a procedure to establish a reproducible temperature

characteristic was determined. Even when the room temperature

characteristic was reproducible, small negative e.m.f.'s

($\sim$ 10 mV) were apparent across the crystal in thermal equili-

brium, i.e. the cathode electrode became slightly positive.

These voltages were biased off with a suitable voltage from

t he potentiometer.

Typical current-voltage characteristics, measured over

the range -28^OC to 76^OC, are shown in Fig. 7.4.3. In order

to avoid possible damage to the crystal the characteristic

was not measured beyond the steeply rising portion. After

each measurement the crystal was shorted and heated to 100^OC

for several minutes, to eliminate injected, stored charge.

After these characteristics had been obtained the traps

filled limit voltage was determined at room temperature.

EFFECT OF HEAT TREATMENT ON I/V CURVE

FIG 7.4.2

Curve legend (upper left of graph):

i heating to 100°C for 5 mins
ii "   "   45
iii "   "
iv "   178°C   5
v "   100   19 hrs
vi "   -   10 mins
vii "   -140   2 hrs

Crystal A

TEMP. 22°C

LOG H

LOG V

Crystal A

2·5 sq cms
4·25 cms

TYPICAL I/V CURVES

AT DIFFERENT

TEMPERATURES

FIG 7.4.3.

76°C
51°C
33°C
21°C
-28°C
-43°C

LOG H

LOG V
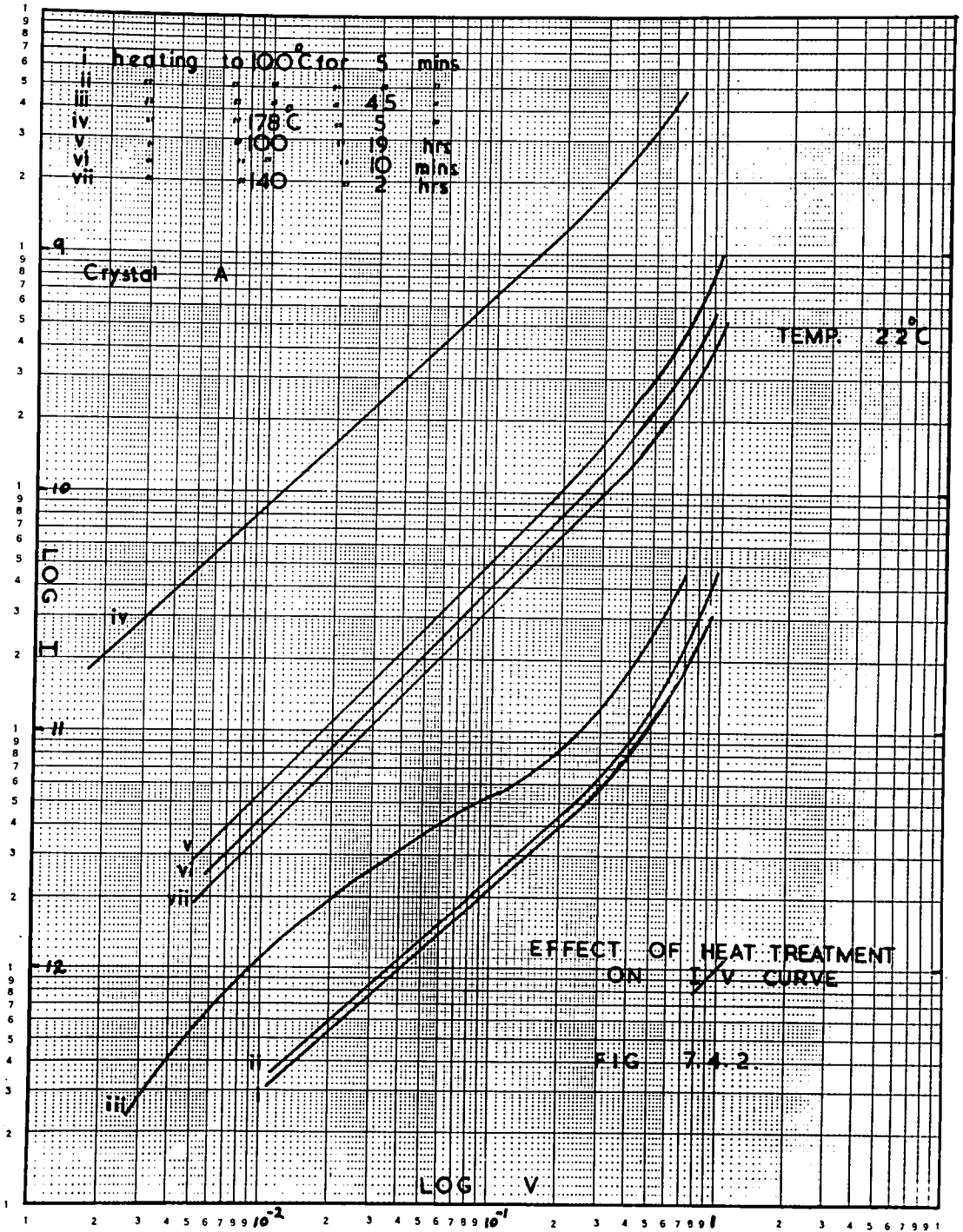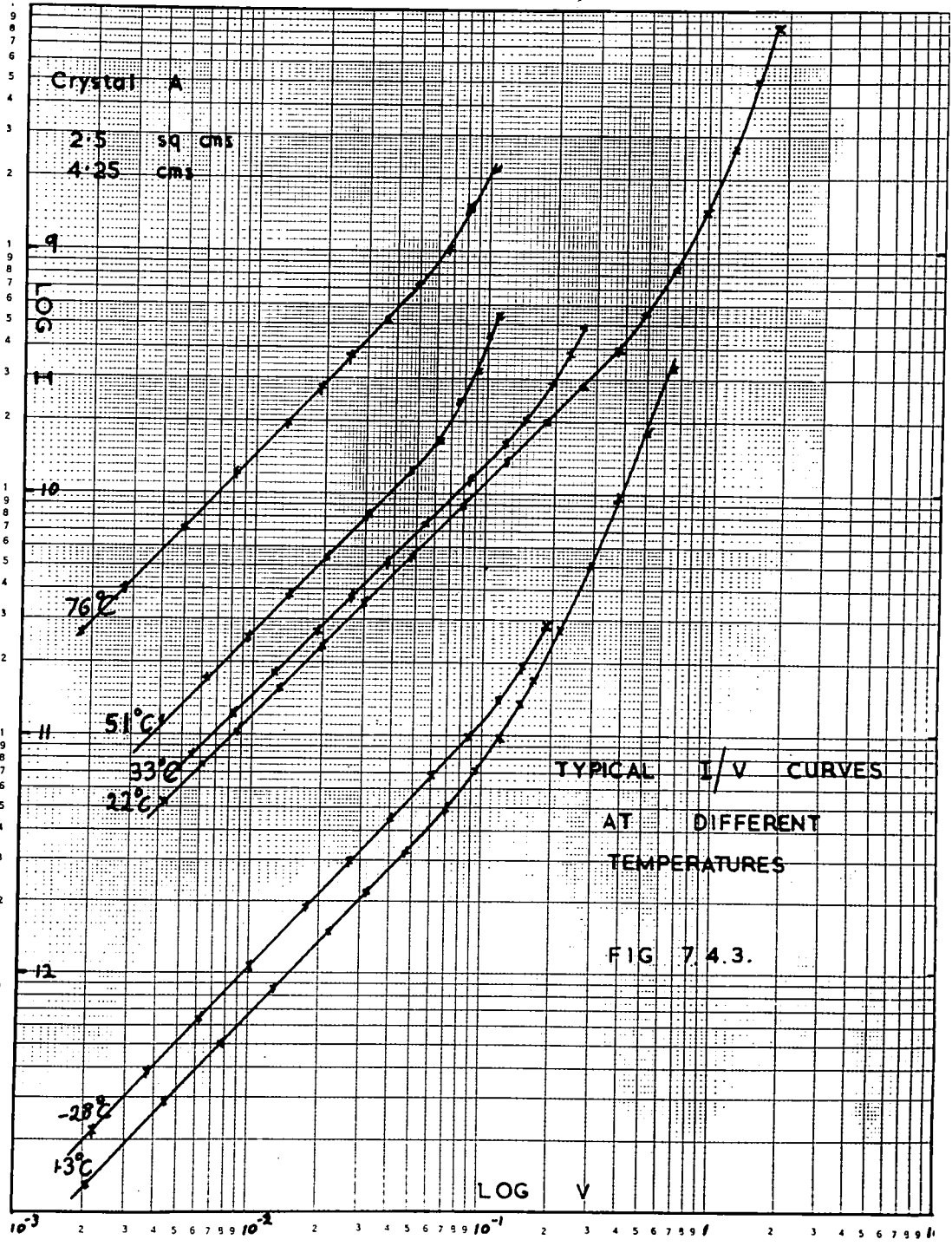
The analysis of the characteristics shown in Fig.
7.4.3., is presented in section 9.1. Results are also given
of similar experiments on two other crystals. The conclusions
are compared with those from earlier work.

7.5. Thermally Stimulated Currents

The object of the experiments described in this section
was to determine whether the steep rise in current, (c)
Fig. 7.4.1. could be associated with trap filling or trap
emptying. If traps were emptying in this region, by field
or collision ionisation, the discrepancy between the two
techniques of determining the trap density, N_t, would be
resolved.

Thermally stimulated currents were measured in cadmium
sulphide platelets after the current-voltage characteristic
had been determined. The same cryostat and current measuring
apparatus were used. Initially the measurements were made
in the temperature range $20^{o}C$ to $140^{o}C$. A stable room
temperature resistivity was first established as described
in the last section. The technique was then as follows.
The conductivity of the crystal was measured while the crystal
was heated at a uniform rate. Typical heating rates were
$10^{o}C$/minute, obtained by dissipating 11 watts in the platinum
heater. This rate was uniform to within $\pm$ 10% over the
temperature range required. The conductivity was measured by

applying a voltage V_1 below that required for injection,
i.e. V_1 lay in region (a) Fig. 7.4.1. The current passed by
the crystal was displayed on the pen recorder as the
temperature increased. The voltage V_1 was less than the
injection voltage over the whole range of measurement. This
procedure established the equilibrium ohmic resistivity
over the range of temperature employed. The crystal was then
shorted and allowed to cool to room temperature. A voltage
V_2 was then applied, which was sufficiently large to allow
the injection of excess carriers to occur. The current passed
by the crystal was above the Ohm's law current for the
neutral crystal, i.e. the current was in region b, Fig. 7.4.1.
The initial current decayed with time for a period of minutes
before it became stable. After the passage of this current
the applied voltage was reduced to V_1 and the conductivity
of the crystal again monitored over the range $20^{\circ}C$ to $140^{\circ}C$.
This cycle was then repeated using higher values of V_2.
Currents were passed which corresponded to regions (b),(c)
of Fig. 7.4.1. Care had to be taken at the high current
end of the characteristic to avoid destroying the crystal
by the heat dissipated. However, it was just possible to
reach the beginning of region (d) Fig. 7.4.1 without affecting
the electrical properties of the crystal, if the high current
was only passed for 1 minute.

Typical experimental results are shown in Fig. 7.5.1.

TYPICAL THERMALLY STIMULATED CURRENTS

Crystal A

FIG 7.5.1.

1. injection with 1·6 10⁻⁹ amps.
2. " " 2·8 10⁻⁶ "
3. " " 1·0 10⁻⁴ "
4. " " 1·0 10⁻² "
5. " " 1·0 10⁻² "

Monitoring voltage 100 mV
Vᵢ fig 7.5.2.

Δ σ × 1·7 10⁻⁸ OHMN⁻¹ CM⁻¹
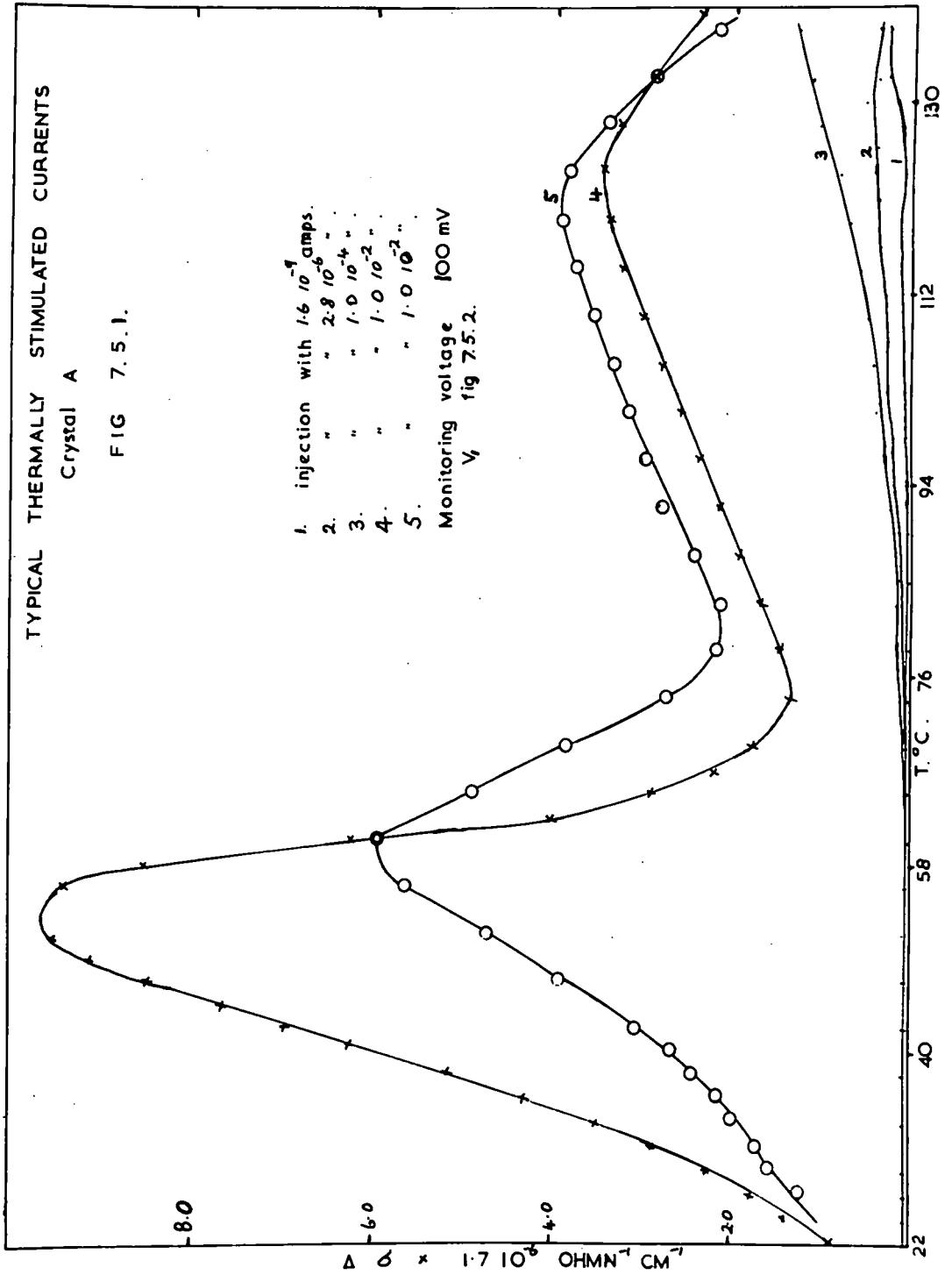
where the change in conductivity $\Delta\sigma$ is plotted against temperature. The full current-voltage curve at room temperature is shown in Fig. 7.5.2. It was necessary to calculate the conductivity at each temperature as the signal voltage was, in general, a significant fraction of the applied voltage. The four regions of the characteristic, (a), (b), (c), (d), discussed in the last section are indicated in Fig. 7.5.2. From Fig. 7.5.1. it may be seen that the change in conductivity due to the release of trapped injected electrons was small unless currents well into region (c) had previously passed through the sample. If a voltage V_2 was used, which was above the traps-filled-limit voltage, i.e. the current was near the top of region (c), the change in conductivity was high. This indicated that traps are being filled as the current rises steeply. It has already been pointed out (5) that for voltages near V_{TFL} the initial current, instead of decreasing with time tends to increase over a period of minutes. This effect was again observed here. At liquid nitrogen temperatures, this particular crystal obeyed the theoretical Child's law at voltages above V_{TFL}.

A similar experiment was performed with the monitoring voltage in region (b), i.e. above the transition from Ohmic conduction. The voltage lay well below V_{TFL}. In this region the equilibrium current is given by the reduced square law,

I/V CHARACTERISTIC OF CRYSTAL A AT 22 °C. FIG. 7.5.2

O MINUS 193 °C

CHILD'S LAW

4+5

5.3

c

←2

b

←1

a

1,2,3,4,5, ARE INJECTION CURRENTS (FIG. 7.5.1)

V₁ V₂ MONITORING VOLTAGES

LOG I

LOG V

V₁ V₂
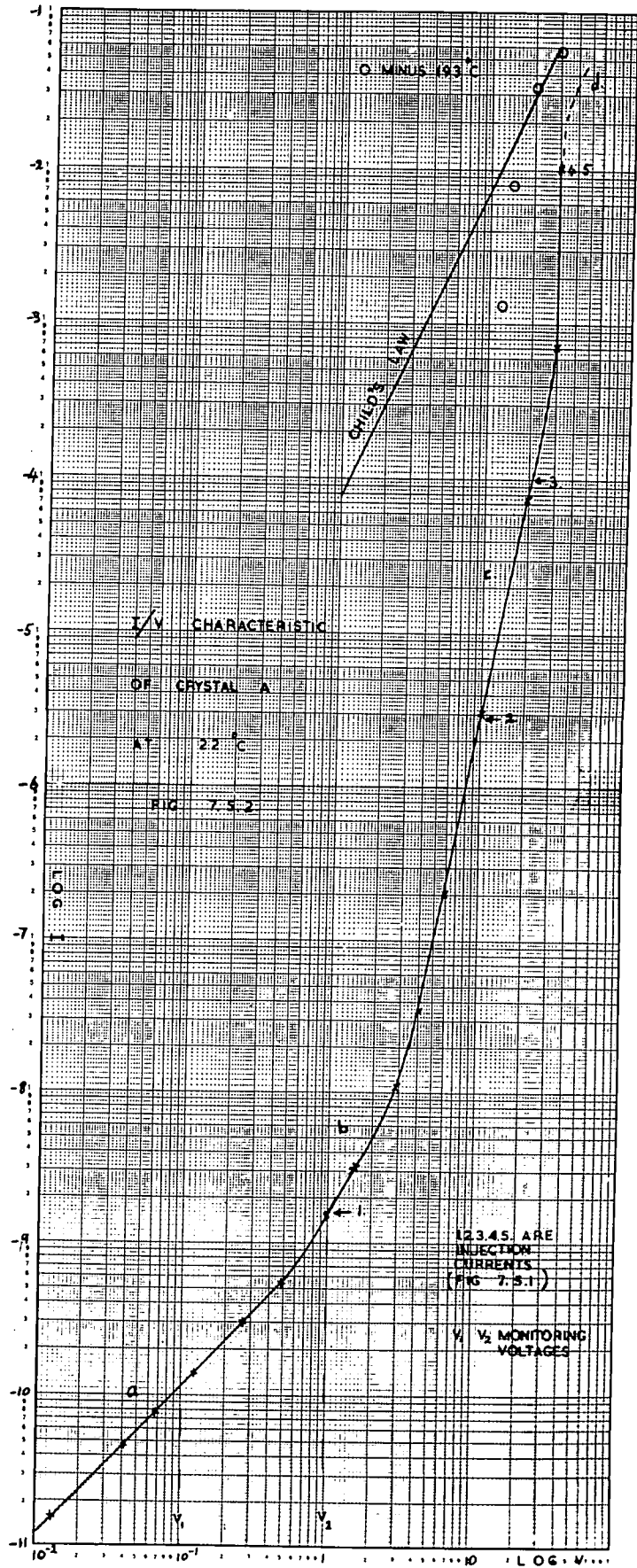
equation 3.2.1. An effective conductivity, K, was therefore defined, such that $I = KV^2$. The results of this experiment are plotted in Fig. 7.5.3. where the variation of K with temperature is shown before and after injection.

The analysis of the curves of Fig. 7.5.1. and 7.5.3., together with an analysis of curves similar to Fig. 7.5.1. obtained on a different crystal, is presented in section 9.2.

7.6. Investigation of Spurious Voltages

The term spurious voltages in this section refers to those voltages which appeared across the measuring resistor when the voltage source was shorted out. After mounting a crystal, spurious negative voltages were observed across the 10^{10} ohm series resistor. These voltages increased with temperature and sometimes became as large as 400 mV at 140°C. The variation of this e.m.f. with temperature, and the effects of the successive heating on the crystal, are shown in Fig. 7.6.1. In the sample illustrated, the negative voltage was initially high, and it was necessary to heat the crystal at 140°C for several hours to reduce the voltage to a few millivolts. The effect of carrier injection on this e.m.f. is shown in Fig. 7.6.2.

With some specimens, the spurious voltage was small immediately after mounting the crystal in the cryostat. The effect of carrier injection in this case is shown in Fig. 7.6.3. When the crystal was irradiated with light with

THERMALLY STIMULATED A.
CURVE. CRYSTAL A.

Monitoring voltage 1 volt
V_2 fig. 7.5.2.

FIG 7.5.3.

T °C

i no injection
ii passing 6·4·10^{-9} amps

$K \cdot 10^{-6}$

1·5

1·0

0·5
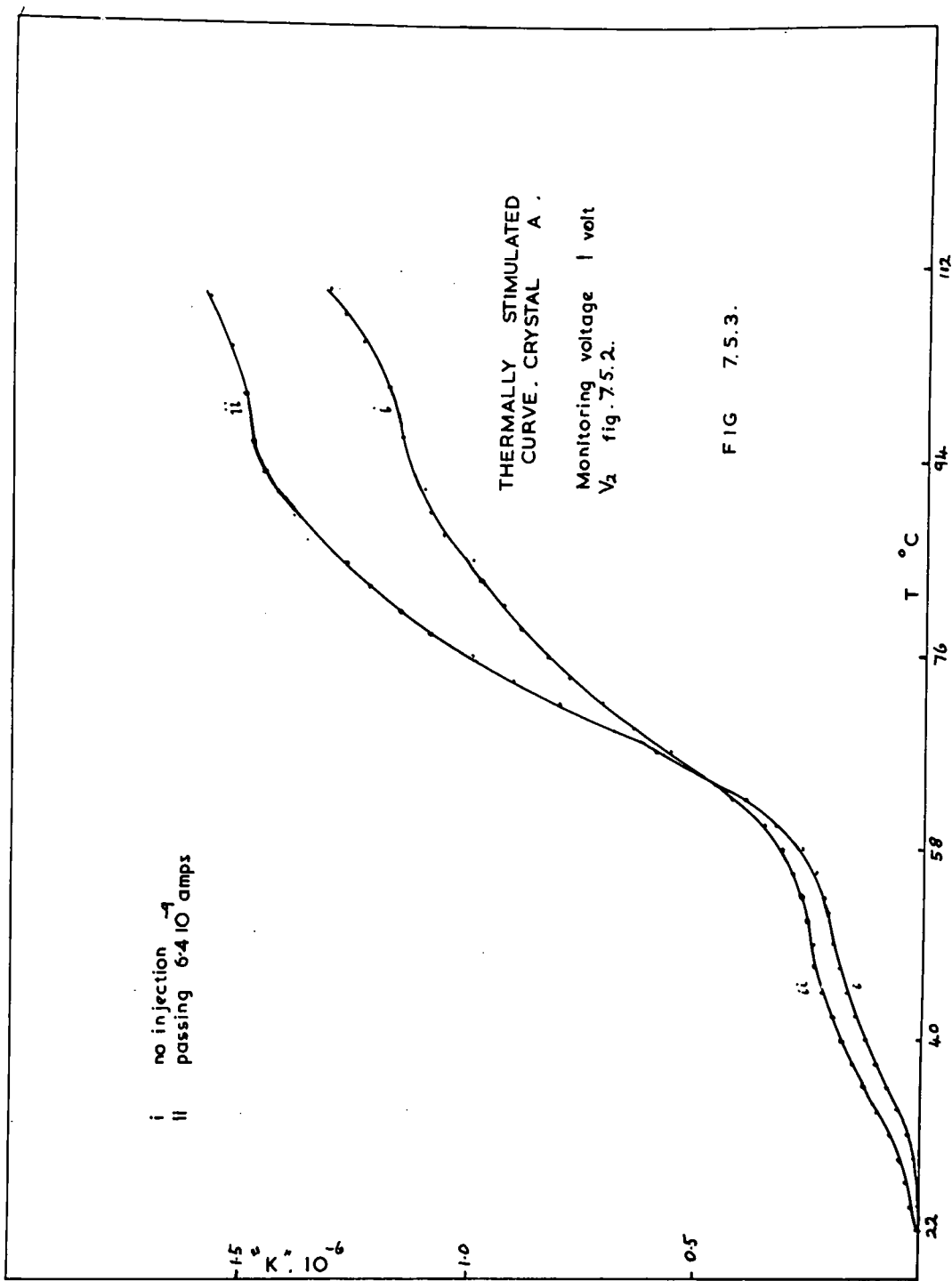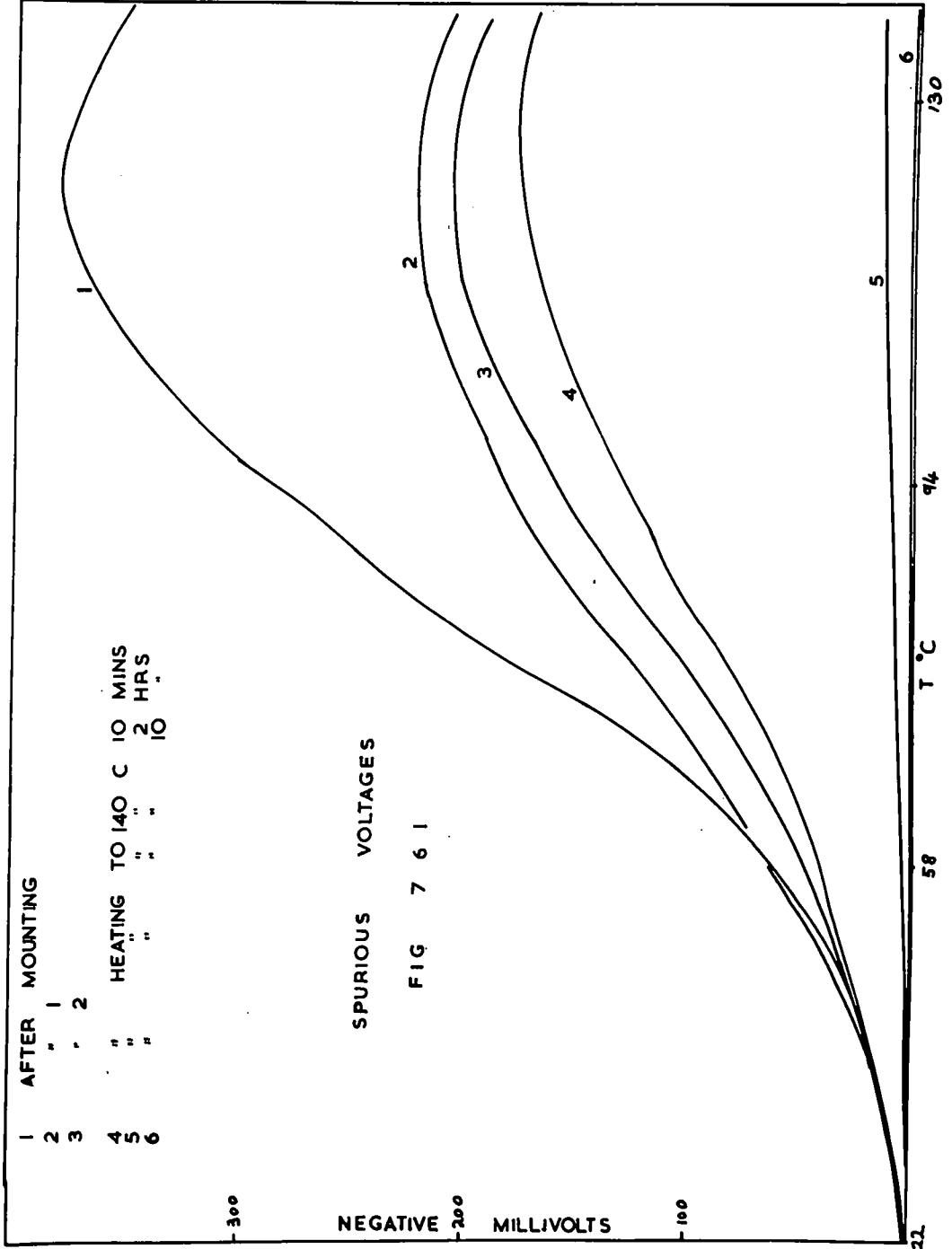
AFTER MOUNTING

1 AFTER MOUNTING
2 " " 1
3 " " 2   HEATING TO 140 C   10 MINS
4 " " "   " " 2 HRS
5 " " "   " " 10 "
6

SPURIOUS   VOLTAGES

FIG   7   6   1

NEGATIVE   MILLIVOLTS

T °C

VARIATION OF SPURIOUS VOLTAGE

WITH INJECTION

FIG 7.6.2.

1 AFTER HEATING AT 140 C. 12. HRS.
2 PASSING 4·0 10⁻⁸ AMPS.
3   "   1·0 10⁻³ "

NEG MV

-15

-10

-5

T °C

22   58   94   130

1.

2.

3.

30 mV

15 mV

NEGATIVE.

O

AFTER PASSING

1.   5·0 10^{-12} amps :
2   5·0 10^{-4} "
3.   5·0 10^{-5} "
4   5·0 10^{-3} "

Crystal B

40   58   76   94   112   130

T °C

SPURIOUS VOLTAGES
AFTER INJECTION

FIG   7. 6. 3

1.

2.

3.

4.
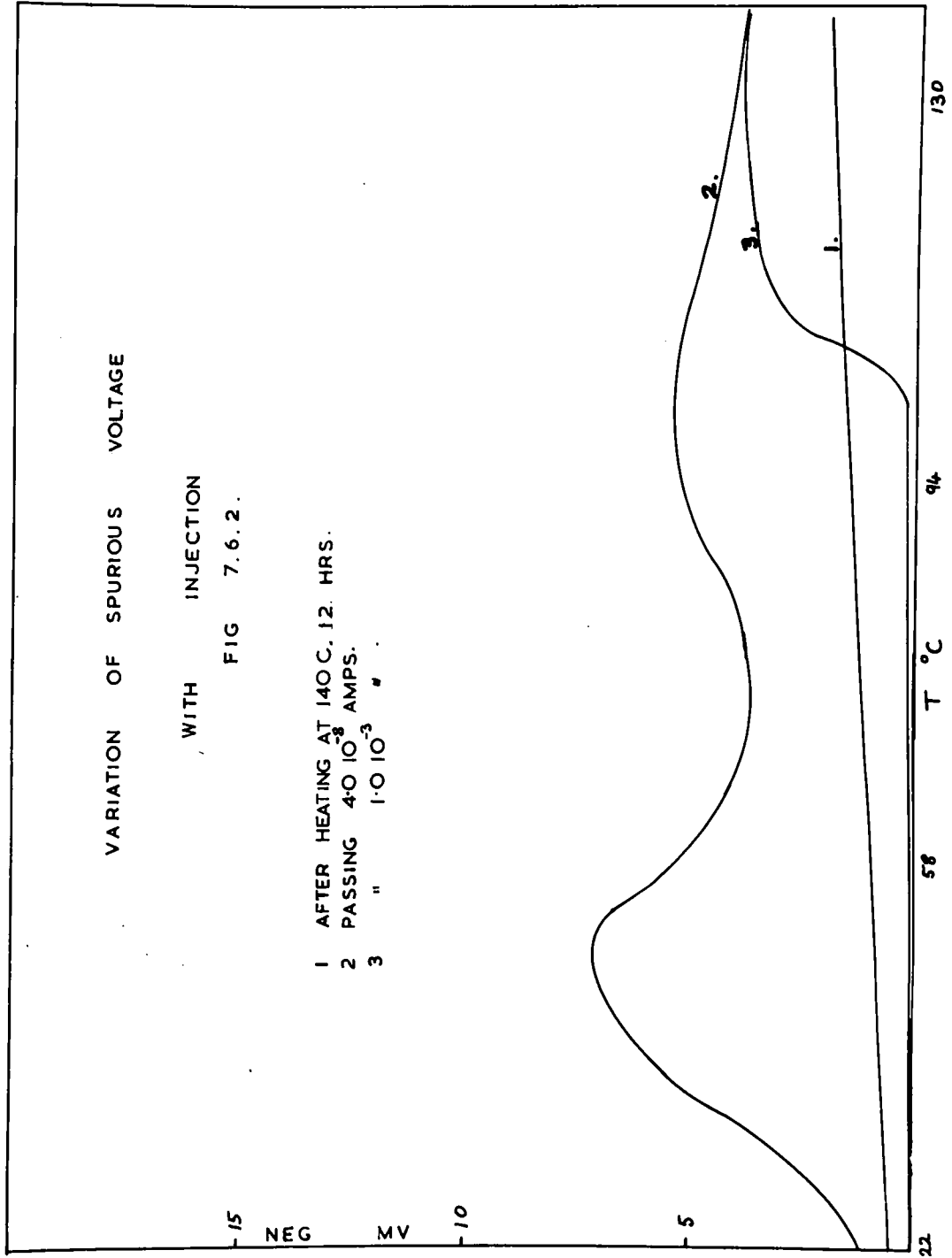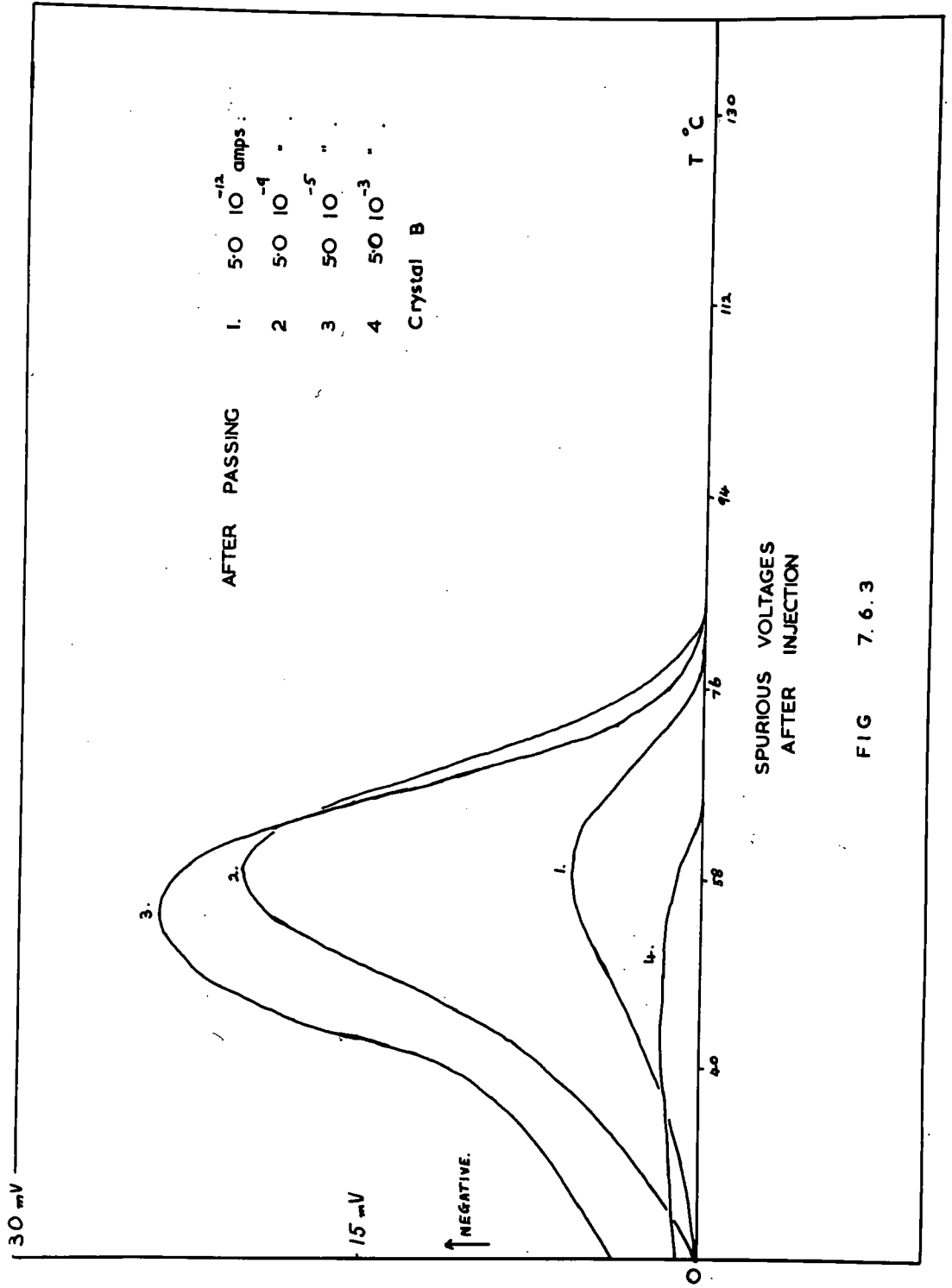
wavelength close to that of the absorption edge, the spurious voltage became large. The magnitude of the voltage at a particular temperature increased with the intensity and duration of the illumination. To eliminate this voltage it them became necessary to heat the crystal for several hours at 140°C. On the other hand, infra-red light with wavelength $>$ one micron, did not have this effect. This suggests that the spurious voltages are associated with trapped electron space charges. The effect of band-gap light on the thermal equilibrium dark current is described in detail in section 7.9., which also includes a description of the light source employed. All the optical measurements in this chapter were made with the light striking the anode (top) contact first. It was noted, however, that if the electrical connections to the crystal were reversed, the spurious voltage was reversed. Thus the light always made the upper face of the crystal negatively charged with respect to the face soldered to the cover slip.

7.7. Thermal Equilibrium Conductivity of Crystal B.

The measurements described in this, and the subsequent sections, of this chapter refer to one particular crystal, termed B. After crystal B had been mounted the spurious voltages shown in Fig. 7.6.3. were observed. On completion of these measurements, crystal B was heated to 140°C for

several minutes. This eliminated the spurious voltages completely. The crystal was then cooled to 77°K and its Ohmic conductivity measured as the temperature was raised uniformly to 140°C. A plot of the dark current as a function of temperature is shown in Fig. 7.7.1. A large peak in the dark conductivity was observed near 10°C. The same peak was also observed when the crystal was cooled. The temperature of the crystal was raised and lowered at different rates in the range -10°C to +30°C repeatedly. The peak remained unchanged. The voltage used to monitor the current (either 100 mV or 200 mV) was reversed. The peak was still present. The curve of Fig. 7.7.1. remained unaltered when the crystal was heated for periods of 20 hours at 140°C. It was concluded that the curve of Fig. 7.7.1. represents the variation with temperature of the equilibrium Ohmic conductivity of the sample. The maximum is not associated with trapped charge.

7.8. Current-Voltage Characteristics of Crystal B

The static, dark current-voltage characteristics of crystal B are shown in Fig. 7.8.1. Before each curve of Fig. 7.8.1. was obtained the crystal was shorted to earth for 2 hours at the particular temperature of measurement. This was to allow thermal equilibrium to be established between the electrons in the conduction band and the levels

CONDUCTIVITY OF CRYSTAL B VS. TEMPERATURE

FIG. 7.7.1

Crystal B

6·5 10^{-3} cms.
2·5 10^{-2} sq. cms.

LOG AMPS

137°C

89°C

-22°C

4·5°C

22°C

-68°C

LOG VOLTS

T/V CHARACTERISTICS
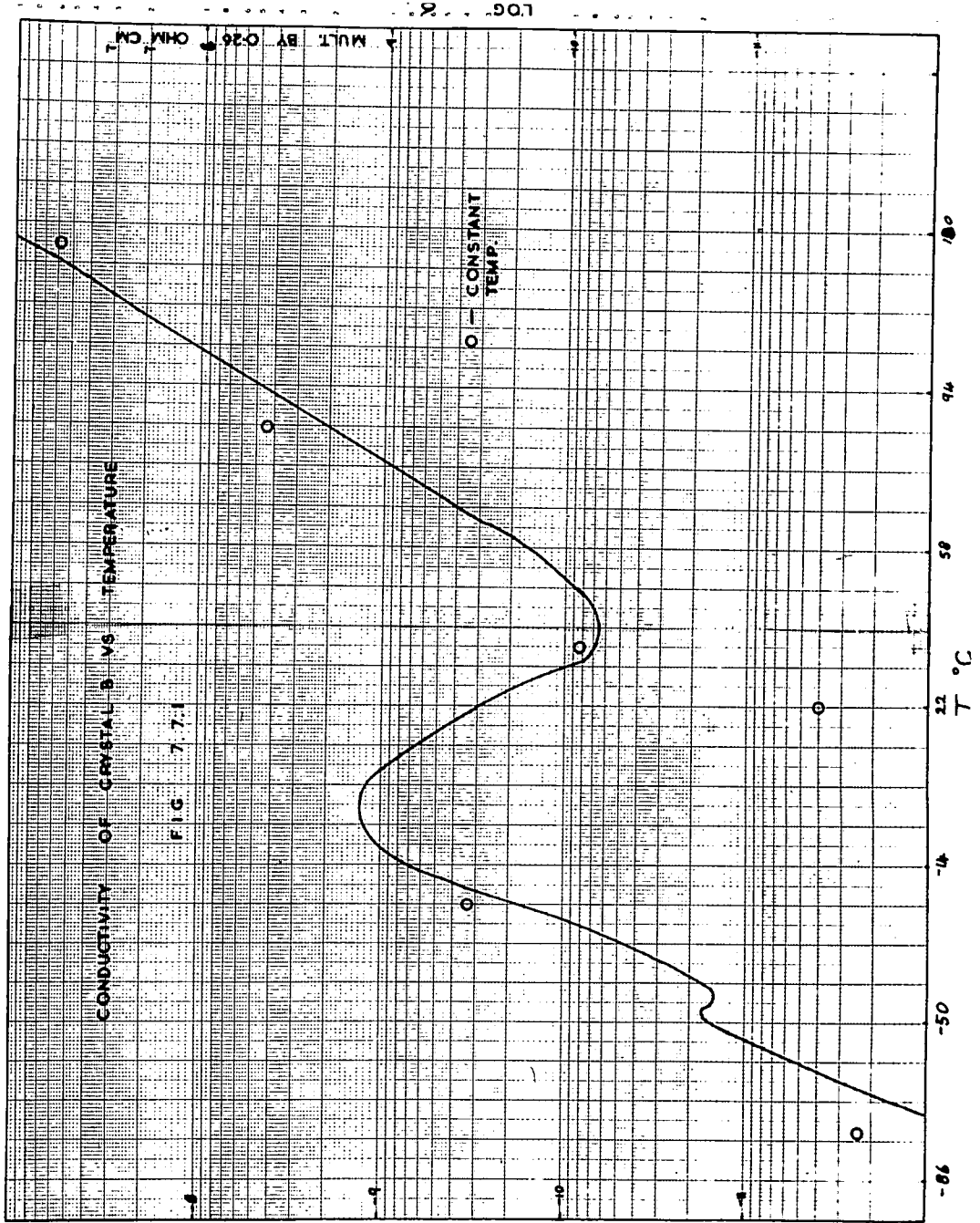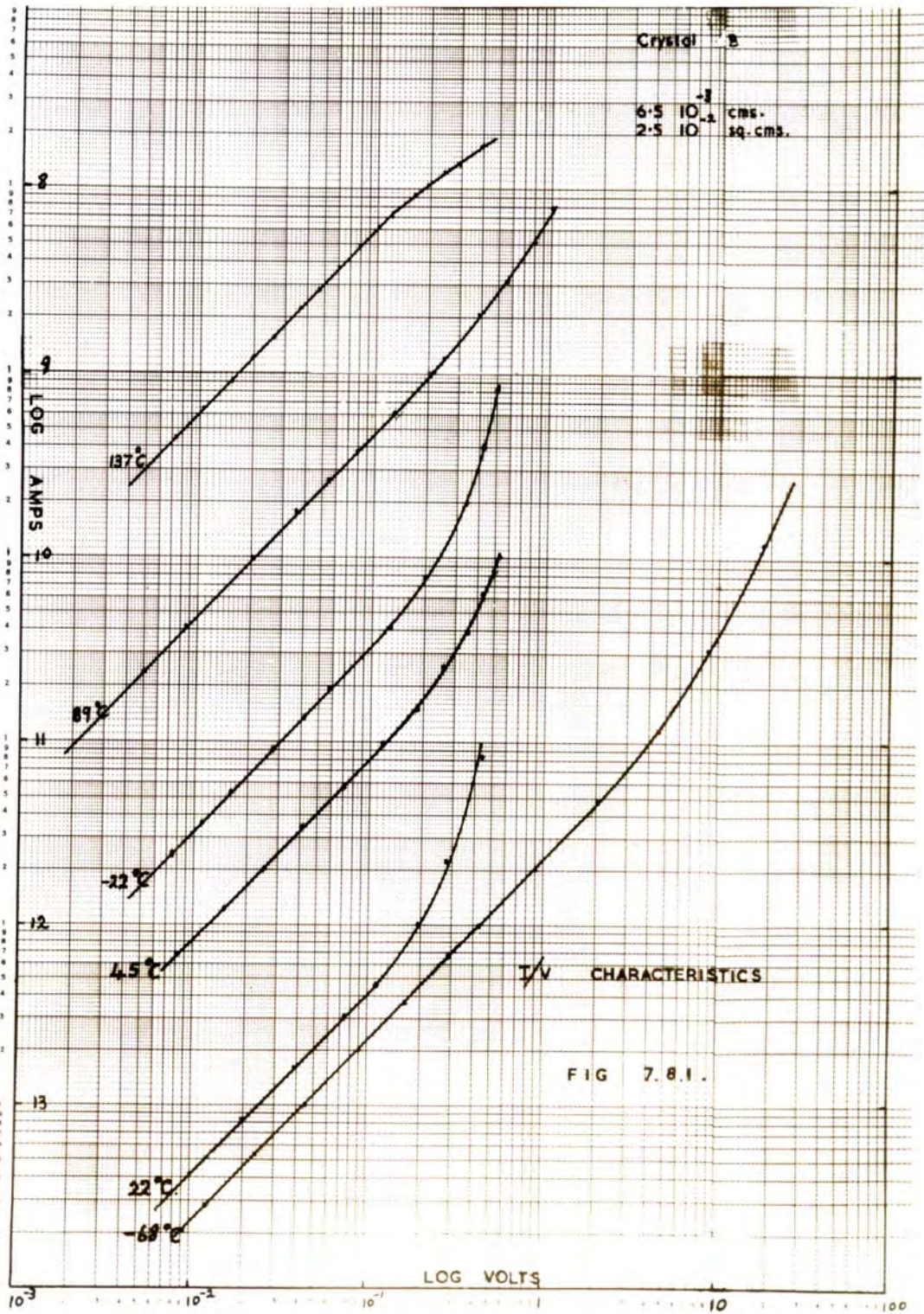
FIG 7.8.1.

within the forbidden gap. The crystal was heated to 140^OC
after each current-voltage curve was obtained. No spurious
voltages were observed. The curves in Fig. 7.8.1. also
indicate that the maximum in the conductivity at 10^OC is
a genuine effect. The interpretation of the results reported
in this and the preceding section, can be found in section
9.4. The conductivity maximum is attributed to a change in
the structure of the defect levels within the forbidden gap,
and a consequent change in the density of carriers thermally
present in the conduction band.

7.9. <u>Thermally Stimulated Currents in Crystal B.</u>

Thermally stimulated current curves for crystal B
are shown in Fig. 7.9.1. It was not possible to pass a
significant current ($>10^{-12}$amps) at 80^OK using applied
voltages up to 200 volts. However by passing 5 milliamps
at room temperature and cooling with the field still applied,
the crystal could be excited at low temperature. Thus a
thermally stimulated current curve was obtained from 80^OK
to 413^OK.

Thermally stimulated currents were also measured in
crystal B using optical excitation. The crystal was illumin-
ated at 80^OK with filtered tungsten light from a Beck
microscope lamp. The light was focussed on to the crystal

THERMALLY STIMULATED CURRENTS
CRYSTAL 8

FIG 7.91

DARK CURRENT
2 PASSING 5·0·10⁻⁷AMP'S (22°C)
3 " 5·0·10⁻⁷ " (")
4 " 5·0·10⁻⁹ " (80°C)
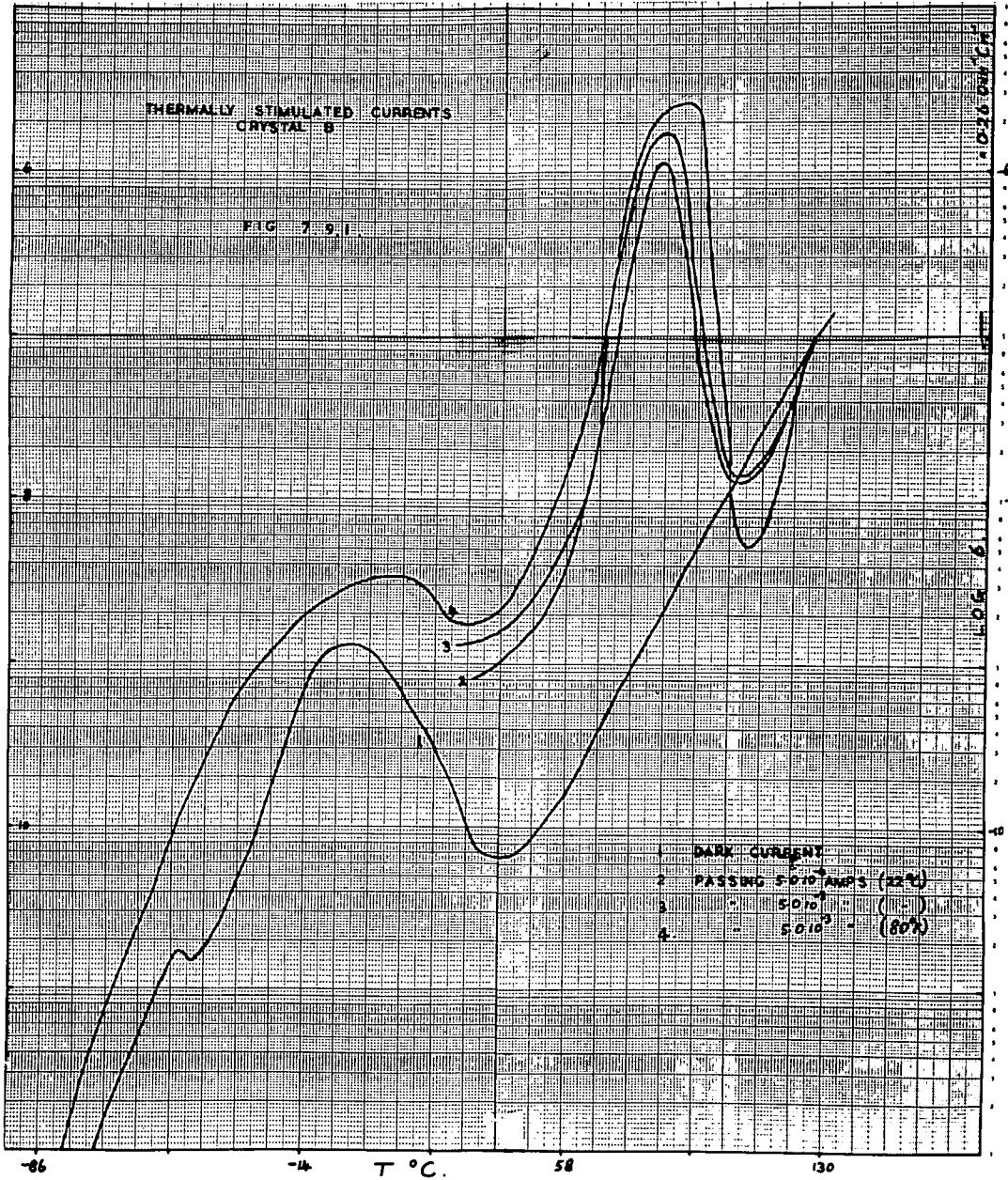
through a silica window covering the side entrance of the
cryostat. After illumination the crystal was heated in the
dark in the usual way. Chance glass filters were used to
give predominantly band-gap or infra-red excitation. The
former was obtained by insertion of a filter type ON22 into
the beam. The latter was obtained by insertion of filters
OX2, OB2 and OR1. The transmission curves of these filters
are illustrated in Fig. 7.9.2. The silica window was
essentially transmitting up to 3.5. microns.

The thermally stimulated current curves obtained using
optical excitation are shown in Fig. 7.9.3. In marked
contrast to the curve obtained by electrical injection the
curve obtained with band-gap excitation shows a depression
at about 85^OC.

Band-gap light at 80^OK did not introduce significant
spurious voltages across the crystal, (section 7.6.) after
the thermally stimulated current measurement of Fig. 7.9.3.
(4). However, the thermal equilibrium dark current was
depressed. The new dark current is shown in Fig. 7.9.4.(2).
Successive heating of the crystal showed that the dark current
increased to its equilibrium value. This is also illustrated
in Fig. 7.9.4. The depression of the dark current was not
associated with the spurious e.m.f.'s. Infra-red illumination
in the temperature range 80^OK to 413^OK did not introduce
typical spurious voltages. A positive voltage was observed
across the series resistor, at 140^OC, when the crystal was
irradiated with infra-red light. This voltage disappeared

OR I

OX 2

CHANCE FILTERS

FIG 7.9.2

OB 2

ON 22

0·4   0·6   μ.   1·0   4·0   μ.

CRYSTAL B
1 DARK CURRENT
2 INJECTION
3 AFTER I.R. (80°K)
4 VISIBLE (80°K)

OPTICAL AND ELECTRICAL THERMALLY STIMULATED CURRENTS

FIG. 7.9.3

$LOG \ 6 = 0.26 \ 4 \ OHM^{-1} CM^{-1}$

T °C

-158   -86   -14   58   130

DE-RPESION OF DARK CURRENT
CRYSTAL B
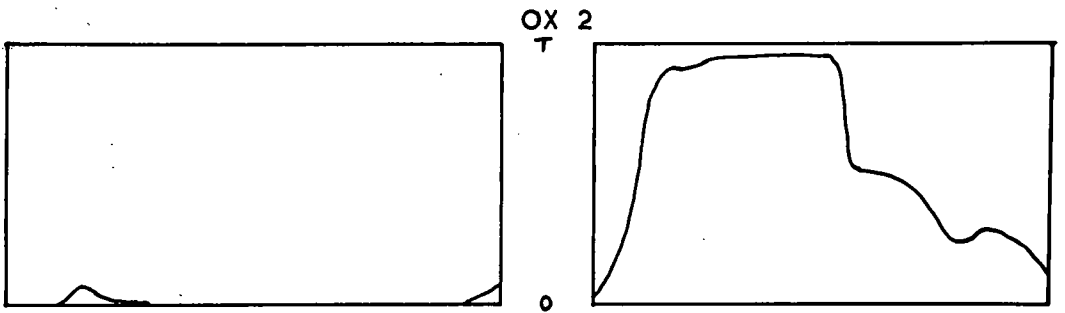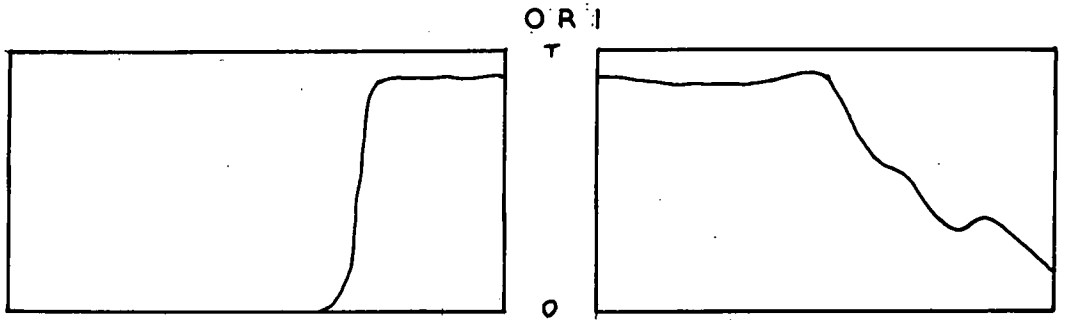
FIG. 7.9.4.
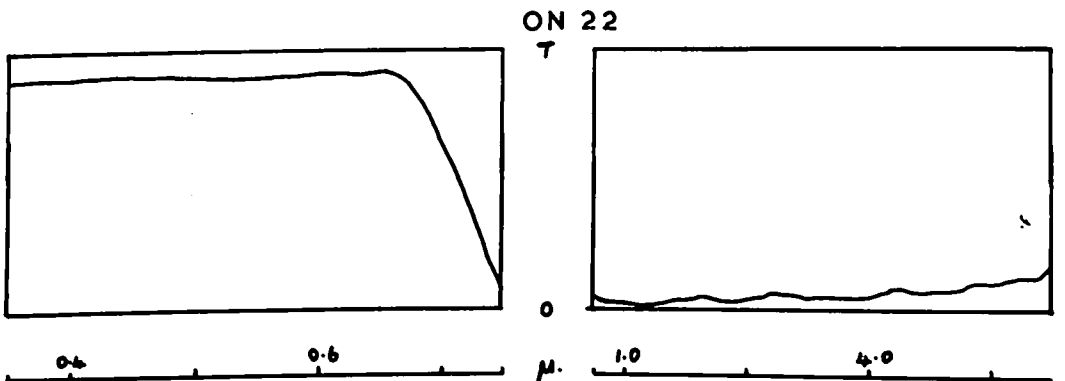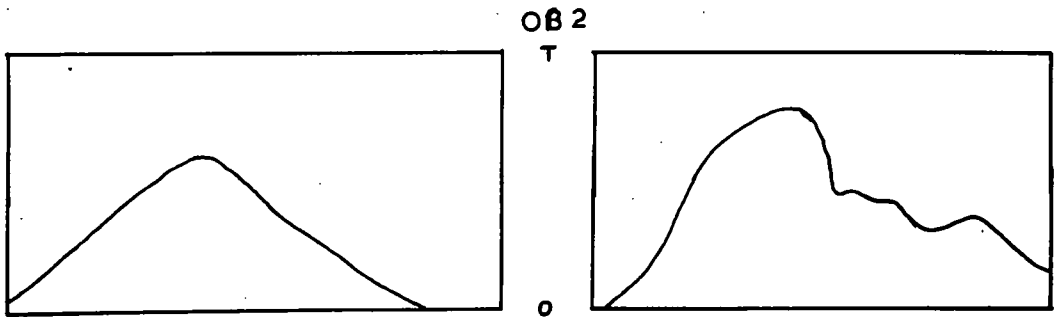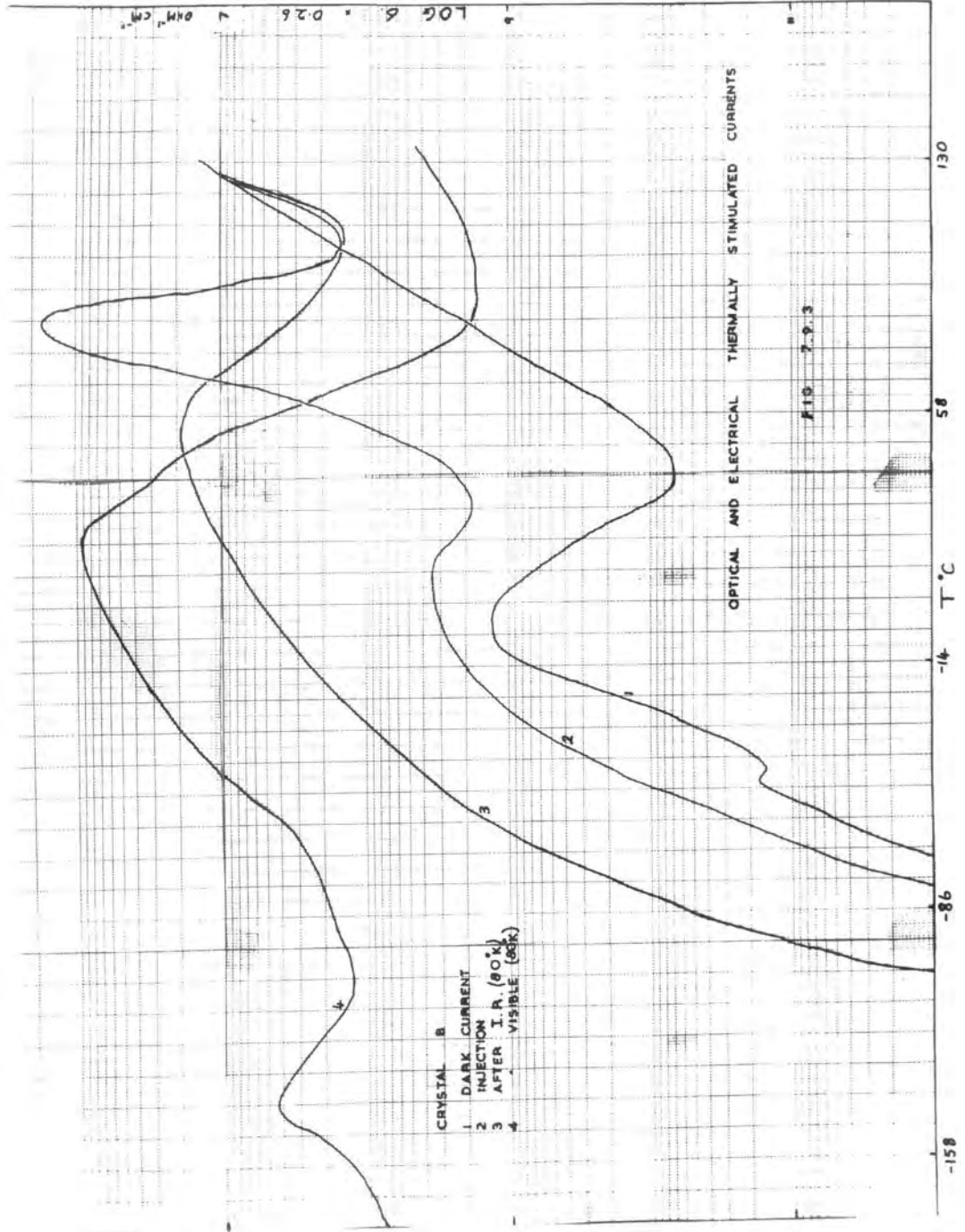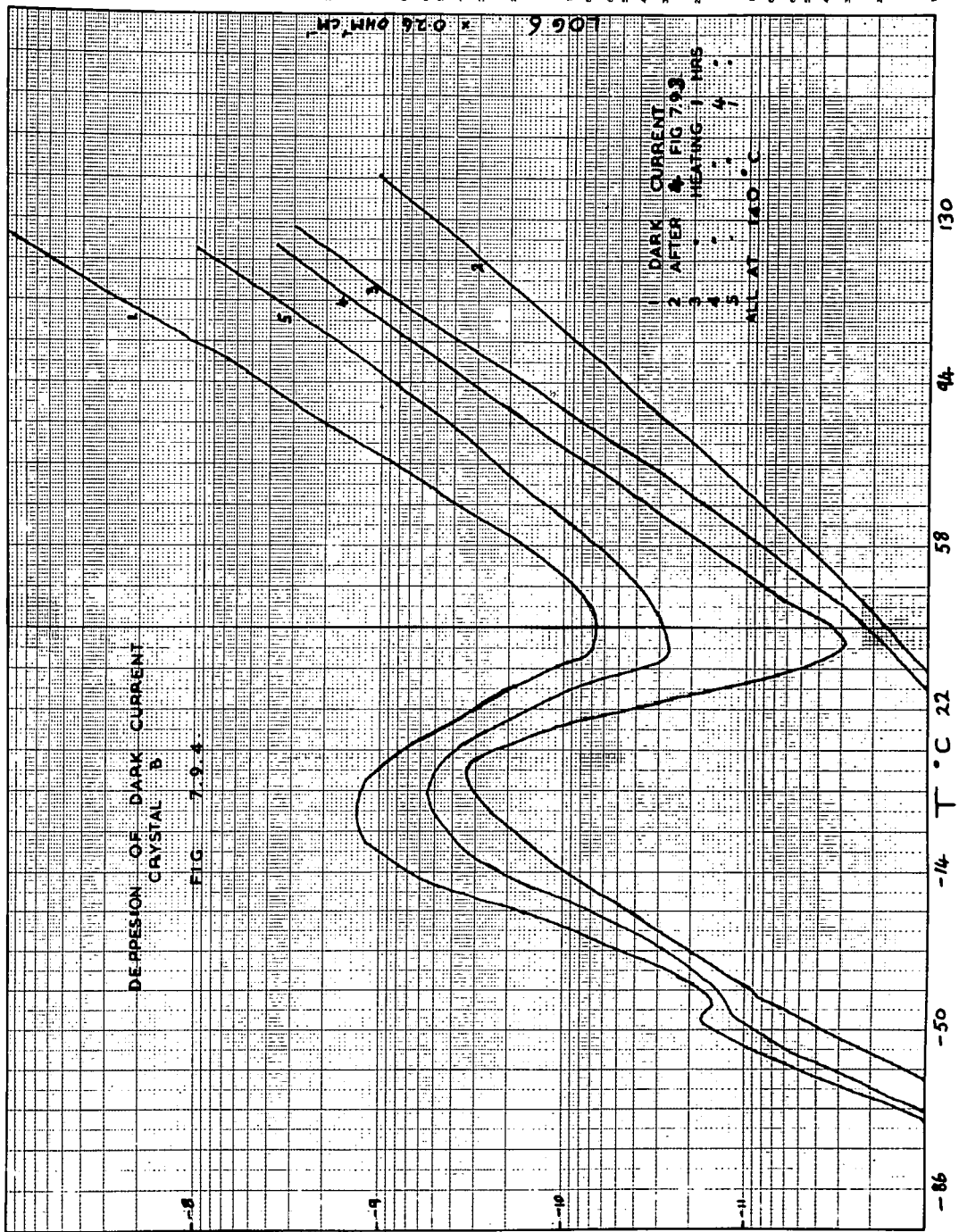
within minutes of removing the excitation.

7.10.   Sensitivity of Crystal B.

The response of this crystal to different intensities
of visible and infra-red light has been measured. This was
achieved by performing a number of experiments in which the
crystal was illuminated with a variety of constant
intensities while the temperature was increased slowly.
The results are shown in Fig. 7.10.

Five intensities were obtained in the visible region
by changing the input to the microscope lamp and making use
of an additional chance filter ON10. The filter ON10 is
a neutral filter with 7% visible transmission. Three infra-
red intensities were used. These were obtained by altering
the input to the microscope lamp. The intensity of band-gap
excitation was measured with a selenium photovoltaic light
fluxmeter. The infra-red intensity was measured with a
lead sulphide photocell. The intensity of the light falling
on to the crystal in absolute units was not determined.

7.11.   Sensitivity of Crystal B to Gamma-rays

The response of this crystal to γ-rays is also shown
in Fig. 7.10. A radium 226 source was used which emits
γ-rays with an energy of 0.187 MeV. The half-life of radium
226 is 1620 years. The source was on loan from the Radio-

INCREASING INTENSITY OF VISIBLE LIGHT

SENSITIVITY OF CRYSTAL B

F I G 7 I.O.

INCREASING INTENSITY I.R.

DARK CURRENT
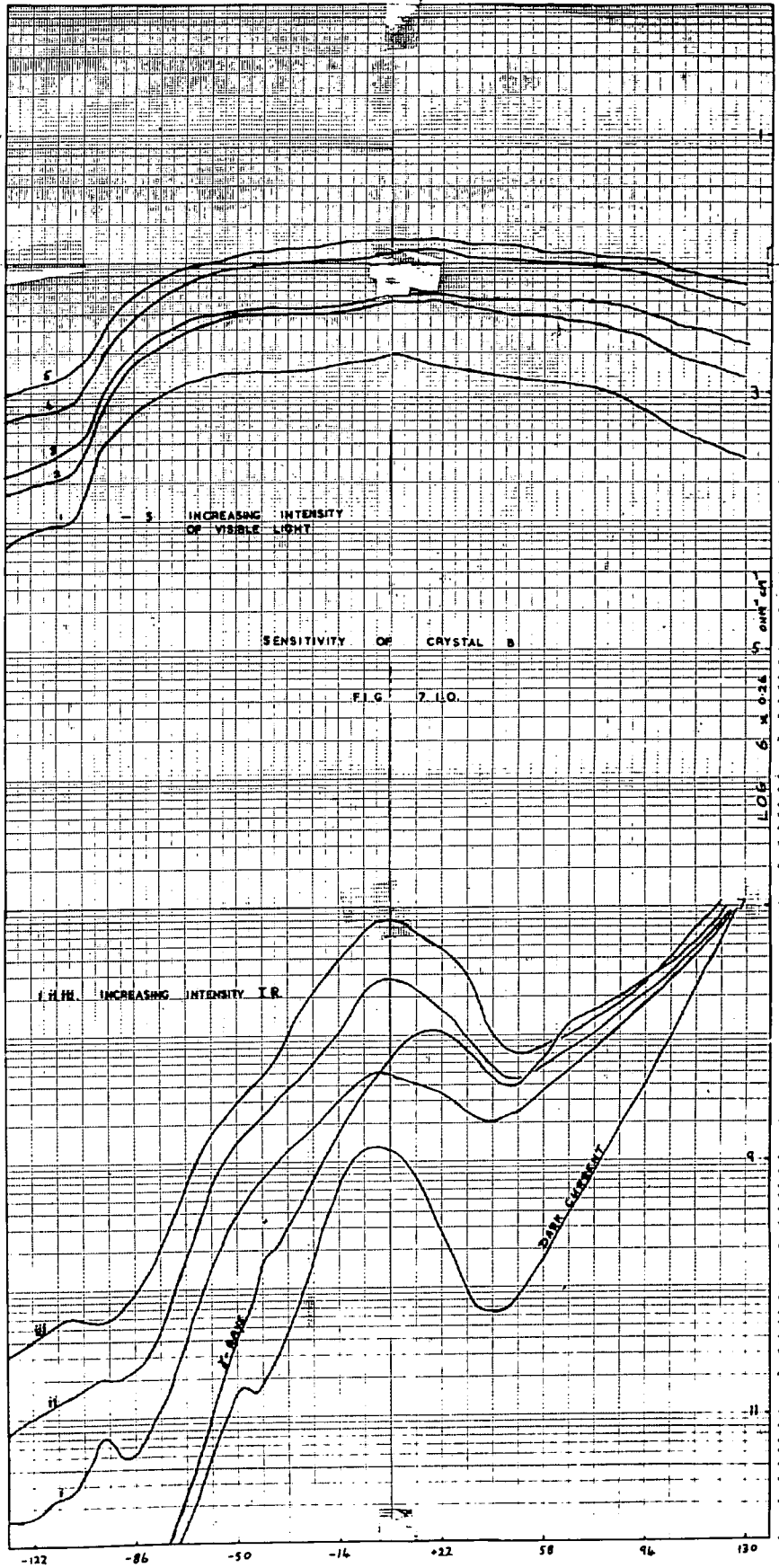
chemistry Department and its history is uncertain. The exact γ-ray emission spectrum arising from decay products was therefore not known. The approximate strength of the source was one milli¢ curie. The tube containing the radium 226 was placed outside the cryostat approximately 7 cms from the crystal. In view of the small response, measurements with lower intensities of irradiation were not attempted. It was not possible to increase the intensity by moving the source closer to the crystal with the present cryostat.

Crystal B responded to the γ-rays in a time of the order of one second. No changes in the dark conductivity were apparent, after an exposure of several hours, after removal of the source. At room temperature and above the γ-induced current was of the order of 10 times the dark current. Below room temperature the sensitivity decreased rapidly with temperature.

CHAPTER VIII

Optical Measurements

8.1. Introduction

The spectral emission distribution of the luminescence of cadmium sulphide crystals, excited by ultra-violet light, has been measured over the range 0.48 to 3.5 microns. In the apparatus with the best resolution the wavelength range covered was between 4800 $\overset{o}{A}$ and 1 micron. The measurements were performed at liquid nitrogen temperature using pure crystals, and crystals doped as described in section 6.3. The spectral distribution of the electro-luminescent emission at $77^{o}K$ has also been measured over the same wavelength range for pure crystals. In a second apparatus the long wavelength limit was extended and the ultra-violet excited photo-emission, at room temperature and $77^{o}K$, was measured from 0.5 to 3.5 microns. The crystal used in the first apparatus to determine the electro-luminescent spectrum, was also examined in the second.

8.2. Apparatus

(a) Measurements between 4800 $\overset{o}{A}$ and 1 micron.

The crystal under observation was placed opposite the silica window of the glass cryostat illustrated diagrammatically in Fig. 8.2.1. Araldite was used to obtain a

vacuum tight seal between the silica window and the wall
of the cryostat. The crystal was fixed on to the outer
face of the inner glass wall with a binder which consisted
of nitrocellulose in butyl acetate. The space between the
walls of the cryostat was evacuated to about 10^{-2} mms with a
rotary oil pump. Liquid nitrogen in the container formed by
the inner glass wall of the cryostat cooled the crystal to
$77^{\circ}K$. The luminescence was excited by using a condensing
lens (10 cm. diameter) to focus the output of a 125 watt
Osram high pressure mercury vapour lamp on to the crystal.
The lamp emitted most of its radiation at 3650 Å . Visible
light was filtered out by the Woods' glass envelope surrounding
the discharge tube. The cryostat was arranged in front of
the entrance slit of the spectrophotometer. Experimentally,
it was found that a maximum amount of light was detected when
a plate-like crystal was aligned edge-on to the entrance slit
of the spectrophotometer. This is due to the high refractive
index of cadmium sulphide, (2.6), which means that most of
the emission is totally internally reflected and is eventually
emitted at the edge of the plate. When rod-like crystals
were being examined, the axis of the rod was placed parallel
to the slit. This gave satisfactory results although the most
intense emission appeared from the ends of the rods.

The first apparatus used to analyse the emission was an
Optica spectrophotometer, Model CF4/DR. I am grateful to

the Chemistry Department for permission to use this instrument, and to J. Collier for advice as to its operation. The CF4/DR is a single-pass, double beam, grating instrument. The monochromator employs a ruled grating with 15,000 lines per inch, and has a maximum resolution of the order of 2 Å. In the experiments to be described the resolution varied between 8 Å and 36 Å depending on the slit width required to obtain a measurable signal. The resolution is marked on each spectral diagram presented later in this chapter. Two photomultiplier detectors are used in the instrument to cover the spectrum over the visible and infra-red to 1 micron. The E.M.I. No. 6256B covers the range 1850 to 6700 Å, while the Dumont 6911 is used from 6700 Å to 1 micron. To employ the CF4/DR for luminescent emission measurements, the instrument has to be operated in its single beam mode. With this arrangement, the input signal is compared with a steady reference signal. The difference is amplified and fed to a Honeywell potentio-metric chart recorder. The recorded trace of the emission spectrum requires a correction to allow for the spectral response of the detector. The spectral response of an E.M.I. 6256B photomultiplier is shown in Fig. 8.2.2. This detector is a thirteen stage device with a CsSbO photo cathode deposited on quartz. The response of the Dumont photomultiplier was not known. Although edge emission was readily measurable no luminescence in the wavelength range 6000 Å to 1 micron

EMI 6256B SbCsO (S.13) PHOTOCATHODE

L.O.G.

SPECTRAL RESPONSE OF PHOTOMULTIPLIER

FIG 8.2.2.

electrons per photon

1.0

0.1

0.01

0.2A   0.4A   0.6A

0   0.2   0.4   0.6
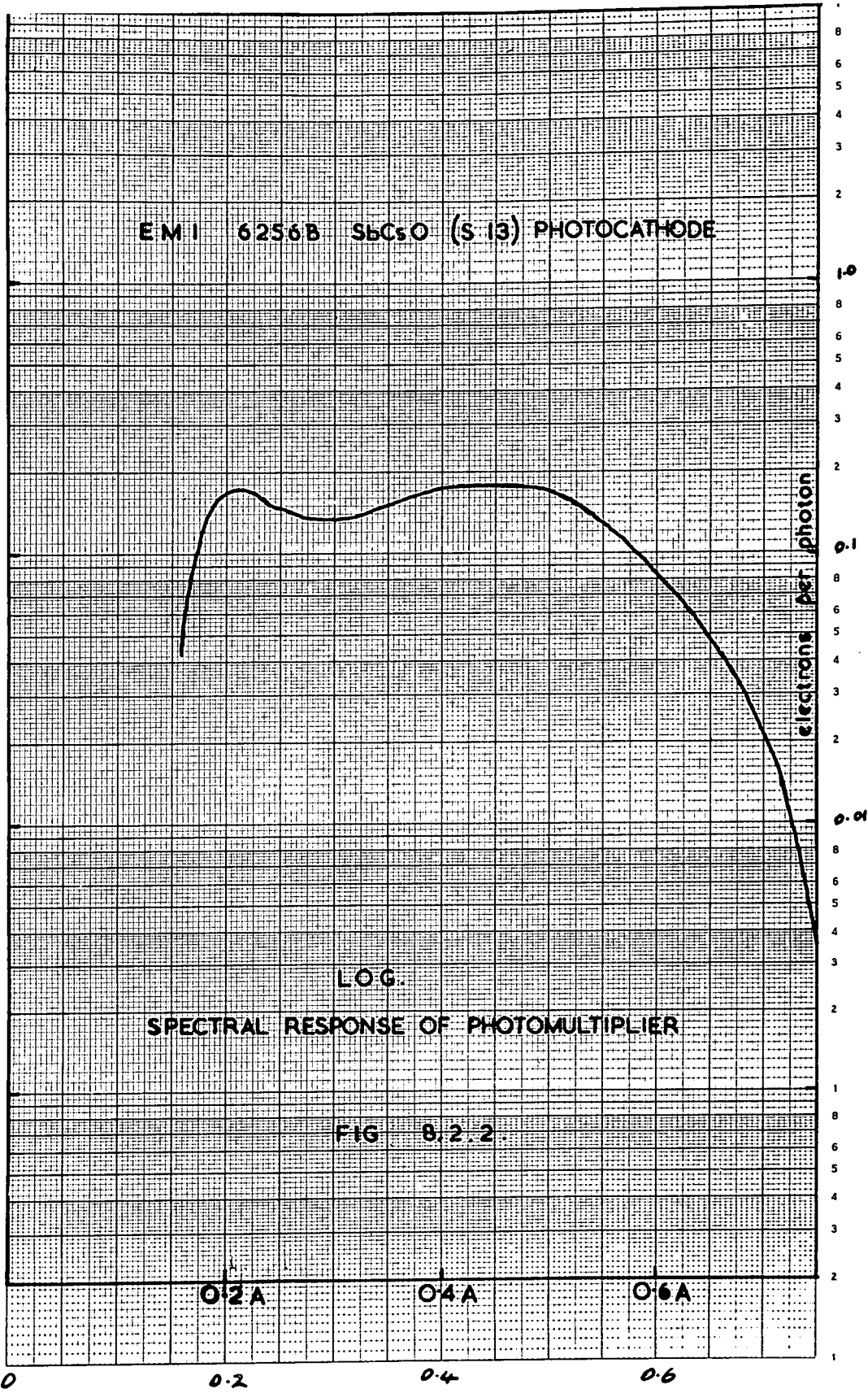
was detected with this apparatus. However the nitro-
cellulose binder, used to mount the crystal in the cryostat,
showed several strong absorption peaks in this range, and its
absorption became strong at 5900 $\overset{o}{A}$. The fact that no emission
was observed between 6000 $\overset{o}{A}$ and 1 micron may have been due to
absorption in the binder rather than an inherent insensitivity
of the detector. No signal at all was discernable over the
whole wavelength range when the crystal was maintained at
room temperature.

The spectral distribution of the electroluminescence
emitted from a platelet of cadmium sulphide was also obtained
using the spectrophotometer just described. The crystal was
mounted in a copper cryostat similar to the one described
in section 7.2. Further details of this experiment are
given later in this chapter.

(b) Measurements between 0.5 and 3.5 microns.

In the second apparatus, in which the wavelength range
was extended to 3.5. microns, the crystal under observation
was placed in the cryostat shown in Fig. 8.2.1. Care was
taken in mounting this crystal to ensure that the binder was
confined to the rear face of the crystal. The sample was
plate-like, and had been previously used for the electro-
luminescent experiment.

The crystal was excited by the more intense radiation
from an Osram 250 watt high pressure mercury vapour lamp.

This compact discharge lamp emits predominantly at 3650, 4040, 4358, 5460, and 5790 Å. The 3650 Å radiation was selected using four filters as follows:- Two Chance filters ON22 to absorb infra-red; a Chance filter OX7 to absorb in the visible; and a 1 cm path of a 10% aqueous solution of copper sulphate to eliminate the infra-red. The output from the lamp was filtered, collected by a 10 cm diameter condensing lens, and focussed on to the crystal with a 5 cm diameter, 5 cm focal length, convex lens.

The emission from the crystal was analysed using a Hilger and Watts prism monochromator, Model D285. A rock salt prism was employed. The emission entering the monochromator was chopped at 800 cycles/sec using a multi-bladed disc. A Mullard lead sulphide photo cell, type 61 SV, was used in conjunction with a tuned amplifier, to detect the radiation at the exit slit. The Barr and Stroud amplifier, type EL7921, fed from a stabilised power supply type EL7907, provided a maximum gain of 5.10^8 with an inherent noise level of 0.04 μV. A direct current bias, variable up to 250 volts, was available from this equipment for the operation of the photocell. The output signal was displayed on a 6 inch meter. The maximum resolution of the monochromator varied from a few angstoms to 80 angstroms with a slit width of 0.02 mms.

The results of experiments made with this apparatus are described later in this chapter.

8.3. Emission Spectrum of Pure Cadmium Sulphide

The spectral distribution of the ultra-violet excited edge emission of a pure crystal of cadmium sulphide is shown in Fig. 8.3.1. Small luminescence peaks can be seen on the short wavelength side of the main emission bands. A broad emission band, near 5800 Å is also present. This band is shown more clearly in Fig. 8.3.2. which was obtained by repeating the measurement using wider slits. A discussion of the emission spectra described here is deferred until Chapter X.

8.4. Emission Spectra of Oxygen Doped Cadmium Sulphide

The emission spectrum of a cadmium sulphide crystal grown in the presence of oxygen is shown in Fig. 8.4.1. Two prominent peaks can be seen on the high energy side of the main emission. It was found that after passing a high frequency gas discharge(using a Tesla coil) in the vicinity of the crystal, the heights of these short wavelength peaks were reduced relative to those of the main bands. The effects of a two minute discharge between measurements led to the reduction in relative magnitude illustrated in Fig. 8.4.2. This suggests that the short wave bands are associated in some way with the surface of the crystal. The spectrum of a second crystal containing oxygen is shown in Fig. 8.4.3. and

FIG. 8.3.1

PURE 8 Å

FIG 8.3.2.

PURE 3.6 Å

FIG 8.41

OXYGEN 36 Å

FIG 8.4.2.

OXYGEN 36 Å

after h.f. discharge

FIG. 8.4.3

OXYGEN 9 Å
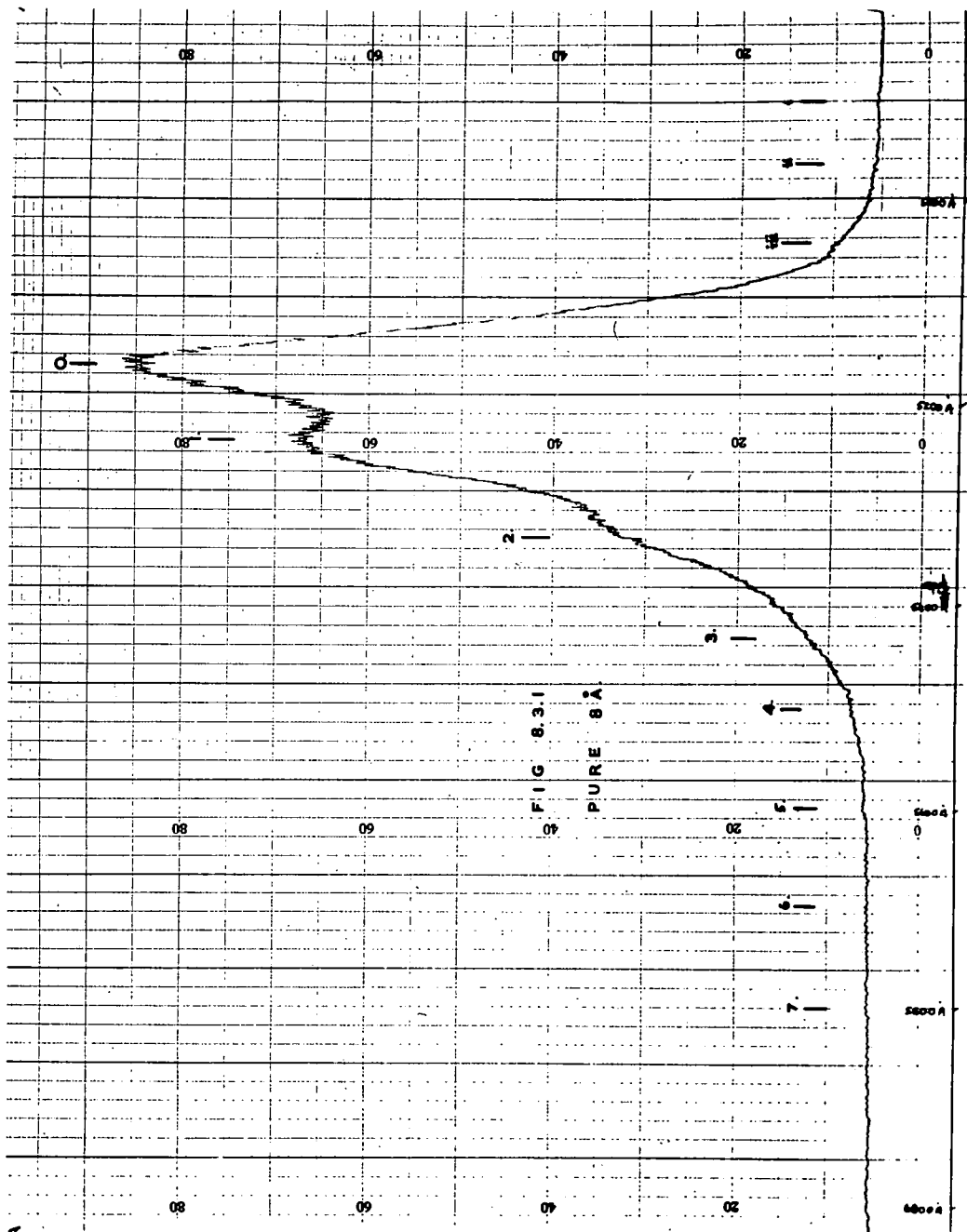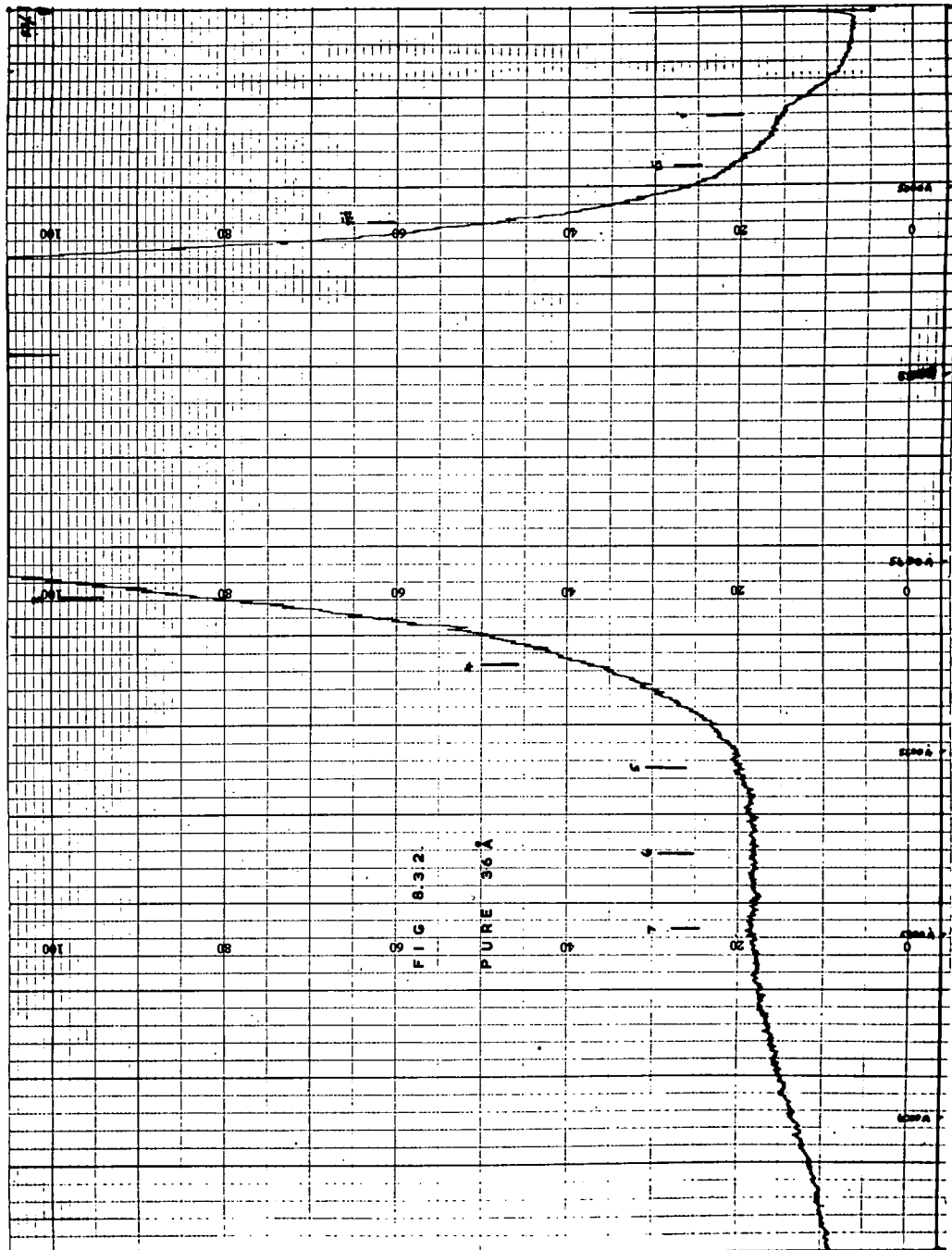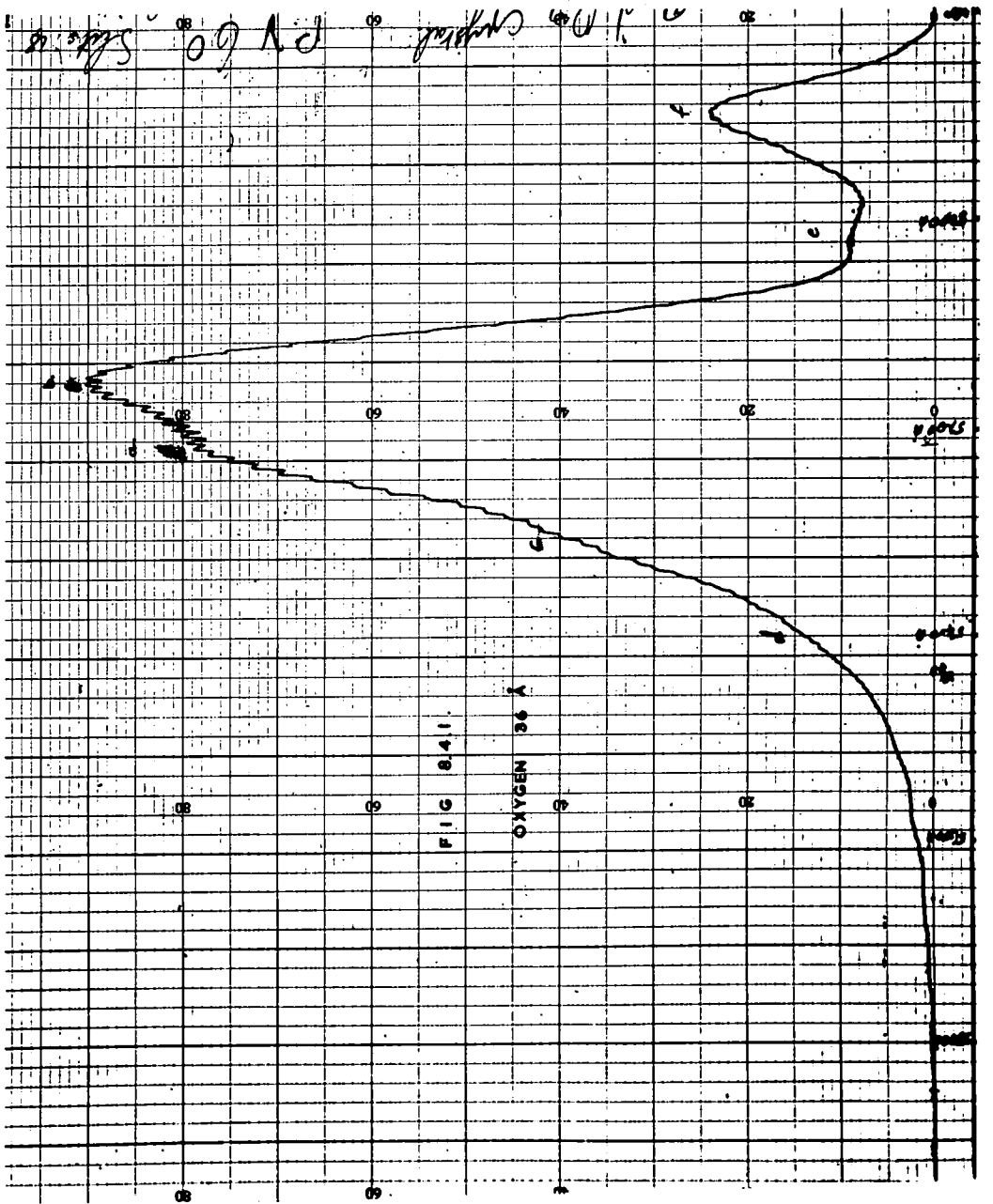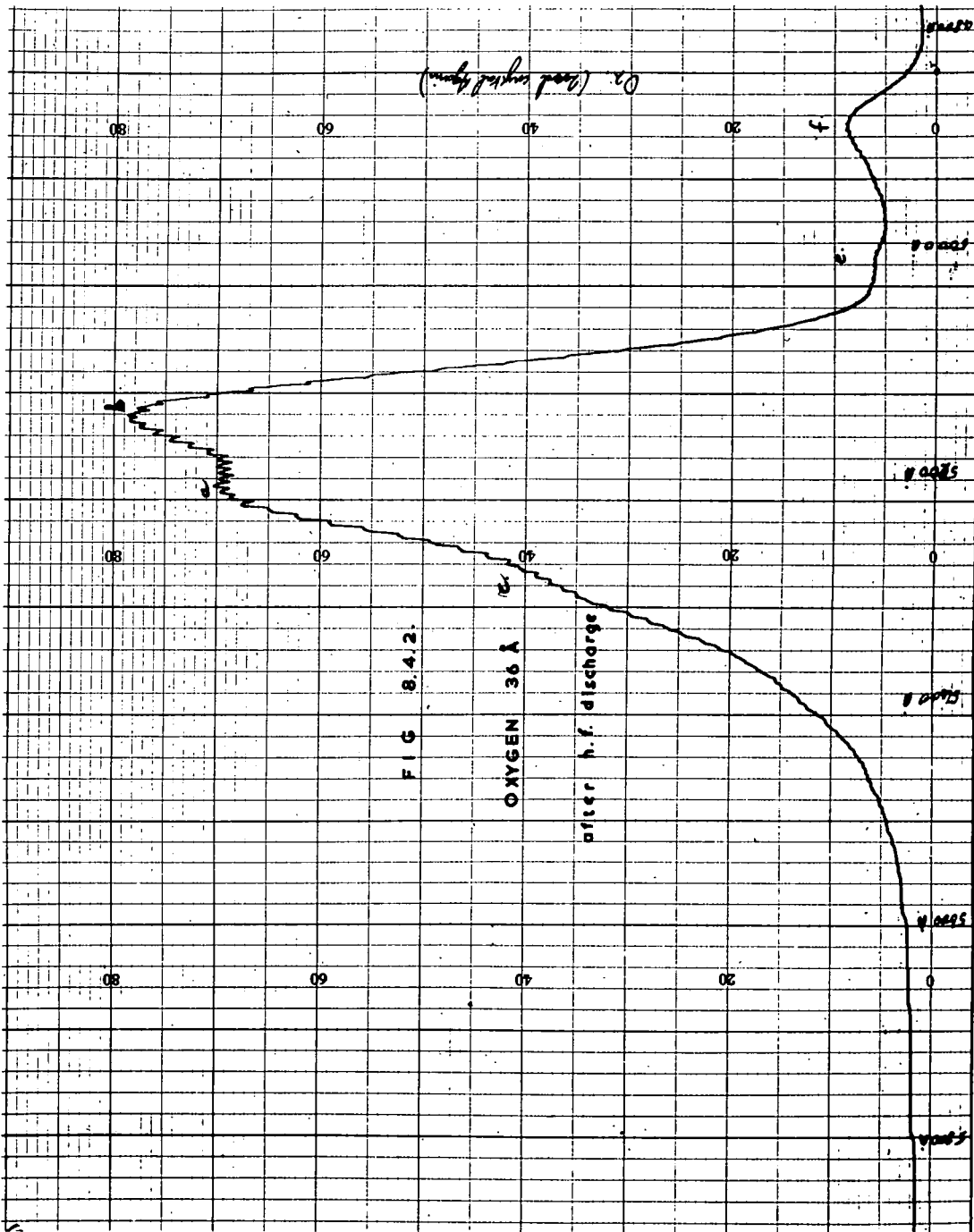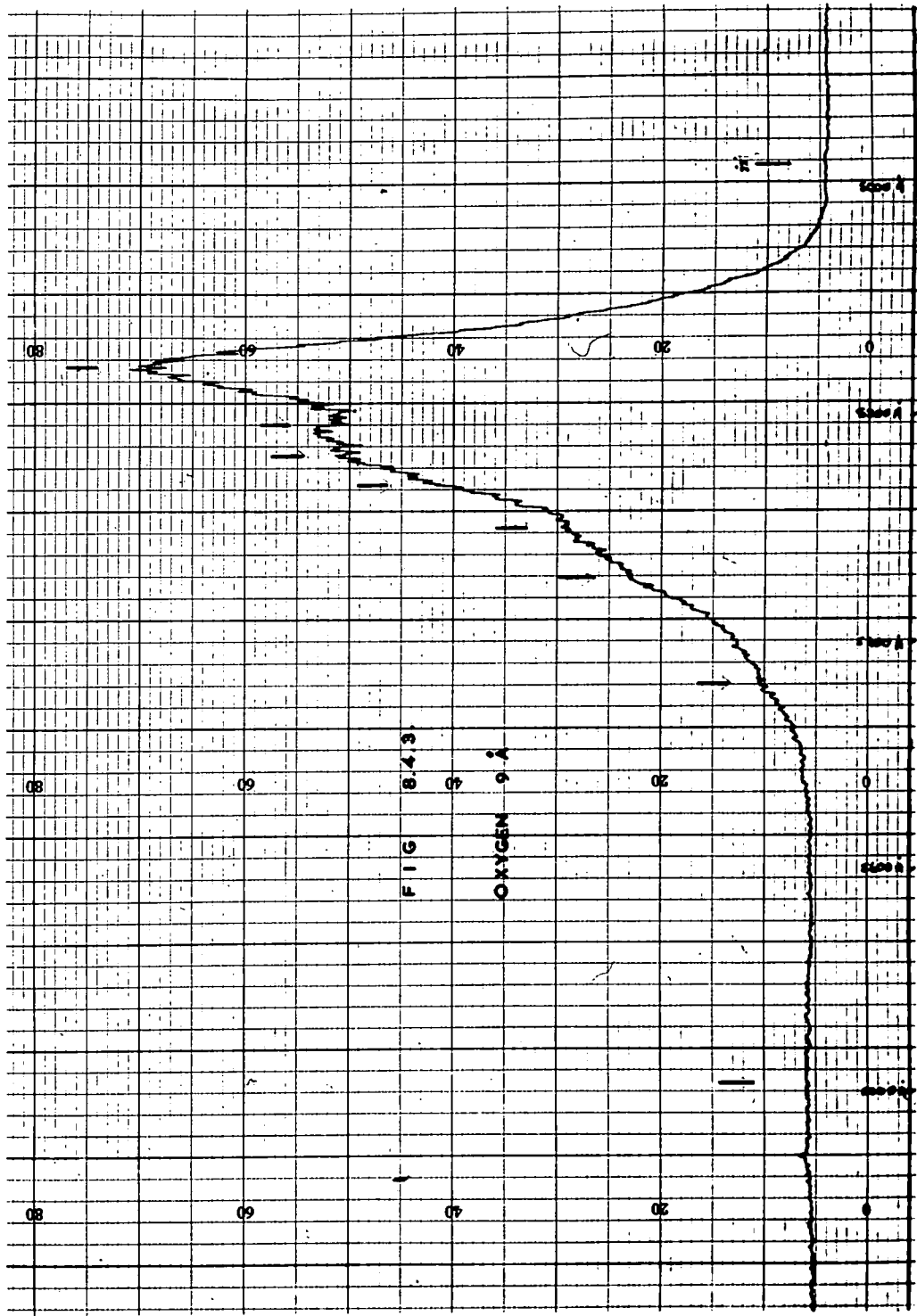
Fig. 8.4.4. The emission from this sample was similar to that of a pure crystal, but additional structure was apparent in the edge emission. The broad band at 5800 Å was also very prominent in some crystals, Fig. 8.4.5. This yellow band was not observed in crystals which displayed large peaks on the high energy side of the main emission.

8.5. Emission Spectrum of Hydrogen Doped Cadmium Sulphide

The emission spectrum of a crystal grown in the presence of hydrogen is shown in Fig. 8.5.1. Additional structure is again apparent in the edge emission spectrum. No other peaks were recorded outside this wavelength region (i.e. 5100 - 5600 Å).

8.6. Emission from Crystals Grown in Water Vapour

Crystals grown in water vapour had the emission spectrum shown in Fig. 8.6.1. Only the edge emission lines were observed. Though the luminescence appeared more intense to the eye, difficulty was experienced in recording these spectra because of the low level of light entering the spectrophoto-meter. The explanation may lie in the fact that the surface texture was such that the light emitted was more diffuse from these crystals.

FIG 8.4.4

OXYGEN 16·Å

FIG 8.4.5

OXYGEN 12 Å

FIG 8.5.1.

HYDROGEN 12 Å
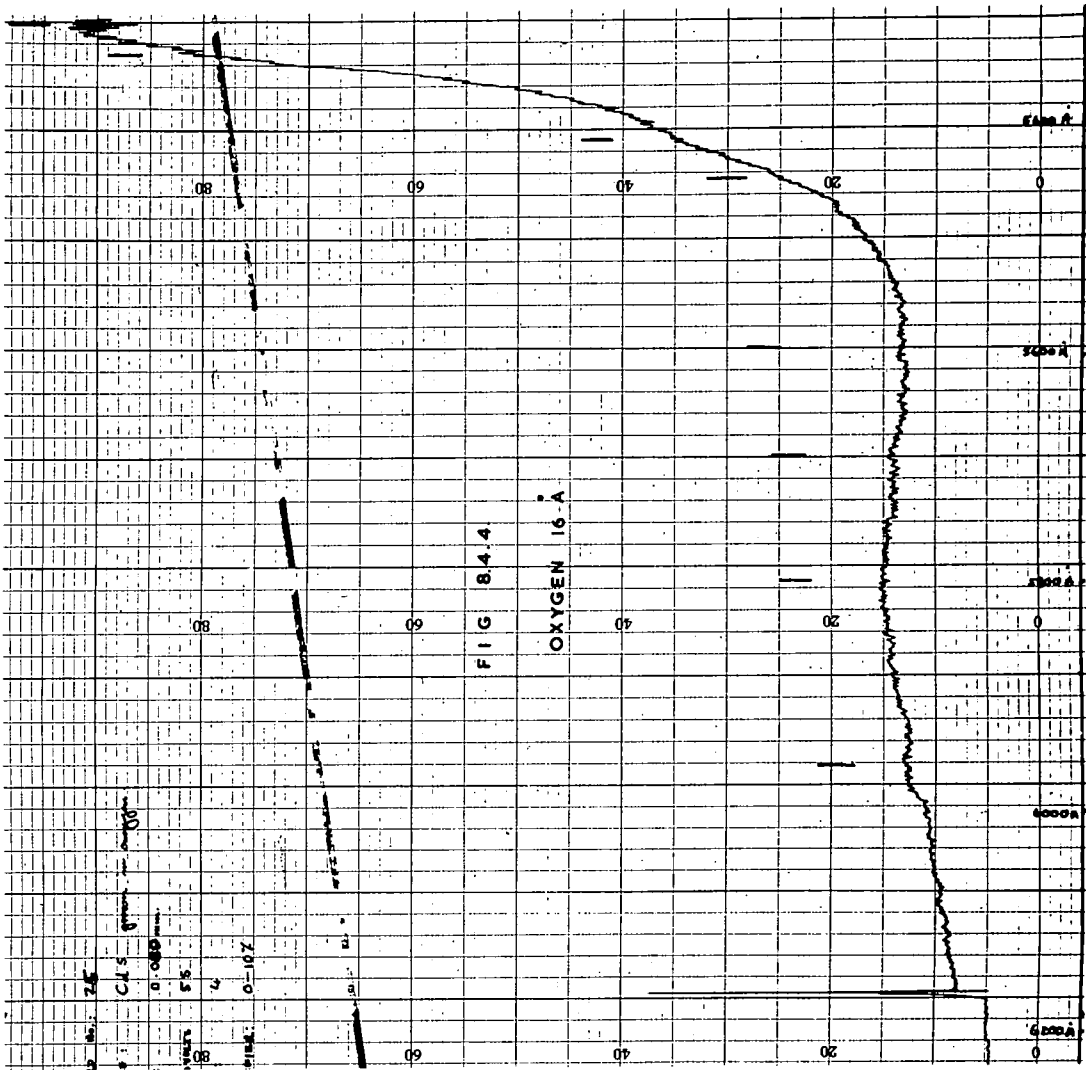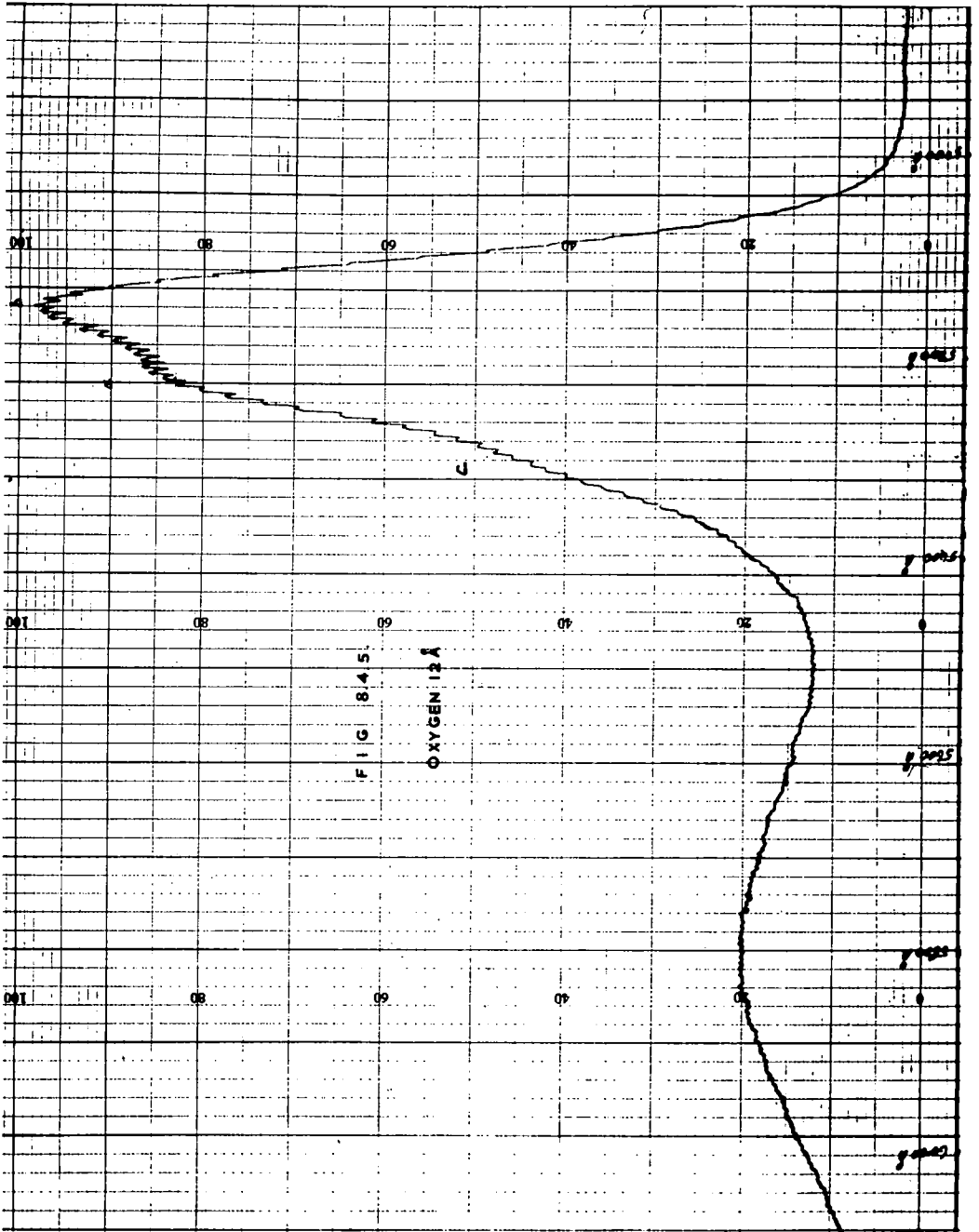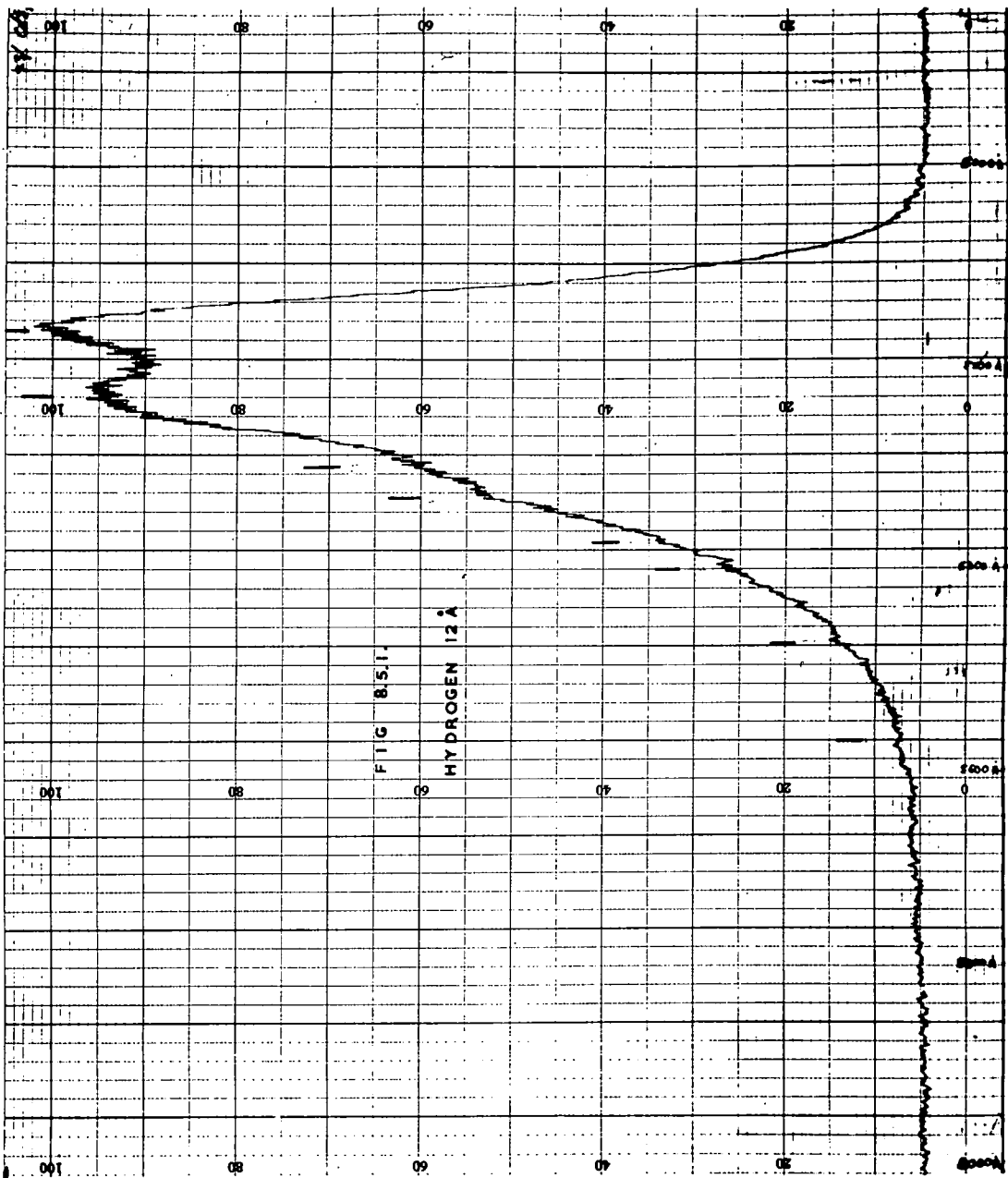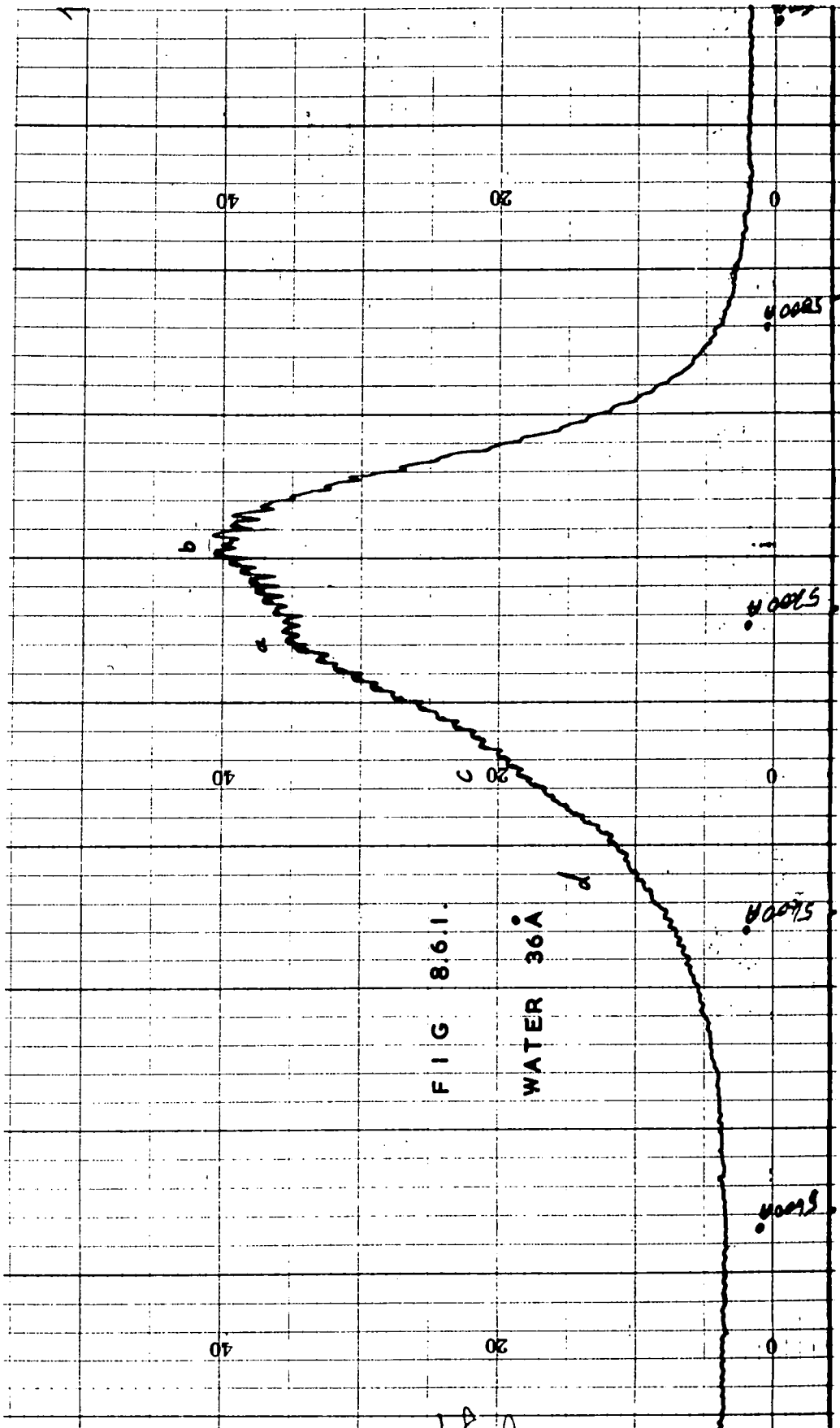
FIG 8.6.1.

WATER 36Å

8.7. Emission from Crystals Doped with Chlorine

A marked change in the emission spectra was found with chlorine doped crystals. This is illustrated in Fig. 8.7.1. The first peak of the edge emission series was depressed relative to the remainder. No band outside the range of this series was observed.

8.8. Emission from Silver Doped Cadmium Sulphide

The silver doped crystals available were rather small. The emission spectrum was obtained by exciting a small number of these single crystals simultaneously. The spectrum is illustrated in Fig. 8.8.1. The edge emission series was affected in a manner similar to the previous section. These crystals may also contain chlorine in addition to silver.

8.9. Emission from Indium Doped Cadmium Sulphide

The indium doped crystals led to the spectrum depicted in Fig. 8.9.1. The edge emission is very nearly swamped by the broad structureless band produced by the incorporation of indium. A small emission band was also observed at a higher energy than the main band.

8.10. Emission from Crystals Grown by Iodine Transport

Crystals grown containing iodine had the emission spectrum shown in Fig. 8.10.1. The relative intensities of

FIG. 8.7.1.

CHLORINE 36 Å

FIG 8.8.1

SILVER 12 Å

FIG 8.9.1.

INDIUM 12 A

FIG 8.10.1.

IODINE 12

a b c d

80   60   40   20   0

80   60   40   20   0

80   60   40   20   0

5500 A
5300 A
5400 A
5200 A
5600 A
5000 A
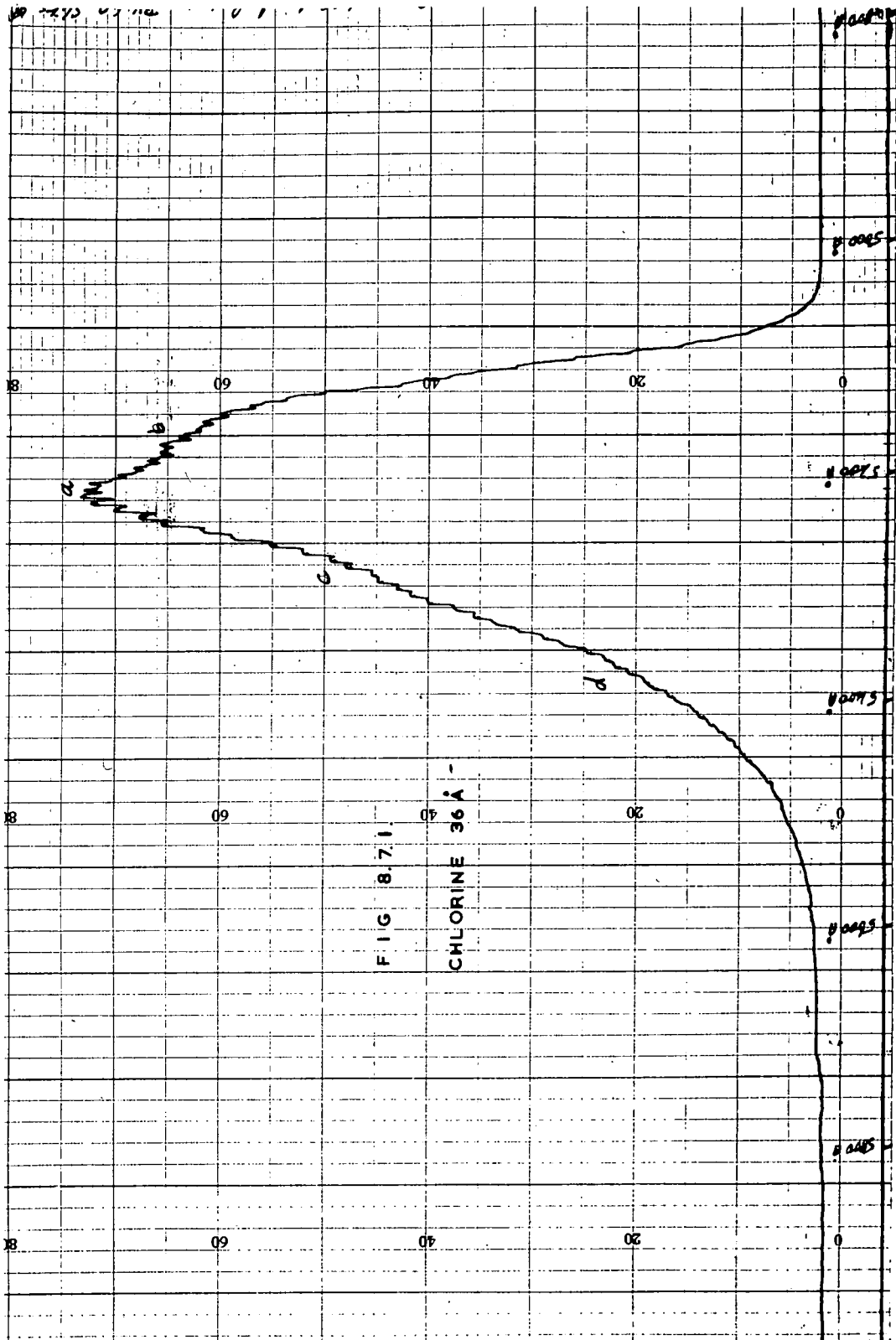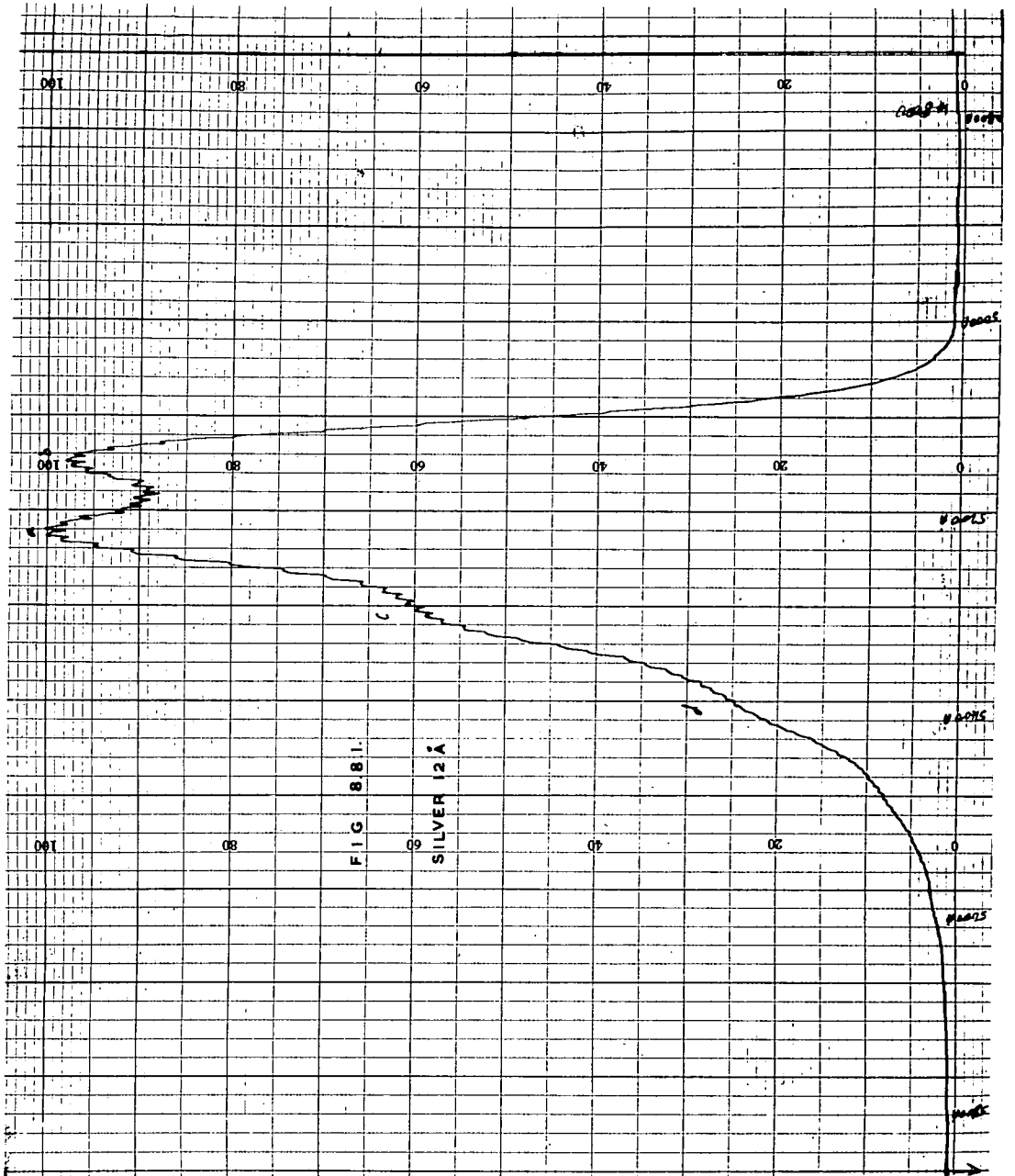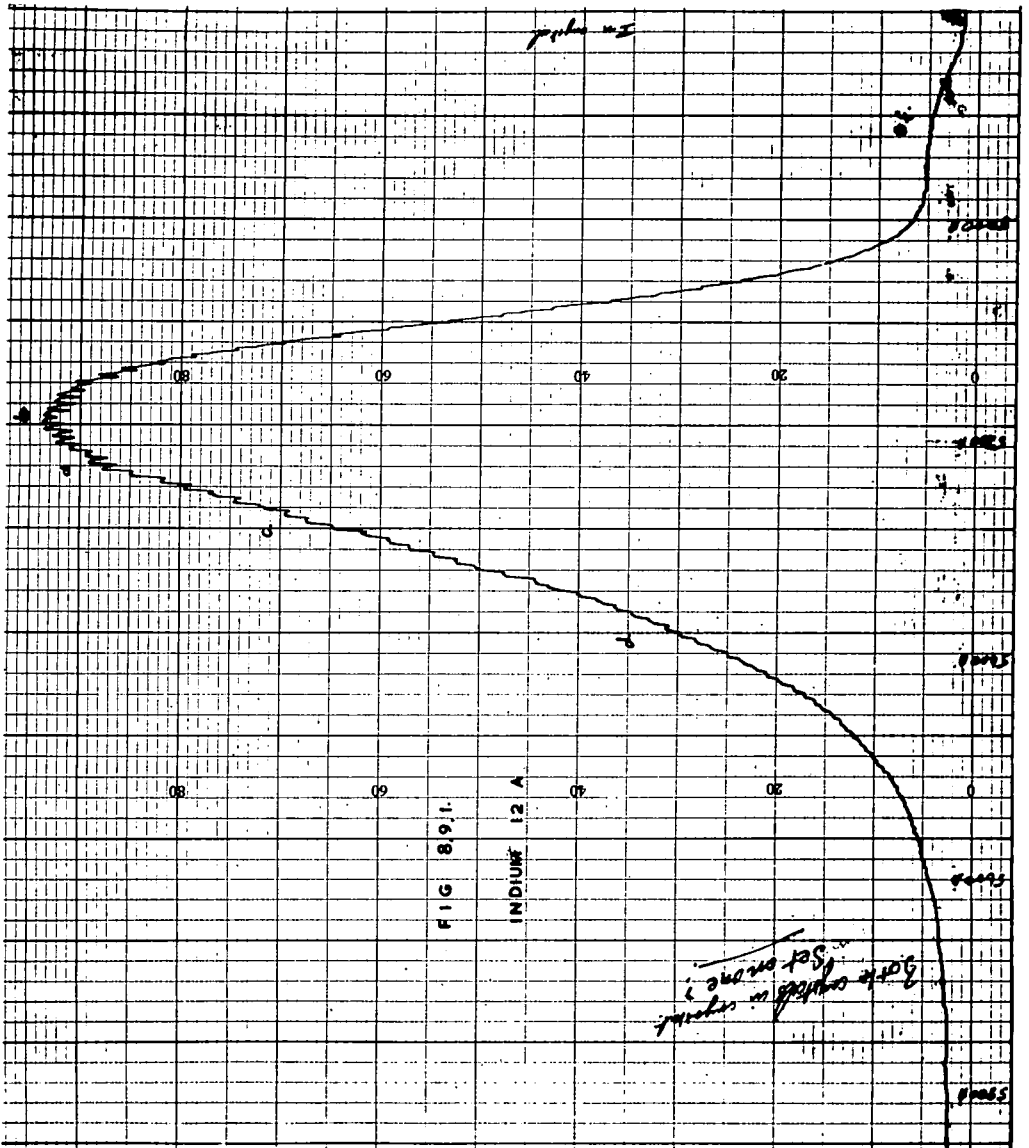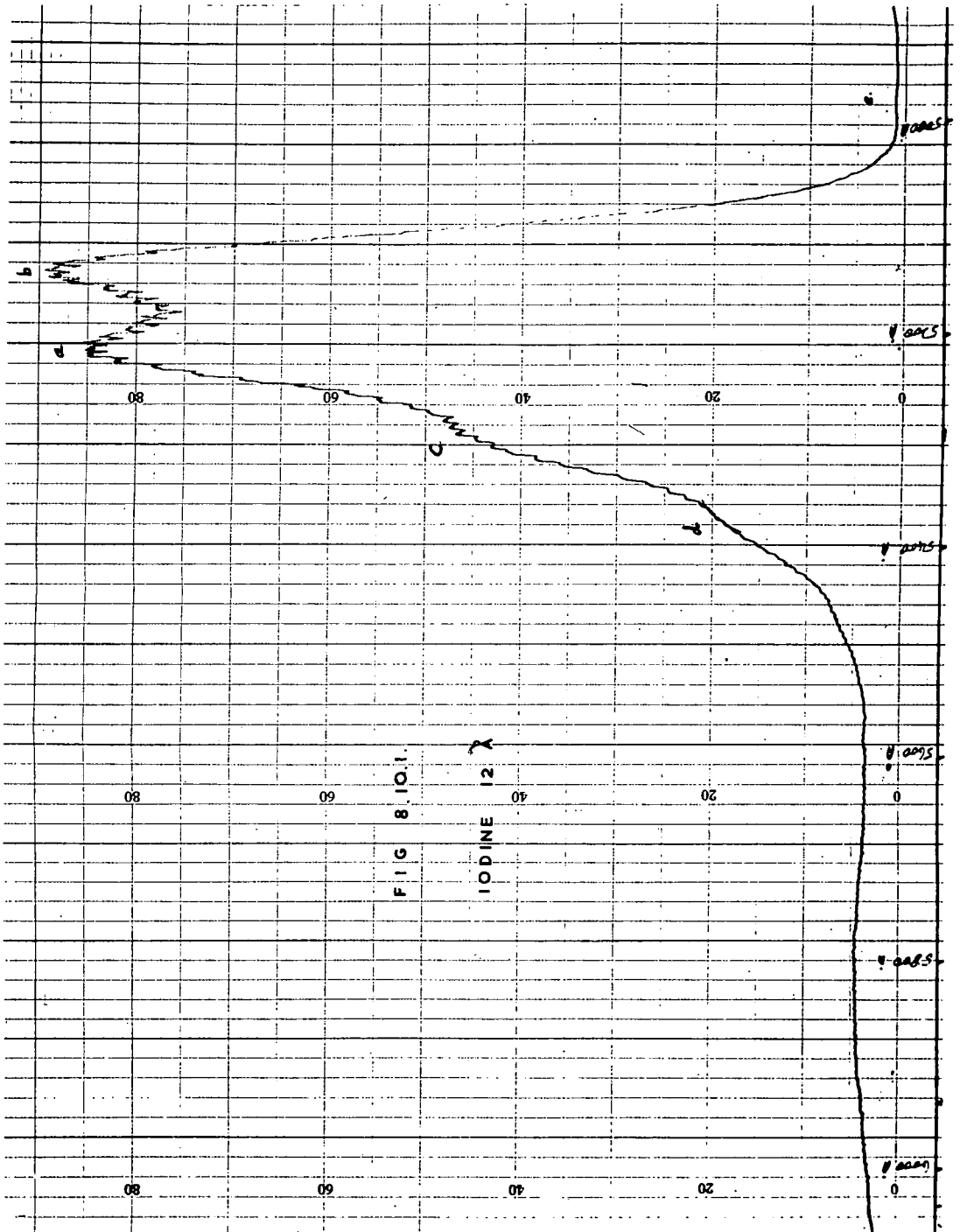
the first two edge emission peaks are different from those of a pure crystal. The broad band at 5800 $\overset{\text{o}}{\text{A}}$ was also observed in these crystals.

8.11. Spectral Distribution of Electro-luminescence

Low field electro-luminescence was produced in a thin, pure platelet of cadmium sulphide by attaching suitable electron and hole injecting contacts. The indium cathode was prepared in the usual way (section 7.3.). The anode was silver painted on to the crystal from a colloidal suspension prepared by Acheson Colloids Ltd. The crystal was mounted on to a copper plate which in turn was secured to the central copper block of a metal cryostat in order to assist the dissipation of heat. I am grateful to A. Rushby of this department for applying the contacts to this crystal. A current of 50 milliamps passed through the crystal when a constant voltage of 40 volts was applied at 77°K. The spectral distribution of the recombination luminescence is illustrated in Fig. 8.11.1. Bands, corresponding to those of the ultra-violet stimulated edge emission, were observed, together with two bands at shorter wavelengths. The thickness of the crystal was of the order of 30 microns, and the area of the contacts $2.5.10^{-2}$ sq.cms.

8.12. Emission Measurements from O.5 to 3.5 microns.

The crystal which provided the electro-luminescent
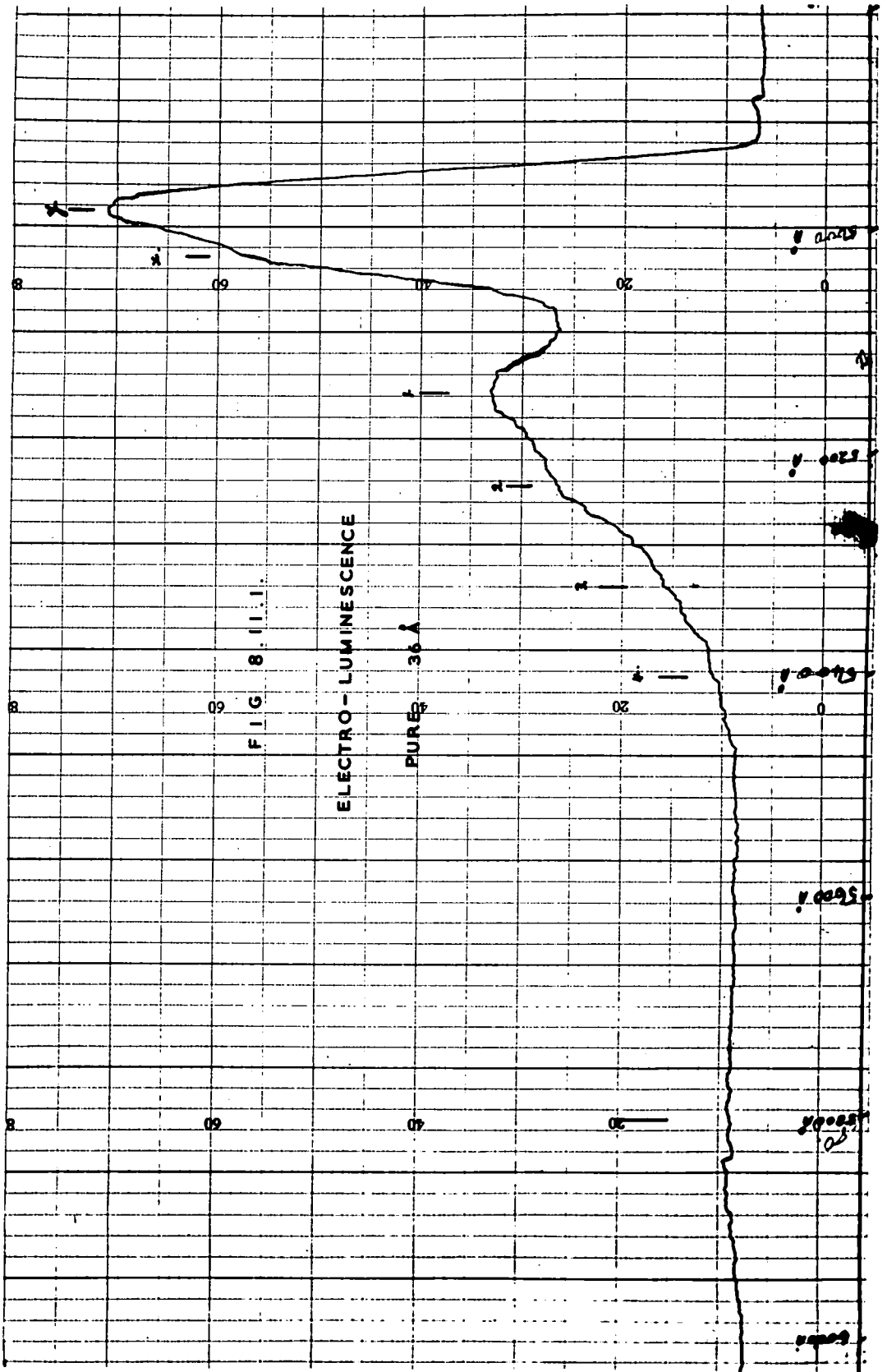
FIG 8.11.1.

ELECTRO-LUMINESCENCE

PURE₀   36 Å

measurements was also used as a fluorescent source with the
apparatus described in section 8.2.(b). The spectrum
obtained under ultra-violet excitation is shown in Fig.
8.12.1. The emission was measured at 77°K and room temper-
ature. The results are corrected for the variation in
dispersion of the prism monochromator. It was necessary
to use the manufacturer's data to correct for the spectral
sensitivity of the lead sulphide cell, because the differential
thermopile contained a broken compensating junction. The
resolution decreased from approximately 50 Å to 0.2 microns
with the wide slits ($\sim$ 0.5 mms) required to obtain a detectable
signal. The bias across the lead sulphide photocell was
100 volts. The silica window was thin (1 mm) and did not
cause appreciable absorption. The effect of water vapour in
the atmosphere, with an absorption band at approximately
2.7 microns was not known. A discussion of the peaks
observed, principally at 0.66 μ, 1.3 μ and above 3.5 μ, will
be found in Chapter X. A subsidiary experiment was carried
out to detect possible reflected radiation from the mercury
discharge lamp. This was done by focussing the filtered
radiation from the lamp directly into the monochromator. The
spectrum obtained has a maximum at 2.3 microns and showed
that the contribution from this lamp to the measured spectrum
was negligible. During the course of this investigation it
was observed that the infra-red emission above 2.5 microns

FIG. 8.12.1.

PURE. 50Å → 0·2μ

—— 7·7 °K
- - - 2·95 °K
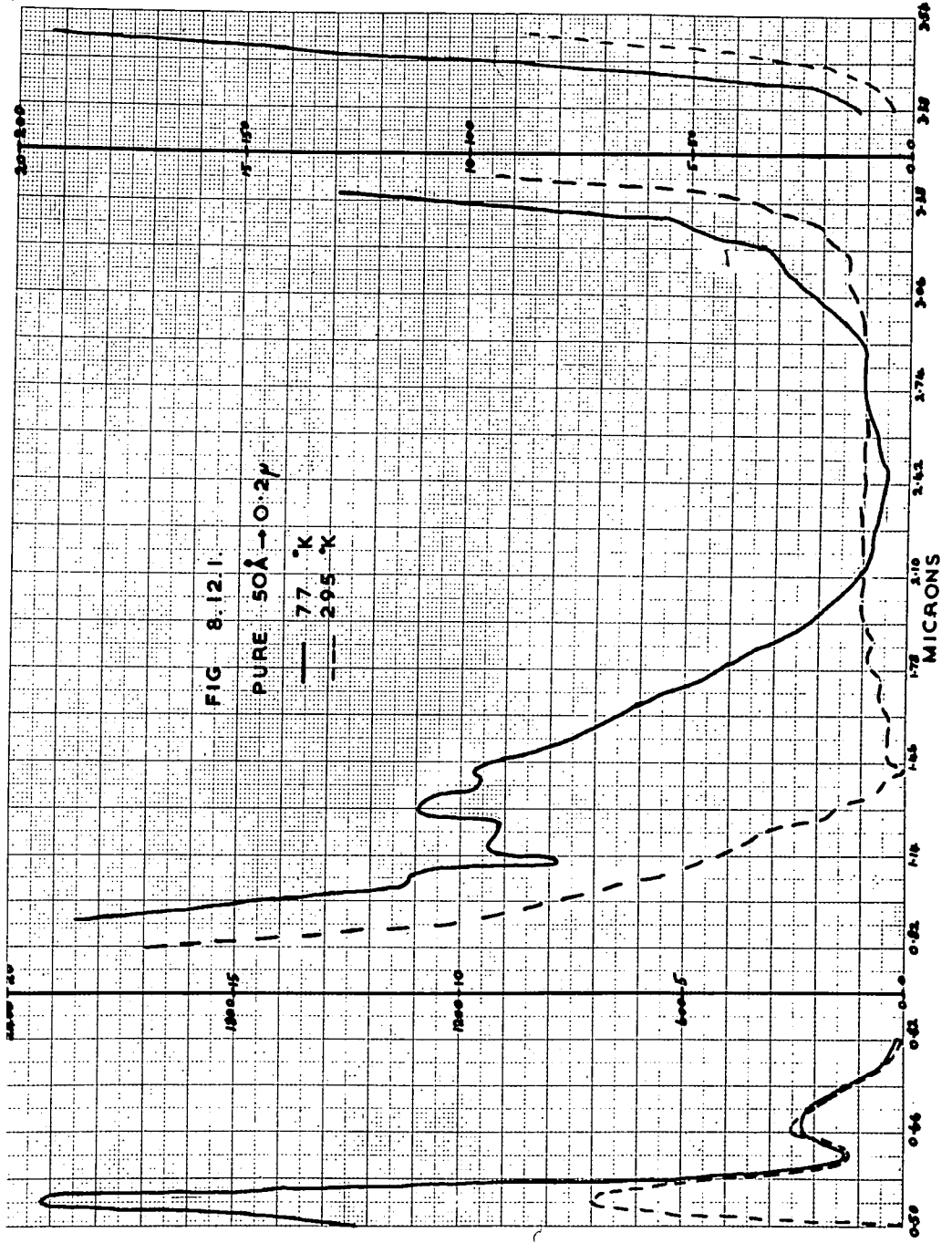
MICRONS

could be quenched with radiation from a small lamp with

a peak output at 1.6 microns.

Unfortunately it proved impossible to measure the

edge emission from this crystal using the grating spectro-

photometer because insufficient light could be directed into

the entrance slit.

CHAPTER IX

Interpretation of Electrical Measurements

9.1. Analysis of the Temperature Variation of the Direct Current-Voltage Characteristics

The large variation found in the resistivity of cadmium sulphide as the result of successive heat treatments at temperatures above $100^{\circ}C$, see Fig. 7.4.2., indicates that care must be taken to establish reproducible current-voltage characteristics. In order to achieve this the crystals used here had to be heated in the dark for a minimum period of 2 hours at $140^{\circ}C$, whilst shorted to earth.

The current voltage curves shown in Fig. 7.4.3, and similar ones for two other crystals, have been analysed, assuming that two discrete sets of centres exist within the forbidden gap (65). These centres are associated with (1) shallow donor levels of density N_D cm^{-3} and (2) deep acceptor levels with a density N_A cm^{-3} and depth E_A eV below the conduction band. The acceptors compensate the shallow donors to produce high resistivity crystals. (71). The thermal equilibrium electron concentration in these circumstances is

$$\bar{n} = \frac{N_c}{\chi} \exp - \frac{E_A}{kT} \qquad 9.1.1.$$

if $\chi = N_A/N_D \gg 1$. N_c is the effective density of states

in the conduction band. (equation 1.5.5.). Assuming
that the mobility varies as $T^{-3/2}$ in the temperature range
employed (40), the electrical conductivity, σ, can be
expressed as

$$\sigma \quad = \quad \frac{e \, \mu_o \, T_o^{3/2}}{\chi} \quad 2 \left(\frac{m_e^* \, k}{2\pi \, \hbar^2} \right)^{3/2} \exp - \frac{E_A}{kT} \qquad 9.1.2.$$

where μ_o is the mobility at temperature T_o. A plot of log σ
against 1/T should yield a straight line from which χ and
E_A can be determined. A typical experimental plot is shown
in Fig. 9.1.1. Below room temperature the points do not
lie on the straight line, since in this range the conductivity
was too high. Values of χ and E_A determined from the
straight line portion of the curves for the three crystals
mentioned are (i) χ = 240. E_A = 0.61 eV. (ii) χ = $1.8.10^5$.
E_A = 0.61 eV. (iii) χ = 141. E_A = 0.61 eV. Values of
μ_o = 210 cm^2/volt.sec. (36) and 0.2 m_e (37) were assumed
for the electron mobility at 300^oK (T_o) and the effective
mass respectively.

A second analysis can be made from the characteristics
of Fig. 7.4.3. as follows. According to equation 3.2.3.
the voltage, V_o, at which the curve departs from Ohm's
law is

$$V_o \quad = \quad \frac{ed^2}{2\epsilon\theta} \quad \bar{n} \qquad\qquad 9.1.3.$$

where θ is the ratio of free to trapped charge (21) and

ANALYSIS OF I/V CHARACTERISTIC
FIG 9.1.1.

see fig. 7.4.3
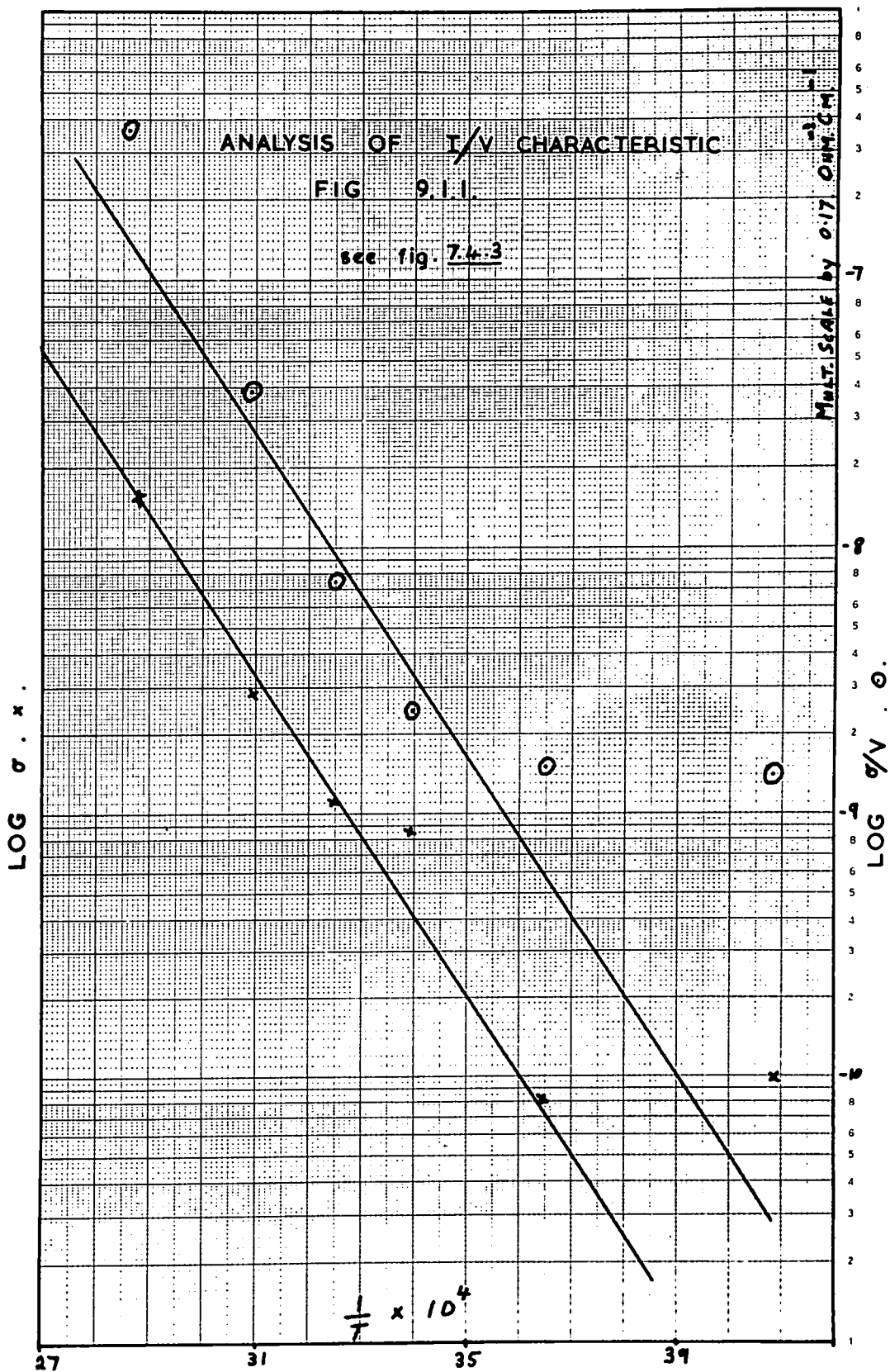
$$\Theta \ = \ \frac{N_c}{N_A} \ \exp \ - \ \frac{E_A}{kT} \qquad\qquad 9.1.4.$$

Equations 9.1.3. and 9.1.4. can be combined to eliminate Θ. If $\mu \ = \ \mu_o T_o^{3/2} \ T^{-3/2}$ then

$$\frac{\sigma}{V_o} \ = \ \frac{2\xi\mu_o T_o^{3/2}}{N_A \ d^2} \ 2 \left(\frac{m_e^* k}{2\pi \ \hbar^2} \right)^{3/2} \exp - \frac{E_A}{kT} \quad 9.1.5.$$

A plot of log σ/V_o against $1/T$ should also lead to a straight line from which N_A and E_A can be determined. Such a plot is shown in Fig. 9.1.1. in addition to the log σ versus $1/T$ line already described. Above room temperature, a satisfactory straight line is again obtained. Values of N_A and E_A obtained in this way for the three crystals are (i) $N_A = 2.4.10^{14}$ cm^{-3}. $E_A = 0.61$ eV. (ii) $N_A = 3.1.10^{16}$ cm^{-3}. $E_A = 0.61$ eV. (iii) $N_A = 6.8.10^{14}$ cm^{-3}. $E_A = 0.61$ eV.

The two sets of values obtained from the two independent lines of Fig. 9.1.1. can be combined to determine the density of donors N_D. The values obtained are (i) $N_D = 10^{12}$ cm^{-3} (ii) $N_D = 1.7.10^{11}$ cm^{-3} (iii) $N_D = 4.8.10^{12}$ cm^{-3}.

According to Lampert's theory of s.c.l. current-flow with trapping, the total trap density, N_t, can be determined by inserting the traps-filled-limit voltage, V_{TFL}, in equation 3.2.2. The experimental values of N_t are (i) $N_t = 3.0.10^{13}$ cm^{-3} (ii) $N_t = 1.7.10^{11}$ cm^{-3} (iii) $N_t = 4.8.10^{12}$ cm^{-3}. If Lampert's theory is correct one would expect that

$N_t = N_A$.

The values of N_A, N_D, N_t, E_A and χ for the three crystals examined are tabulated in Table 9.1.2. The results marked (i) refer to a similar analysis of yet another crystal described in earlier work (65). From Table 9.1.2. it can be seen that $N_t = N_A$ in one crystal only. The value of N_t for crystal (ii) is five orders of magnitude smaller than N_A. The calculations based on the temperature variation of the current-voltage characteristics clearly give a more realistic estimate of the total trap density, but immediately require an explanation for the failure of Lampert's theory. In an attempt to resolve this problem the technique measuring thermally stimulated currents was used to obtain independent information concerning the trapping spectrum.

9.2. Analysis of Thermally Stimulated Current Curves.

1. Methods of Analysis

There are many methods by which a thermally stimulated current curve (section 7.5.) can be evaluated. Nicholas (46) has recently investigated the validity of several methods of analysing glow curve data obtained from crystals similar to those used in this work. The following four methods have been applied here.

a) The Garlick and Gibson method.

The method used by Garlick and Gibson (72) relies on the

	E_A(eV)	N_A(cm^{-3})	N_D(cm^{-3})	N_t(T.F.L.)(cm^{-3})	χ
(i)	0.61	$2.4 \cdot 10^{14}$	$1.0 \cdot 10^{12}$	$3.0 \cdot 10^{13}$	240
(ii)	0.61	$3.1 \cdot 10^{16}$	$1.7 \cdot 10^{11}$	$3.0 \cdot 10^{11}$	$1.8 \cdot 10^{5}$
(iii)	0.61	$6.8 \cdot 10^{14}$	$4.8 \cdot 10^{12}$	$1.0 \cdot 10^{13}$	141
(iv)	0.61	$2.2 \cdot 10^{13}$	$9.1 \cdot 10^{10}$	$2.0 \cdot 10^{13}$	242

Values of N_A, N_D, N_T and E_A

TABLE 9.1.2.

fact that after the traps have been filled at room temperature or 77^OK the current carried by electrons released from the traps is given by $\Delta I = $ const. exp. $(-\frac{E}{kT})$, provided the crystal is heated at a uniform rate. This relationship is independent of the kinetics of the recombination mechanism of the excited carriers. In the present work, the concept of recombination is rather different from that usually considered and refers to the removal of trapped electrons which have been injected into the crystal and therefore constitute a net negative charge. In the normal situation, charge neutrality prevails and free electrons recombine with trapped holes. A plot of log $_e$ ΔI against 1/T for the initial rise of the thermally stimulated current should give a straight line of slope $-E/k$. Energy depths obtained from these plots will be referred to as E_{GG}.

b) Grossweiner's Approximation

An approximation due to Grossweiner (73) is applicable when thermally freed carriers are not appreciably retrapped before recombination occurs. The depth of the trapping levels according to Grossweiner is given by

$$E_G = \frac{1.5 \ kT^* T'}{T^* - T'}$$

where T^* is the temperature of the thermally stimulated current maximum and T' the temperature, lower than T^*, at which the thermally stimulated current reaches one half its

maximum value.

c)   Lushchik's Method

The method devised by Lushchik (74) is applicable
when fast retrapping occurs.   The trap depth is then given
by

$$E_L \quad = \quad \frac{kT^{*2}}{T'' - T^*}$$

Here T'' is the temperature above the maximum at which
the thermally stimulated current is one half its peak value.

d)   Bube's Fermi Level Analysis

Another technique which can be used under fast retrapping
conditions is due to Bube (18. p.292).   Bube assumes that
the trapping levels are half filled when the stimulated
current reaches its maximum value.   The depth of the trapping
levels then coincides with the quasi Fermi level.

$$E_B \quad = \quad kT^* \log_e \frac{N_c}{n^*}$$

Here n^* is the density of electrons in the conduction
band when the stimulated current reaches a maximum.

2.   Results of the Analysis applied to Measurements
     made under Ohmic Conduction Conditions

Thermally stimulated currents have been measured in
two crystal plates using a monitoring voltage in the Ohmic
range. (section 7.5.).   The trap depths determined using
the above four analyses are tabulated in Table 9.2.1.   The
values listed under (iv)a, (iv)b refer to two separate sets

	Peak at 54°C				Peak at 121°C			
	(iv)a	(iv)b	(ii)		(iv)a	(iv)b	(ii)	
E_G	0.76	0.79	1.57	eV	0.49	–	0.84	eV
E_L	1.02	0.68	0.73	eV	0.63	0.78	0.96	eV
E_B	0.59	0.63	0.85	eV	0.75	0.75	0.93	eV
E_{GG}	0.71	0.42	0.87	eV	0.28	0.18	0.64	eV

(iv)a, (iv)b apply to crystal (iv) Table 9.1.2.
    See also curves 4 and 5 respectively
    Fig. 7.5.1.

(ii) apply to crystal (ii) Table 9.1.2.

Analysis of Thermally Stimulated Currents

TABLE 9.2.1.

of measurements made on the same crystal, and are those
obtained from the curves 4 and 5 of Fig. 7.5.1. respectively.
Typical Garlick and Gibson plots of $\ln \Delta I$ versus $1/T$ are
shown in Fig. 9.2.2. The total trap densities obtained
from the two analyses of the last section showed that $N_t = N_A$
for this crystal. The values listed under (ii) refer
to the crystal in which the largest discrepancy between N_t
and N_A was found. (see Table 9.1.2.).

Nicholas (46), using similar crystals, observed three
conductivity glow maxima in the temperature range 20°C to
140°C, namely a double peak near 50°C, and a single peak
near 120°C. The double peak was associated with energy
levels at 0.41 eV and 0.83 eV, while the 120°C peak was
thought to be due to a trap at 0.63 eV. This trap had a
very large cross-section for electron capture. The suggestion
was put forward that an energy of 0.83 eV was required to
destroy a complex defect while simultaneously ejecting an
electron. All three maxima disappeared after heating the
crystal above 100°C in the dark. It will be seen that the
three major glow peaks observed in the present work can be
identified with the 0.41 and 0.83 eV double peak and the
0.63 eV level described by Nicholas.

The two conductivity glow curves shown in Fig. 7.5.1.
indicate that the injection of excess charge alters the
distribution of the two trapping levels. The relative

(iv) a. fig 7.5.1.(4)

slope 0.71 eV

slope 0.28 eV

LOG ΔI

LOG ΔI vs. 1/T

FIG 9.2.2

1/T × 10⁴
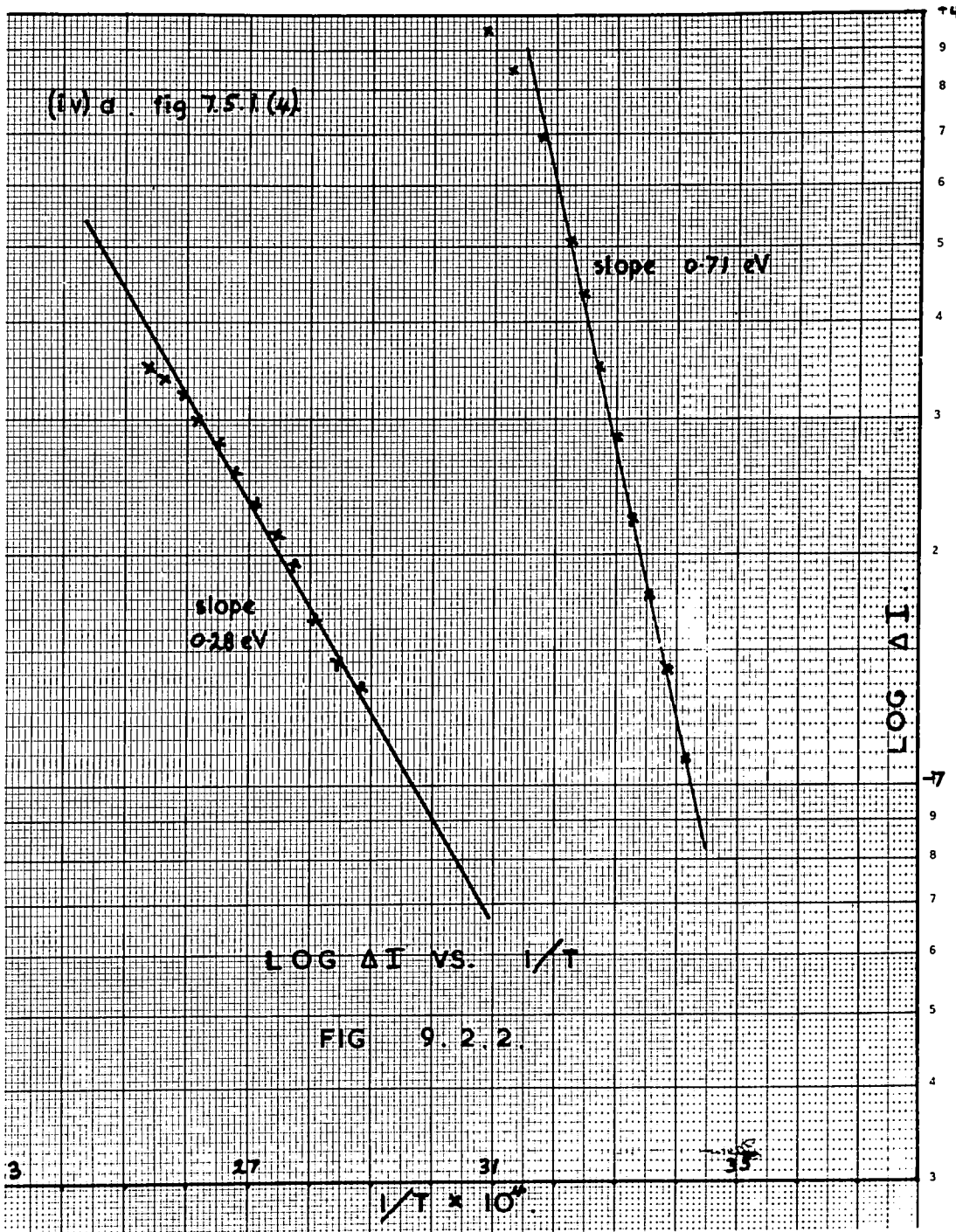
heights of the two thermally stimulated current maxima
are not the same in the two experiments which were performed
using the same injection current. A reduction in the
maximum near 120°C is accompanied by an increase in the peak
near 50°C. The passage of a high current, altering the
distribution of the 0.41 eV and 0.63 eV levels, could assist
in explaining the discrepancies in total trap densities
calculated from the current-voltage characteristics by the
techniques described in the preceding section. The traps-
filled-limit voltage would not then necessarily be related
to the total trap density as suggested by Lampert, even
though a trap-filling mechanism still determines the main
features of the current-voltage characteristic. This is
discussed further at the end of this chapter.

The values obtained by applying the four analytical
methods to conductivity glow curves obtained after charge
injection must be treated with reserve for two main reasons;
(1) the neglect of diffusion and (2) the fact that no thermal
cleaning was done.

(1) The contribution of carrier diffusion processes
to the current flow has been neglected. The diffusion term
is small with respect to the drift component provided the
applied voltage $\gg$ 25 mV (20). The values (iv)a.b. were
obtained with an applied voltage of between 50 and 100 mV
(depending on the voltage across the measuring resistor,
section 7.5.) and the diffusion contribution to the total

current may have been significant. In contrast the values
(ii) were obtained with an applied voltage between 2.4 and
2.5 volts. Then, although diffusion would have been
negligible there may have been some injection taking place
while the thermally stimulated current was being measured.

(2) No thermal cleaning of the maxima was done.
Thermal cleaning is a technique advocated by Nicholas (46)
to isolate thermally stimulated current peaks. The procedure
is as follows. The thermally stimulated current is monitored
up to some temperature below T^*. The crystal is then recooled
and reheated while the current is monitored again. In this
way, electrons are removed from unwanted traps and the effects
of overlapping peaks can be eliminated. There was considerable
overlapping of the peaks in our experiments. Differences
in thermal glow peaks, due to the different recombination
mechanism mentioned earlier, are discussed in 9.5.(a).

Nicholas (46) also found that the peaks near $50^{\circ}C$
were associated with monomolecular recombination processes
so that the methods of Bube and Luschik are not applicable.
Grossweiner's technique should be valid, but cannot be
used because of the indeterminate width of the double peak,
and the lack of thermal cleaning. The reasons for relating
the peaks found in this work with the double peak discussed
by Nicholas are the positions of current maxima on the
temperature scale and the values 0.71, 0.42 and 0.87 eV

obtained from the Garlick and Gibson method of analysing glow curves.

On the other hand, according to Nicholas the $120^{\circ}C$ peak should be associated with fast retrapping. Thus Grossweiner's analysis cannot be employed in this case. Overlapping of the thermally stimulated current curves accounts for the low values of E_{GG} quoted in Table 9.2.1. However, Bube's method should now apply. Unfortunately it relies on the crystal dimensions, and uncertainty in these can explain the high values obtained using this method on the $120^{\circ}C$ peak. Similar uncertainty in the position of T'' for this peak, which was near the high temperature limit of measurement, makes E_L uncertain. The one value of 0.63 eV in Table 9.2.1. is the only justification, apart from the temperature of the maximum, for relating the $120^{\circ}C$ peak with this energy level.

All the energy levels labelled (ii) Table 9.2.1. were higher than those determined for the other crystal (iv). This may be due to the higher applied voltage causing some injection of excess charge, or alternatively the high values may be associated with the high trap density (N_A) of this crystal (see Table 9.1.2.).

The activation energy of the curve marked 3 in Fig. 7.5.1. calculated from a Garlick and Gibson plot was 0.51 eV. This suggests that at low injection levels the 0.41 and

0.63 eV level were not being filled. The experimental errors in measuring the stimulated current after even smaller injection (curves 1 and 2, Fig. 7.5.1.) were too large to justify a log ΔI versus 1/T plot. The value of 0.51 eV refers to crystal (iv) and is to be compared with the values of E_{GG}, obtained at higher injection levels, given in Table 9.2.1. No significant thermally stimulated currents were observed at low injection levels when the monitoring voltage was $<$ 200 mV. This is attributed to spurious voltages (section 7.6.) and is discussed in the following section.

The variation of the dark conductivity with temperature measured during the course of the thermally stimulated current experiments, can be analysed according to equation 9.1.2. Crystal (iv) is again typical and a plot of the logarithm of dark conductivity versus 1/T is shown in Fig. 9.2.3. for this crystal. The high slope below $50^{\circ}C$ is typical of all crystals measured. The activation energy of 0.87 eV suggests it may be associated with the destruction of the complex defect. This effect would explain why the static current-voltage curve analysis of section 9.1. could not be applied below room temperature. The complex defect is discussed in more detail later in this chapter. The slopes of all plots like that in Fig. 9.2.3. gave an activation energy of 0.61 eV above $50^{\circ}C$, in agreement with

Crystal (b+)
table 9.1.2

slope 0.8 eV

slope 0.87 eV

LOG σ VS 1/T

FIG 9.2.3

1/T . 10⁴
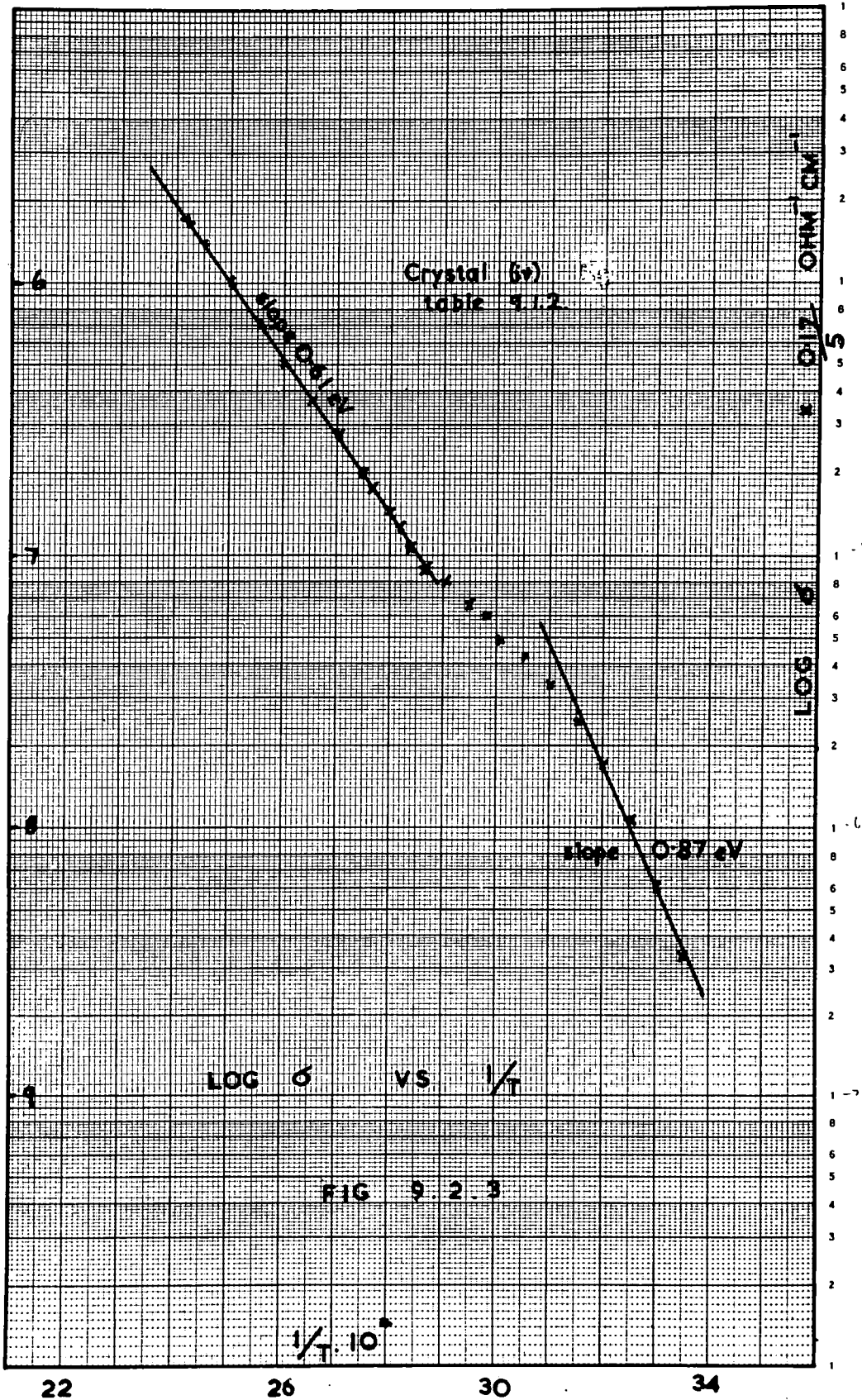
the trap depth obtained from the static current-voltage measurements. The intercepts similarly led to identical values of χ. The conclusions to be drawn from these facts are that the 0.61 eV level is present in the electrically neutral crystal, and that above 50°C this level governs the Ohmic conductivity. On the other hand, below room temperature the Ohmic conductivity is determined by the 0.41 eV level associated with the complex defect. An energy of the order of 0.83 eV is required to dissociate this level.

3. Conduction Conditions Non-Ohmic

The conductivity glow curves of Fig. 7.5.3., which were obtained in the so-called trap-filling region, can be analysed as follows. The "conductivity" $K = I/V^2$ in the reduced square law region is given by equation 3.2.1.

$$K = \frac{9 \Theta \epsilon \mu}{8 \, a \, d^3} \qquad\qquad 9.2.1.$$

Substituting for Θ from equation 9.1.4. we have

$$K = \frac{9 \epsilon \mu N_c}{8 \, a \, d^3 \, N_A} \exp - \frac{E_A}{kT} \qquad\qquad 9.2.2.$$

A plot of log K versus 1/T should be a straight line. This is illustrated in Fig. 9.2.4. where it can be seen that above 75°C the slope of the line gives a value for E_A of 0.15 eV. Between 75°C and 50°C the slope is 0.61 eV and below 50°C a

LOG K' vs. 1/T

FIG. 9.2.4.

slope 0.15 eV

slope 0.61 eV

$N_A = 2.1 \ 10^{13}$ traps. cms^{-3}

(see text)

LOG K

25   28   1/T 10^4 31   34
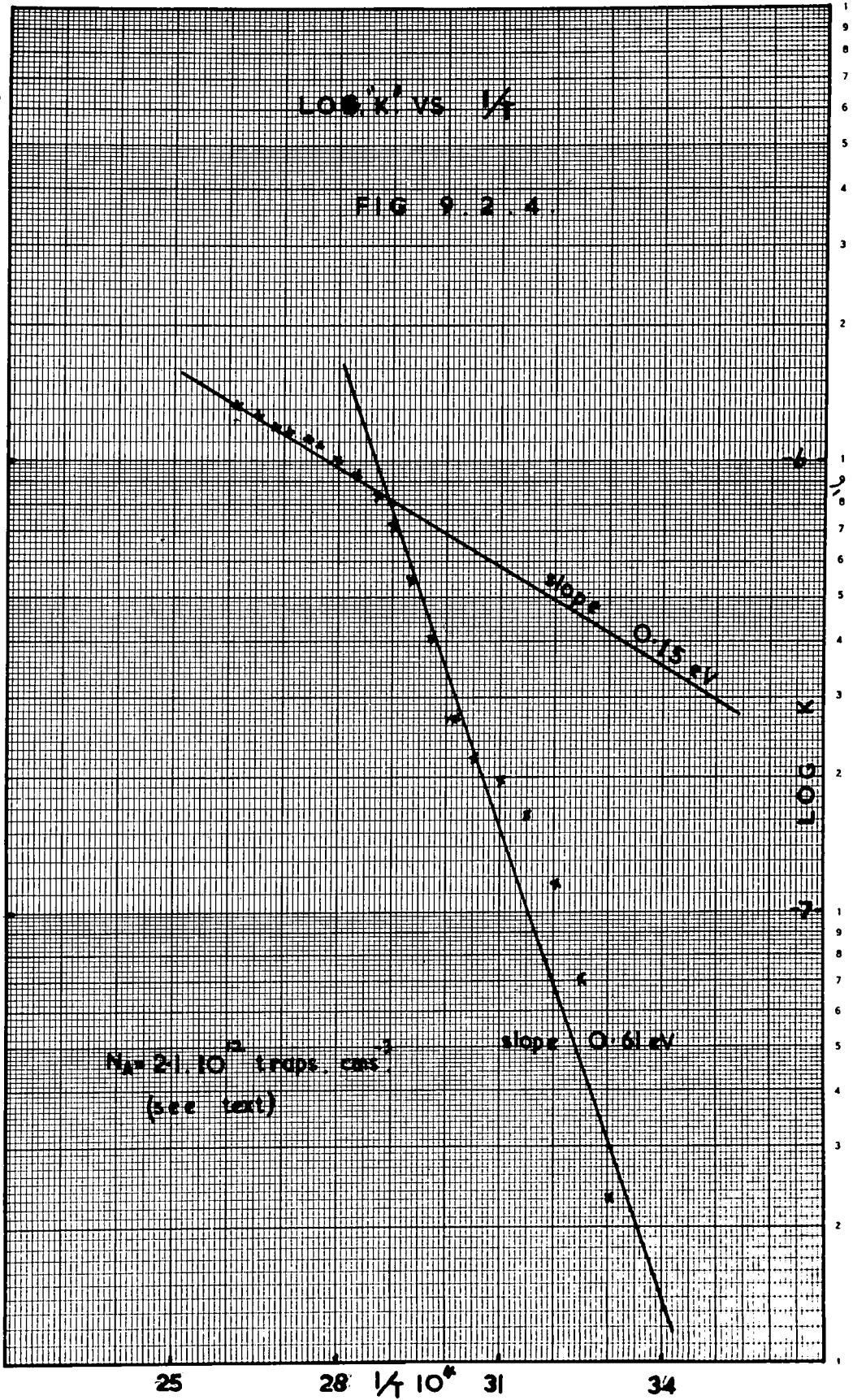
a straight line is not obtained. The high temperature behaviour is almost certainly due to the transient behaviour of the s.c.l. current as the temperature increased. The behaviour below 50°C may again be attributed to the complex level at 0.41 eV in terms of transient effects as the crystal is heated whilst passing a s.c.l. current. The intercept of the line with a slope of 0.61 eV gives a value of $2.1.10^{12}$ traps/cm^3. This is to be compared with a value of $2.2.10^{13}$ deduced from the variation of the current-voltage characteristic with temperature.

Thermally stimulated current maxima were obtained by subtracting the dark "conductivity" in the reduced square law region from the measured curve Fig. 7.5.3. The result is shown in Fig. 9.2.5. The error associated with the lower peak was too large to justify any deductions. A value of 0.73 eV was obtained for the higher temperature peak using Grossweiner's method. The error incurred by subtracting the conductivities made the Garlick and Gibson method unsound. Neither is it clear how Bube's method is applicable to measurements in the s.c.l. region. Furthermore, T'' lay outside the range of measurement and therefore Luschik's technique could not be applied. However, it does seem possible to detect thermally stimulated currents under s.c.l. conditions. If this technique is developed, analyses of

ΔK VS T
FIG 9.2.5.
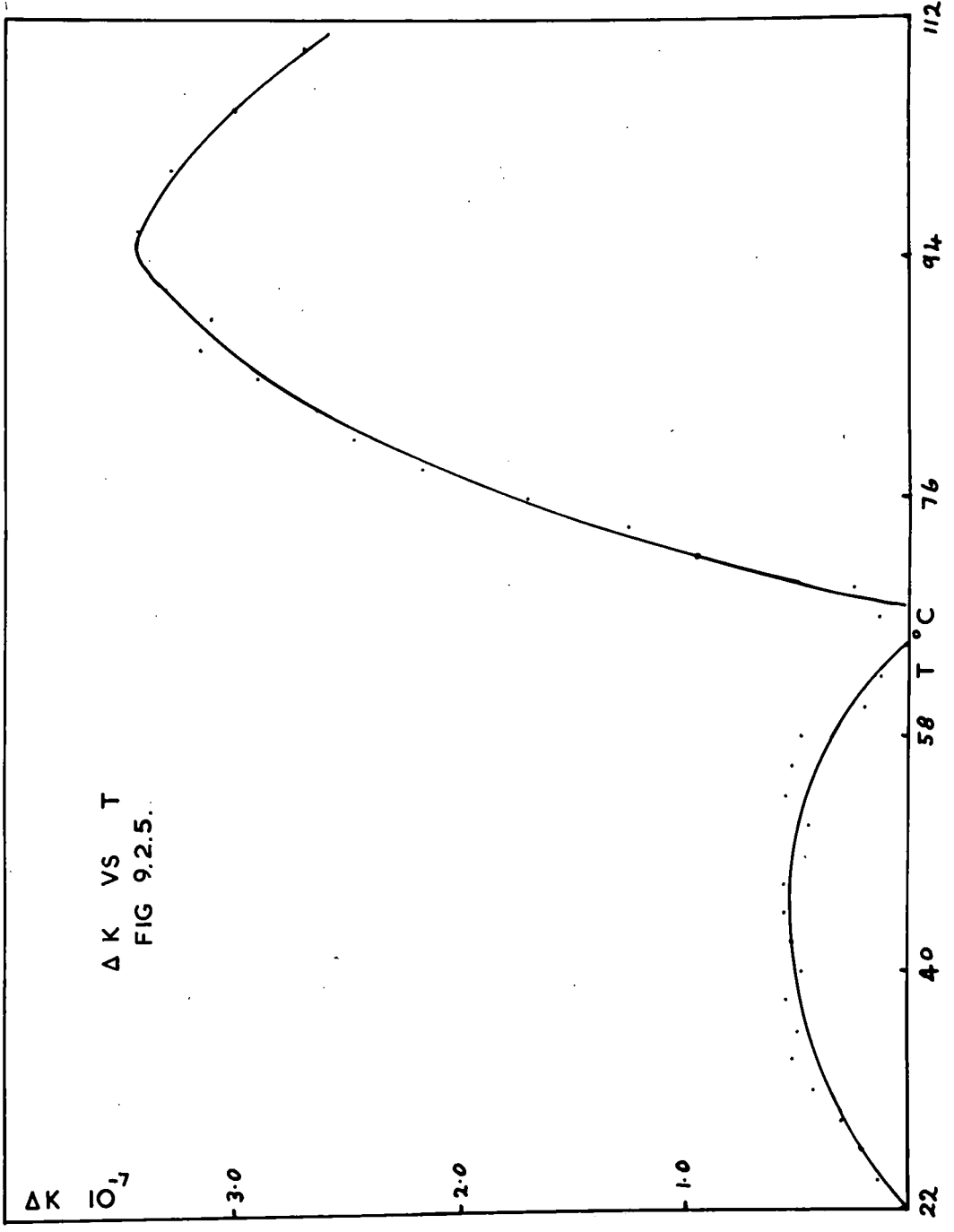
curves taken with voltages $\gg$ 25 mV can eliminate diffusion effects. The peaks were observed with a low (6.4 10^{-9} amps) injection level.

9.3. Consideration of the Spurious Voltages.

The spurious voltages discussed in section 7.6. are of the wrong polarity to be attributed to the Dember effect (75). The Dember effect arises when light is strongly absorbed at a semiconductor surface creating electron-hole pairs. If the electrons have the higher mobility, as they do in cadmium sulphide, they will diffuse away from the surface more rapidly than the holes. In consequence, the surface becomes positively charged. In this work, the anode was irradiated and became negative.

Ludwig (76) has observed photovoltages in cadmium sulphide with the same polarity as the spurious voltages we have found. He attributed the effect to a difference in barrier heights of the two contacts.

The effects described in section 7.6. were observed with two Ohmic contacts of the type illustrated in Fig. 1.9. In thermal equilibrium, there is an excess of electrons in the crystal near each contact. It is convenient for clarity to discuss the situation where the anode is neutral and the cathode is Ohmic for electron flow. This is illustrated in exaggerated form in Fig. 9.3.(a). The difference in
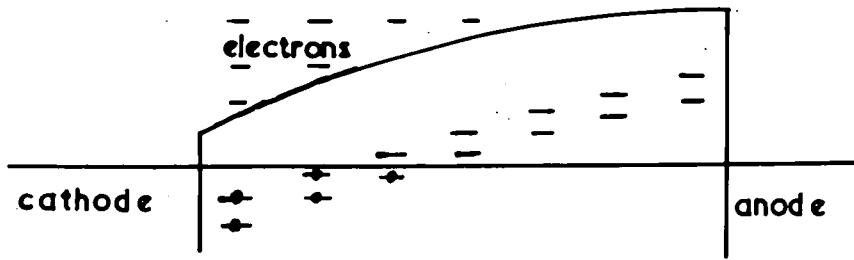
(a) thermal equilibrium

— empty trap   ⊸ filled trap
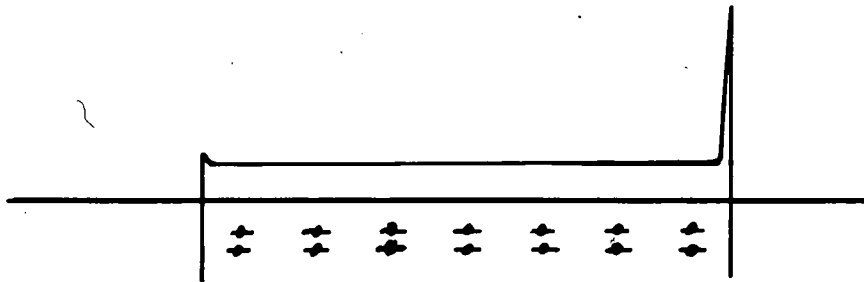
(b) under intense illumination

ORIGIN OF SPURIOUS E.M.F.'s

FIG 9.3

work functions of the crystal surfaces may be due to
surface layers or the better cathode contact may be
associated with an n^+ - n junction (77). It will be assumed
that our crystals have some such asymmetry of the two indium
contacts. In thermal equilibrium the conduction band is
tilted and the distribution of trapped electrons in the
crystal is non-uniform. More electrons are trapped in
the vicinity of the cathode than near the anode. This is
illustrated in Fig. 9.3.(a). With light which is to the
long wavelength side of the absorption edge absorption
throughout the bulk of the crystal creates electron-hole
pairs uniformly and hence increases the bulk conductivity.
This in turn fills all the trapping levels and renders the
distribution of trapped charge uniform. Fig. 9.3.(b). On
removal of the illumination, there is an excess of trapped
negative charge near the anode which is responsible for the
observed voltages. A mechanism of this nature may be used
to explain the sign of the observed voltages. This appears
to be a genuine effect and it would be more appropriate
to refer to the spurious voltages as contact voltages. Infra-
red light would not have the same effect because free
electrons are not created, in fact infra-red quenching
reduces the concentration of both free and trapped electrons.
Thus the observation of a positive e.m.f. at high temperature
with infra-red excitation can be explained in terms of
the preferential release of trapped electrons near the anode.

A possible way to eliminate contact voltages might be to solder a blob of indium to the evaporated cathode layer before mounting the crystal on the cover slip (section 7.3.) to provide two more nearly symmetrical contacts.

An alternative explanation for the observed effects might be sought in terms of the temperature distribution across the sample. Thermo-e.m.f.'s are unlikely to be involved because of the controlled and reproducible way in which the contact voltage can be eliminated, Fig. 7.6.1.

The observation of peaks in the contact voltage versus temperature curves, measured after the injection of electrons, Fig. 7.6.2. and Fig. 7.6.3. suggests that at low injection levels the distribution of excess trapped, injected charge is non-uniform. At high injection levels the peaks disappear. This is probably due to the trapped excess injected charge becoming uniformly distributed throughout the bulk of the crystal although the total negative charge distribution remains non-uniform. The release of the trapped injected charge is observed when an external voltage is applied. (previous section). These measurements indicate that, at low injection levels, the contact voltages introduced by injection can have a pronounced effect on thermally stimulated current measurements. The contact voltage can be invoked to explain why thermally

stimulated currents were not observed until high current densities had passed through the crystal. At low injection levels there is preferential trapping near the anode opposing further injection. The field set up within the crystal is in the opposite direction to the monitoring voltage and effectively reduces it. If the internal voltage is a significant fraction of the applied voltage, thermally stimulated current curves can not be observed. This explanation does not apply when the monitoring voltage is much greater than the contact voltage. Under such circumstances, thermally stimulated current maxima can be observed following quite low levels of injection Fig. 9.2.5. The contact voltages were too small to have a significant effect on V_{TFL}. The reason for the reappearance of contact voltages after passing high currents at high temperatures, Fig. 7.6.2.(3), is not clear. The voltage might be associated with a non-uniform distribution of trapped charge in one level only. Thus it may only be observed when that particular level (possibly 0.61 eV) begins to empty as the temperature is increased.

9.4. The Ohmic Conductivity of Crystal B

The maximum in the equilibrium Ohmic dark conductivity versus temperature curve of crystal B, illustrated in Fig. 7.7.1, can not be attributed to a change in electron

mobility associated with the effects of ionised impurity scattering. The ionised impurity mobility is given by (3.p.166).

$$\mu_I = \frac{2^{7/2} K^2 (kT)^{3/2}}{\pi^{3/2} m_e^{*1/2} q^3 N_I} \left[\log\ (1 + b) - \frac{b}{1 + b} \right]^{-1}$$

where $\quad b = \dfrac{2\, m_e^{*}\, K\, kT(3kT)}{\pi\, q^2\, \hbar^2\, N_I}$

N_I is the density of impurity centres with charge q and K is the dielectric constant.

Using this expression the mobility limited by 10^{14} singly charged impurities per cm^3 would be of the order of 10^8 cm^2/volt.sec. at room temperature. As mobilities add reciprocally, a change from neutral impurity to ionised impurity scattering could not cause the observed change in conductivity.

When the experimental results were plotted in the form of log σ against 1/T, the curve shown in Fig. 9.4.1. is obtained. The two activation energies of 0.77 eV and 0.41 eV obtained from the low temperature part of the curve suggest that the complex defect, discussed earlier, is prominent in this crystal. It seems probable that the dissociation of the defect causes the decrease in conductivity as the temperature rises. Below room temperature the density of carriers

LOG σ vs 1/T

FIG. 9.4.1

Crystal B   O FIXED T
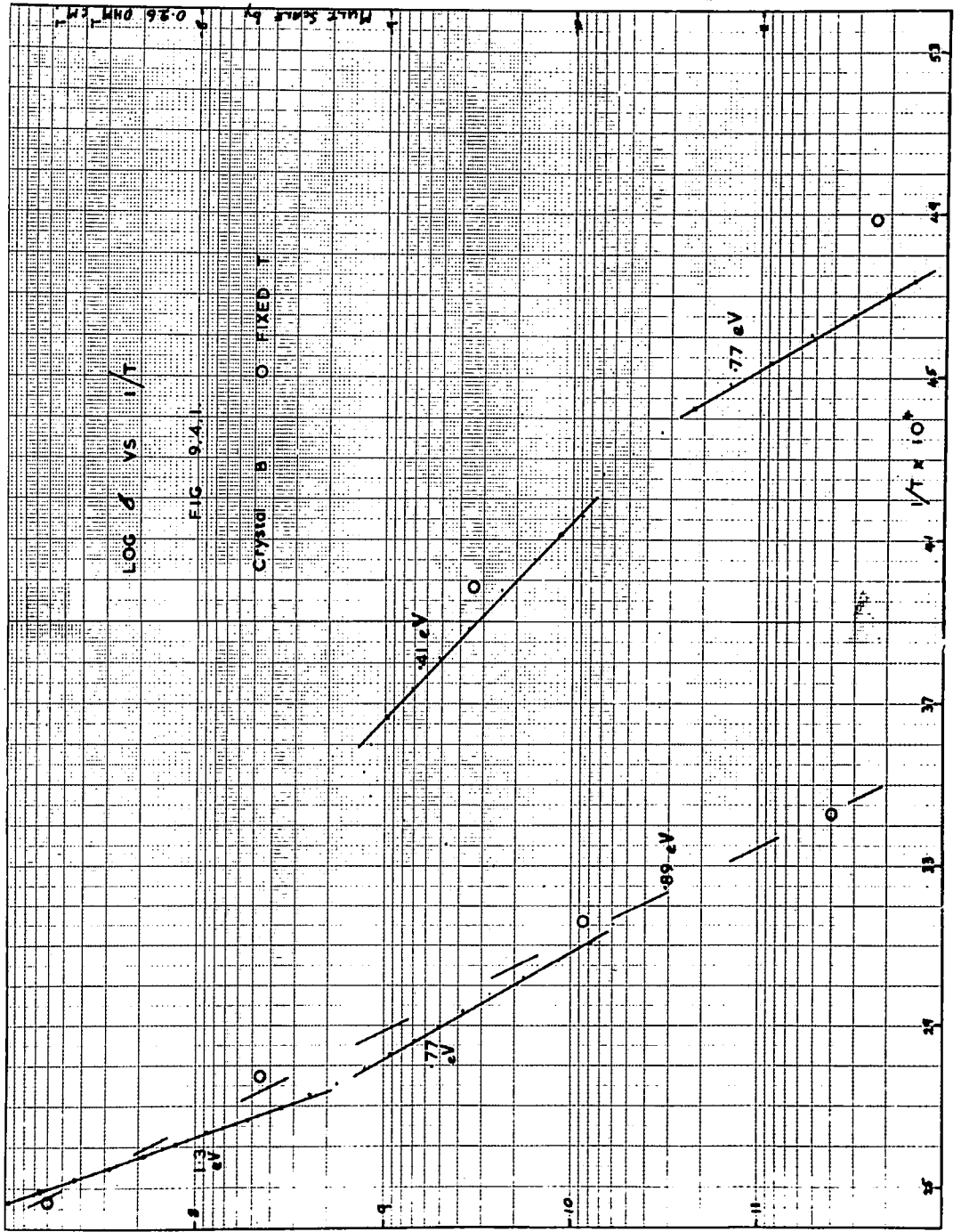
in the conduction band is determined by the level at 0.41 eV. Above room temperature this level is replaced by the 0.61 eV acceptor level with a consequent reduction in the conductivity.

The points obtained from the static-current voltage characteristics (Fig. 7.8.1.) are also plotted in Fig. 9.4.1. These points show that the change in conductivity is more abrupt than indicated by the measurements taken when the temperature was varying slowly. The static current voltage measurements above room temperature lie on a line with a slope 0.89 eV. This contrasts with other crystals where similar plots yield activation energies of 0.61 eV (section 9.1.). The energies of 0.77 eV and 1.3 eV, obtained from the straight line regions of Fig. 9.4.1. above room temperature, are probably due to transient effects. However the value of 0.89 eV may also be associated with the complex defect.

If it can be assumed that the decrease in conductivity which leads to the maximum in the curve is associated with the thermal destruction of an associated complex with the simultaneous ejection of an electron, analytical techniques appropriate to thermally stimulated currents can be employed on the peak. Thus values of E_A can be calculated for the peak in conductivity using the methods of section 9.2. These give values of $E_L = 0.55$ eV, $E_G = 0.50$ eV and $E_B = 0.70$ eV.

Grossweiner's method may well provide the best result
since the other two techniques require fast retrapping to
occur. This would not happen if the defect were destroyed.
However the value 0.50 is very low and none of the three
methods may be suitable.

A more satisfactory explanation of the shape of curve
7.7.1. in terms of a complex defect is as follows. Assume
equation 9.1.1. is valid and that $X \equiv N_A/N_D$ remains constant.
The rapid changes in conductivity are the result of the
destruction of a defect with a level at $E_A = E_1$ and the
simultaneous creation of a level at $E_A = E_2$. Therefore,
the densities of carriers, at lower and higher temperatures
than the conductivity maximum, are given by

$$\bar{n}_1 = \frac{N_c}{X} \exp - \frac{E_1}{kT} \qquad \qquad 9.4.1.$$

$$\bar{n}_2 = \frac{N_c}{X} \exp - \frac{E_2}{kT} \qquad \qquad 9.4.2.$$

If two points are considered, on either side of the peak
where the values of $\bar{n}$ are identical, equations 9.4.1. and
9.4.2. can be equated. Then

$$\frac{T_1}{T_2} = \frac{E_1}{E_2}$$

T_1 and T_2 are the temperatures at which the free
carrier density is $\bar{n}$. Comparing points on the curve of

Fig. 7.7.1. the two energy depths are in the ratio of $E_1/E_2 \approx 0.7$. Thus, assuming the peak is due to the destruction of the 0.41 eV centre, $E_2 \approx 0.60$ eV. The conversion of a complex defect centre with an associated level of 0.41 eV into a centre with an associated level at 0.61 eV, on a one to one basis, seems the most probable explanation for the reduction in conductivity. The activation energy for the transformation is probably of the order of 0.83 eV.

The ratio of the dark conductivity at the peak to that at the minimum (measured at constant temperature) was between 3.4×10^2 and 4.7×10^3. This compares with a value of 1.56×10^3 calculated from the ratio of the right hand sides of equations 9.4.1. and 9.4.2. This agreement lends further support to the proposed mechanism.

The small peak near -44°C may be due to the double nature of the complex defect. A more probable explanation is that it is associated with the complex nature of a different and shallower level. Nicholas (46) observed a trapping level at 0.25 eV which dissociated during intense illumination to be replaced by two centres with levels at 0.41 eV and 0.83 eV. The reaction could be reversed by heating in the dark at 100°C. This effect was observed in crystals rich in cadmium which did not contain a centre with a level at 0.63 eV. Nevertheless, it is possible that both complex defects could be present in the same crystal.

9.5.   Thermally Stimulated Currents in Crystal B.

Thermally stimulated current measurements have been made on crystal B using both electrical and optical excitation.

a) Electrical Excitation.

Three curves obtained after various levels of electrical injection are shown in Fig. 7.9.1. These curves have been analysed using all four methods discussed earlier in this chapter. The values obtained for the depth of the defect giving rise to the peak near $85^{o}C$ are listed in Table 9.5.1. With the exception of Bube's technique, all the methods gave very high values. These high values can be discounted since the methods are either not valid or easily applied to this case. Bube's method, however, does give satisfactory values. The failure of Luschik's method even though the recombination can be regarded as a fast retrapping mechanism may be due to diffusion effects. Luschik bases his analysis on a geometrical approximation to the shape of the peak. Thus it would be particularly sensitive to anomalies intro-duced when the diffusion component of the current becomes large with respect to the drift component. The minimum voltage applied to the crystal under these experiments was of the order of 70 mV.

A more physical explanation of the failure of the various methods of evaluating glow curves generally may be

	2.	3.	4.
E_G	1.45 eV	1.57 eV	1.85 eV
E_L	1.23 eV	1.27 eV	2.5 eV
E_B	0.62 eV	0.63 eV	0.64 eV
E_{GG}	0.73 eV	0.73 eV	0.73 eV

2. 3. 4., refer to Fig. 7.9.1.

Thermally Stimulated Currents in Crystal B.

TABLE   9.5.1.

I

due to the different mechanisms involved in a situation
where the traps are filled by injection compared with one
where the traps are filled by optical excitation. With
electrical injection, excess negative charge within the
crystal is compensated by positive charge on the anode. The
thermal release of the trapped charge and its subsequent
removal from the crystal to recombine with and neutralise the
charge on the anode results in the observed maxima. With
optical trap filling, the crystal remains neutral. The
release of trapped electrons and their eventual recombination
with holes is responsible for the normal thermally stimulated
current. It is probable that the peaks observed after
electrical injection are much sharper than the normal peaks
because the relaxation of excited charge is more rapid.
(i.e. the recombination process is different the gain factor

$\leqslant$ 1 section 2.8.). Further electrons can not enter and
leave the crystal as readily as they do when optical
excitation is used to fill the traps and the crystal is
neutral. The narrow peaks observed experimentally can be
explained on the basis of these considerations. The narrow
peaks in turn lead to the abnormally high calculated energy
values quoted in Table 9.5.1. Bube's method relies on the
position of the Fermi level coinciding with the trap depth
at the maximum of the glow peak. Such a method should be
valid for both excitation mechanisms, provided the recombination

process can be described as one of fast retrapping.

A peak is also observed in the thermally stimulated current curves of Fig. 7.9.1. near room temperature. This is probably due to the thermal emptying of injected charge from the level at 0.41 eV. The peak may also be associated with an increase in the density of the level at 0.41eV by the passage of a high current (discussed in section 9.2.2.). No thermally stimulated current due to the emptying of the suggested level at 0.25 eV was observed. Thus this shallow level was probably not being filled by the injected current.

b) Optical excitation.

The thermally –stimulated current curves obtained with crystal B after optical excitation are shown in Fig. 7.9.3. When band-gap light was employed, the peak near room temperature was large but the thermally stimulated current near 85°C was less than the Ohmic dark current. The absence of the maxima near 85°C associated with the 0.61 eV level can be interpreted as due to transformation of this level into a level at 0.41 eV. Thus band-gap light increases the density of the 0.41eV complex level at the expense of the 0.61 eV level. This is a similar effect to that observed by electrical injection (section 9.2.2.). The depression of the thermally stimulated current below the Ohmic dark current requires some deep level in the forbidden gap. Similarly, the depression of the Ohmic dark current after this measurement, Fig. 7.9.4, can only be explained in terms

of a deep trapping level. It seems probable that these latter effects are due to the destruction of a second complex defect at 0.25 eV, mentioned in the last section. Thus band-gap light dissociated this second defect and creates levels at 0.41 eV and 0.83 eV. This is consistent with the work of Nicholas (46). The small peak near - 145°C, Fig. 7.9.3. may be due to a level at 0.15 eV. Nicholas (46) observed a thermally stimulated current peak in this temperature range with this value.

Infra-red excitation produced a peak near room temperature, no peak near 85°C and did not depress the conductivity. Fig. 7.9.3.(3). This could be due to an increase in the 0.41 eV complex, again at the expense of the 0.61 eV level, without the dissociation of the defect giving rise to the 0.25 eV level. This is supported by the fact that after this measurement, the thermal equilibrium conductivity was not depressed.

In view of the complexity of these effects it is not reasonable to attempt any further analysis of the curves of Fig. 7.9.3. and Fig. 7.9.4.

9.6. Photo-Sensitivity of Crystal B

From the curves of Fig. 7.10, which show the photoconductivity as a function of temperature at various intensities of illumination, a series of plots can be made of photo-

current versus excitation intensity at different temperatures.
These plots are shown in Fig. 9.6.1. and Fig. 9.6.2. for
(i) band-gap and (ii) infra-red excitation.

(i)   The sensitivity of the crystal varied as the
square root of the excitation intensity over the temperature
range $180^{\circ}K$ to $410^{\circ}K$. This behaviour is consistent with fast
recombination through a centre (18,78). The free lifetime
is proportional to the one half power of the excitation
intensity (section 5.2.). It could be attributed to recom-
bination through the 0.83 eV level, created by the destruction
of the 0.25 eV complex on illuminating the crystal.

(ii) The sensitivity of the crystal to infra-red light
varied as the square of the excitation intensity below $70^{\circ}C$
and as the square root above this temperature. This can be
interpreted as follows. Below $70^{\circ}C$ the crystal contains
a level at 0.61 eV and the complex defect with a level at
0.41 eV. The second complex defect with its shallow level
of 0.25 eV is also present but has little effect on the form of
the photosensitivity versus excitation intensity curve. The
infra-red illumination has the effect of transforming the
0.61 eV level into the 0.41 eV complex. Thus the more intense
the illumination, the fewer will be the 0.61 eV centres with
their large electron capture cross sections. This will lead
to a free electron lifetime which increases with intensity
of illumination. This could lead to a dependence of sensitivity

SENSITIVITY OF CRYSTAL B
TO VISIBLE LIGHT

FIG 9.6.1.

· −180°C
◁ −95°C
× 20°C
○ 98°C
□ 136°C

LOG PHOTOCURRENT   amps

LOG INTENSITY
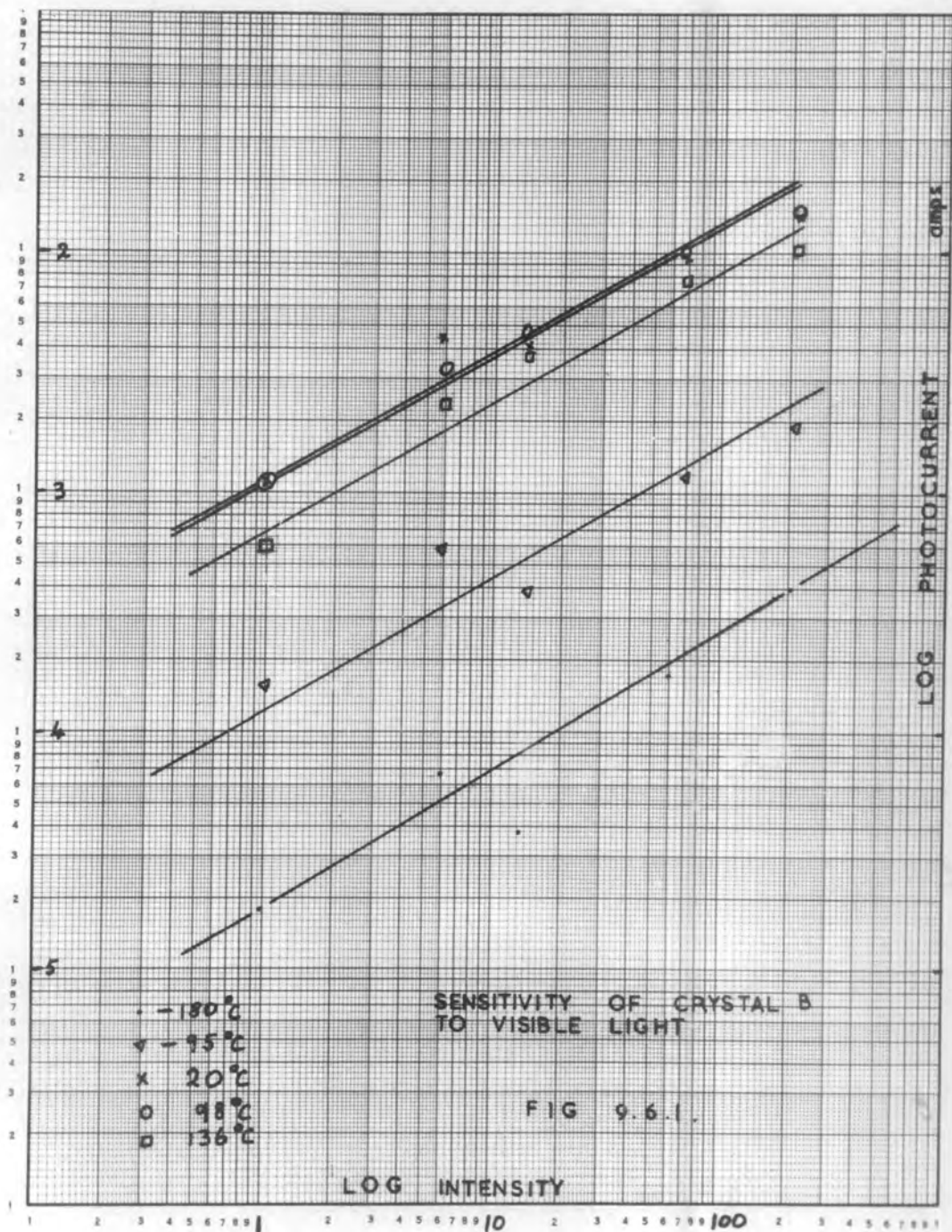
I . R .   SENSITIVITY
FIG 9. 6. 2.
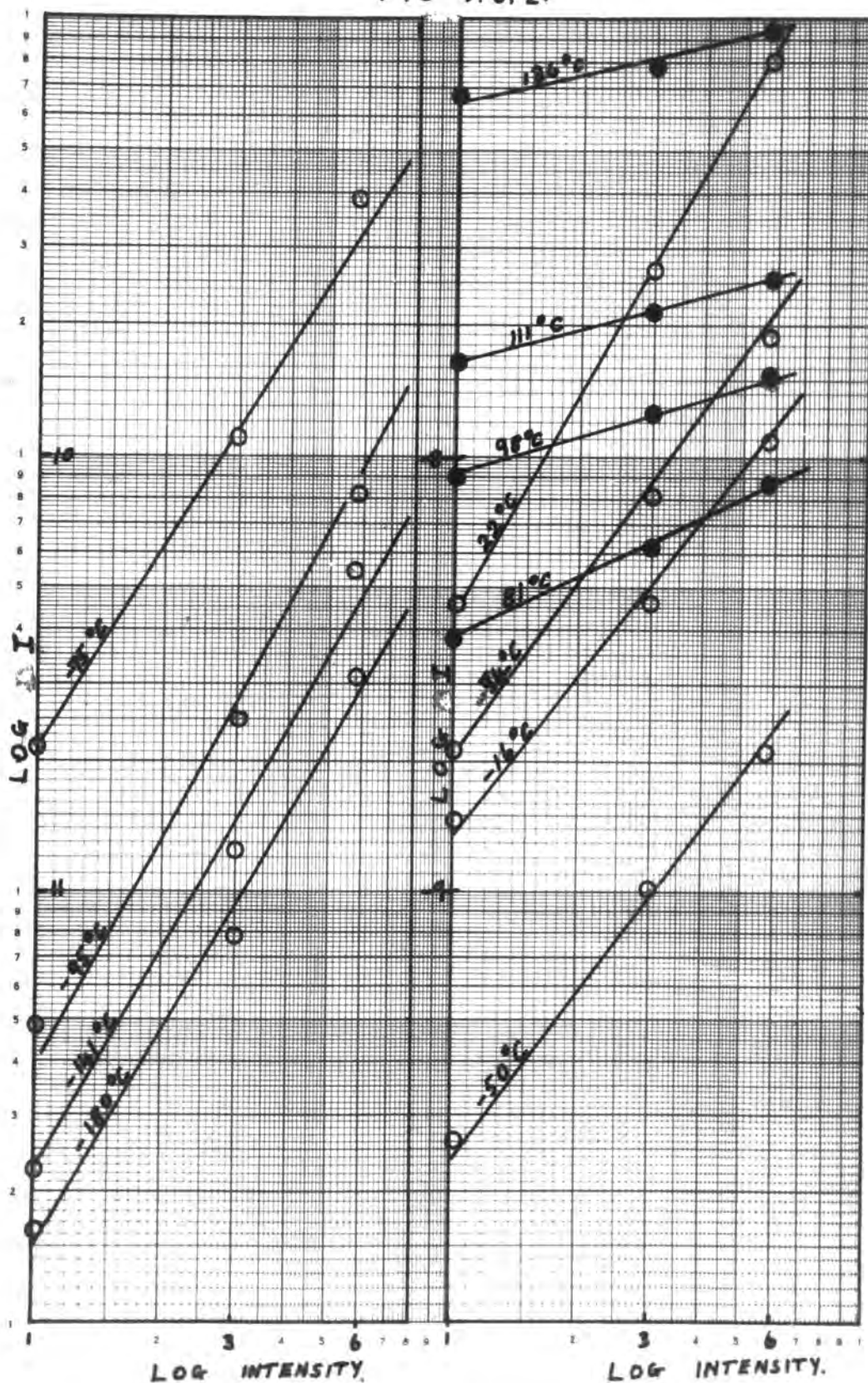
as the square of the excitation. Above 70°C, the rate of
conversion of 0.61 eV levels into levels at 0.41 eV becomes
less than the rate of thermal destruction at the intensities
employed and the 0.61 eV level dominates. Thus the sensitivity
reduces to a square root dependence as the recombination
becomes bimolecular.

The sharp increase in photocurrent with temperature
near -110°C using visible excitation, Fig. 7.10, is probably
associated with a shallow trapping level. As the temperature
rises, this centre ceases to trap electrons with a consequent
increase in their free lifetime. Plots of log I versus 1/T
are shown for the photocurrents, in this temperature range,
in Fig. 9.6.3. The slope of the line gives a value of trap
depth of 0.15 eV. This value again agrees with the work of
Nicholas and this shallow level is probably associated with
luminescent emission in cadmium sulphide discussed in the
following chapter.

The sensitivity of crystal B to γ-rays, Fig. 7.10.
has a maximum near room temperature. No depression of the
thermal equilibrium dark current was observed. This suggests
that γ-radiation has an effect similar to that of infra-red
illumination. (i.e. it can convert the 0.61 eV level into the
0.41 eV complex but is unlikely to affect the 0.25 eV complex).
The comparatively quick response of the crystal to this low
intensity of irradiation ($\sim$ 1 sec. section 7.11.) indicates

LOG PHOTO-CURRENT VS. I/T
(VISIBLE LIGHT)

FIG 9.6.3.

Crystal B
slope 0/5 eV
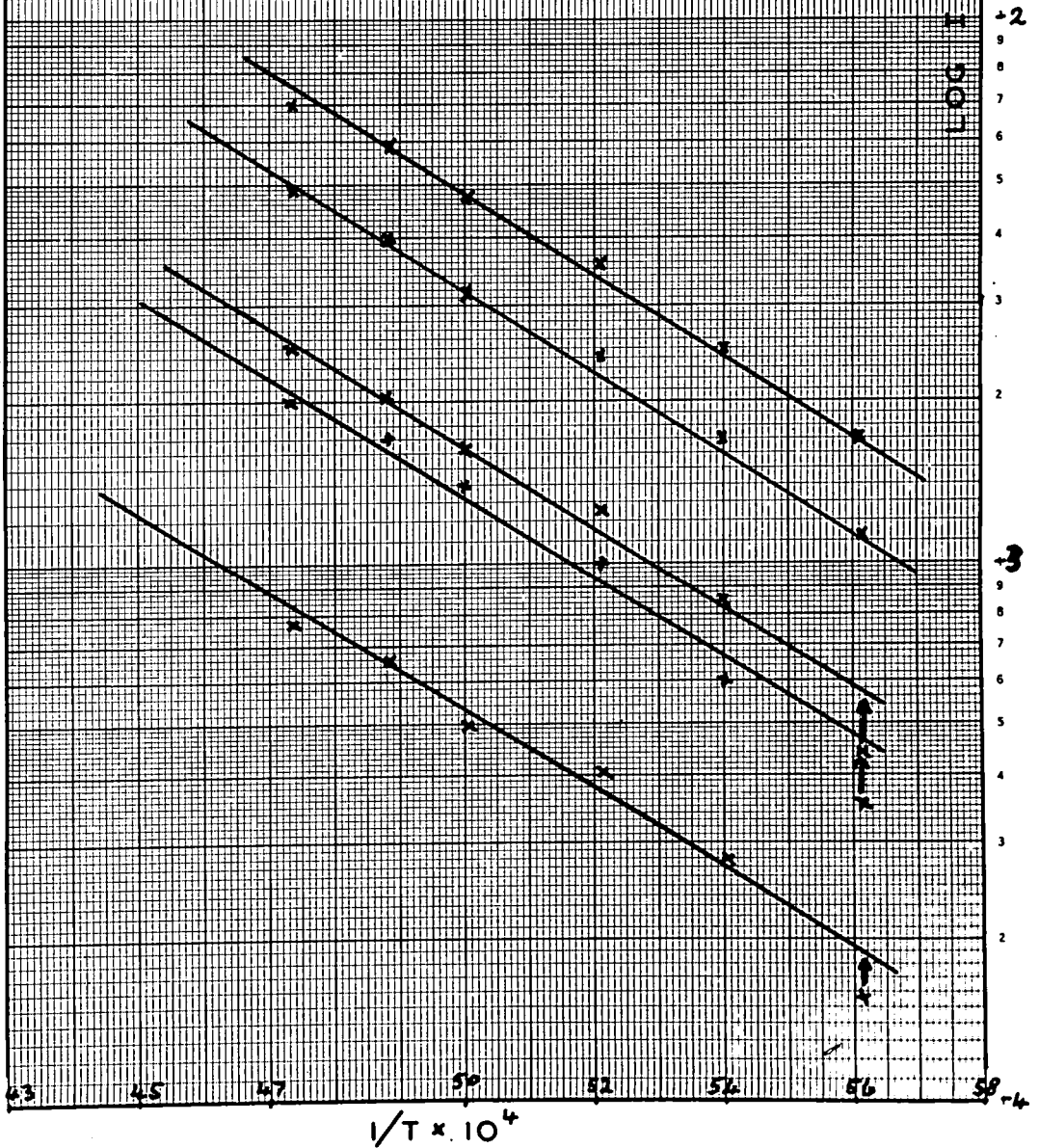
that cadmium sulphide may be useful as a small, fairly sensitive, detector. Further work is needed, however, to clarify the nature and behaviour of the complex defect centres discussed in this chapter.

9.7.   Interpretation of the Traps-filled-limit.

Since electrical injection decreases the density of the 0.61 eV level and increases the density of the 0.41 eV complex, it seems highly unlikely that V_{TFL} will be simply related to the total trap density. However, as V_{TFL} is related to the total excess trapped charge, whether at 0.41 eV or 0.61 eV it is difficult to see how a corrected analysis could give a higher value of N_t. The suggested reason for the discrepancies between N_t and N_A of Table 9.1.2. is as follows. As the voltage increases, trap-filling occurs some way up the steep rise in current. The 0.61 eV levels then start to be transformed into the complex at 0.41 eV as the voltage increases still further. Finally, field ionisation or collision ionisation removes some or all of the trapped charge from the 0.41 eV level. These mechanisms are far more likely from a level at 0.41 eV compared to ionisation from a level at 0.61 eV (65). V_{TFL} may then be related to the residual density of trapped charge after suitable allowances have been made for the ionisation process.

CHAPTER X

Analysis of Optical Measurements

10.1. The Spectrum of Pure Cadmium Sulphide

The results of the analysis of the spectrum of pure cadmium sulphide, Fig. 8.3.1., Fig. 8.3.2., are shown in Table 10.1. The emission bands marked 0 to 7, Fig. 8.3.1. can be satisfactorily attributed to electron-hole recombination accompanied by the emission of 0, 1, 2, 3..... phonons. The energy of the strongest, no phonon, band is 2.39 eV (see section 10.5.). This value is consistent with recombination through a level 0.13 eV from the band edge, assuming the energy of the forbidden gap is 2.52 eV at 77^OK (section 4.3.). The separation of the emission band maxima is of the order of 300 cm^{-1} which is consistent with coupling of the emission to longitudinal optical phonons. (section 5.1.).

The approximate intensities of the emission peaks 1.2.3. relative to that of the first peak fit a Poisson distribution. (equation 5.3.). The broad band, near 5800 Å, could be responsible for the high relative intensities measured for bands 4 to 7. The relative intensities were calculated after correcting the peak intensities for the variation in sensitivity of the detector. Fig. 8.2.2.

The broad band near 5800 Å corresponds to emission of photons with an energy of 2.12 eV. Thus this luminescence

Peak	Wavelength Å	Wave No. 10^4/cm	Separation from 1st peak /cm	Separation from 2nd peak /cm
0	5157	1.939	0	
1	5233	1.911	280	1.300	0
2	5314	1.882	570	2.300	1. 300
3	5429	1.842	970	3.300	2. 300
4	~ 5500	1.820	1190	4.300	3. 300
7	5619	1.780	1590	5.300	4. 300
6	~ 5700	1.755	1840	6.300	5. 300
7	5790	1.727	2120	7.300	6. 300
i	4914	2.035	0	
ii	4971	2.012	230	
iii	5043	1.983	520	

	Approximate Relative Intensity 5233/5157	$I_n = I_0 \frac{(0.87)^n}{n!}$	Approximate Relative Intensity 5314/5233
0.	100	100	
1.	78	87	100
2.	40	38	51
3.	12	11	15.5
4.	3.9	2.6	3.7
5.	1.4	0.4	1.8
6.	0.9	0.06	0.15
7.	0.8	0.007	

Analysis of the Edge Emission of Pure Cadmium Sulphide

TABLE 10.1.

could be due to recombination through a level approximately

0.4 eV from a band edge. The exact position of the maximum

of this emission is uncertain for two reasons.

1. The sensitivity of the detector was beginning to fall

rapidly with increasing wavelength in the region.

2. Absorption in the binder was becoming large (section 8.2.).

It seems probable that this emission is due to recombination

through the level which lies 0.41 eV below the conduction band

edge as discussed in the last chapter.

The small emission bands on the high energy side of

the edge emission, bands, (i), (ii) and (iii) Fig. 8.3.1.

are probably due to recombination via a centre near one of

the band edges. The smaller separation between these higher

energy bands ($\sim$ 260/cm) is probably due to coupling with

the transverse optical phonon ($\nu_{TO_1} = 261$ cm^{-1}, (55), section

5.1.). This agrees with usual observations (17 p.87).

Better resolution is required, however, to justify any firm

conclusion. The energy of the first peak of this series (i)

was ~ 2.516 eV. This indicates recombination through a

level only 0.004 eV from the band edge and the emission might

be due to band to band transitions which have a low probability

Similar emission bands from other crystals are discussed

below.

10.2. Analysis of the Spectra of Oxygen Doped Crystals

The emission spectrum of an oxygen doped crystal, shown in Figs. 8.4.1. and 8.4.2., has edge emission bands similar to those of pure crystals. However two short wavelength bands are prominent. These bands are centred at wavelengths of (f) 4898 (e) 5019. They are not identical with the short wave bands observed in pure crystals. The effect of a high frequency gas discharge was to reduce the intensity of peaks (e) (f) relative to that of the most intense emission band from 27% to 9.7%. This reduction was measured after passing the discharge for 2 minutes. A further reduction was apparent after a second discharge. This suggests that the emission is due to the adsorption of surface impurities which are removed by the discharge and pumped out of the cryostat.

In a second type of oxygen doped crystal, an example of which is shown in Fig. 8.4.5. a broad emission band near 5800 Å was apparent. This band is similar to that discussed earlier, i.e. associated with a level at 0.41 eV. As stated in section 8.4., this emission was not observed in conjunction with the bands (e) (f). It is not known at this stage whether this indicates that the 5800 Å band is associated with a different absorbed surface layer or not. The work of Nicholas (46) indicates that the 0.41 eV level is associated with a bulk defect.

The emission spectrum of an oxygen doped crystal is sometimes very different from that of a pure crystal, Figs. 8.4.3. and 8.4.4. The positions of the main emission bands are marked on the figures. In all, fifteen emission bands were tentatively identified. These are listed in Table 10.2.1. The structure can be associated with the phonon frequencies determined by Marshall and Mitra (section 5.1.) provided the highest energy band (5157 Å) is ignored. The second (5210 Å) and subsequent bands may be tentatively fitted to no phonon emission, and emission with one or more phonons as illustrated in Table 10.2.2. The first emission band (at 5157 Å) did not fit this pattern and is probably due to recombination through a different centre. More emission measurements are required at lower temperatures to clarify the position. An emission band at 4971 Å was also observed in this crystal, which corresponds to a similar peak observed in the luminescent spectrum of a pure crystal. The position of the most intense line suggests recombination through a level 0.13 eV from the band edge.

10.3. Analysis of the Spectrum of Cadmium Sulphide Grown in Hydrogen.

The emission spectrum of cadmium sulphide grown in hydrogen shows a distinctly different structure from that of a pure crystal, see Fig. 8.5.1. The maximum of the first

Angstroms	Intensity %	Angstroms
5157	100	5486
5210	77	5648
5229	72	5702
5252	61	5810
5295	40	5895
5338	30	5948
5412	12	5995
5438		4971 (ii)

Emission Bands in Oxygen Doped Cadmium Sulphide

TABLE 10.2.1.

Distance in wave nos from 1st band	Distance in wave nos from 2nd band	Suggested Combinations
197	O	No phonon
267	70	TA_2
351	154	$TA_1 + TA_2$
505	308	LO
657	460	LO + LA
914	717	$LO + TO_1 + LA$
1002	805	$LO + TO_1 + TO_2$

$LO = 295 \text{ cm}^{-1}$. $TO_1 = 261 \text{ cm}^{-1}$. $TO_2 = 238 \text{ cm}^{-1}$.

$LA = 149 \text{ cm}^{-1}$. $TA_1 = 79 \text{ cm}^{-1}$. $TA_2 = 70 \text{ cm}^{-1}$.

Phonon Emission in Oxygen Doped Cadmium
Sulphide

TABLE 10.2.2.

peak is again displaced by 0.13 eV from a band edge but the remaining emission bands all lie at multiples of approximately 120 wave numbers on the long wavelength side of the most intense band. The emission bands are listed in Table 10.3. together with the estimated relative intensities. One possibility that the structure suggests is that the emission is due to two levels, separated by 120 /cm, the emission from each level having structure associated with phonons of frequency 240 /cm. (ν_{TO_2} = 238 cm^{-1} , section 5.1.). Alternatively, the separation of the two series may be due to emission between the two levels of the split valence band (section 4.4.) and an impurity level 0.13 eV below the conduction band. The splitting of the valence band is $\sim$0.016 eV which is approximately 120 cm^{-1}.

10.4. Analysis of the Emission Spectrum of Crystals Grown in Water Vapour

The emission spectrum of a crystal grown in water vapour, Fig. 8.6.1., showed bands corresponding to those of a pure crystal at 5162 Å, 5219 Å, 5305 Å, 5371 Å. No other emission was detected in this crystal.

10.5. Emission of Chlorine and Silver Doped Crystals

The emission spectra of crystals doped with chlorine and silver were very similar to one another Fig. 8.7.1. and

Wavelength $\mathring{A}$	Separation from 1st peak /cm			Separation from 2nd peak /cm
5157	0			
5221	238	2. 120		0
5290	487	4. 120	2. 120	
5324	608	5. 120	3. 120	
5371	772	6. 120	4. 120	
5398	866	7. 120	5. 120	
5467	1099	9. 120	7. 120	
5576	1457	12. 120	10. 120	

Relative Intensity (5221/5157)	$I_N = I_o \dfrac{(0.87)^n}{n!}$
100	100
94	87
60	38
52	11
32	2.6
25	0.4
13	0.06
5	0.007

Emission from Cadmium Sulphide Grown in
Hydrogen

TABLE   10.3

Fig. 8.8.1. The silver doped crystals were grown at G.E.C. Ltd. by a vapour phase technique using hydrogen sulphide. The H_2S was prepared using hydrochloric acid and it seems likely, therefore, that the form of the emission spectrum of the silver doped crystal is due to substitutional chlorine.

A distinct feature of these spectra was that the emission band at 5157 Å was less intense than that at 5233 Å. The positions of the emission bands were the same as those of a pure crystal, Table 10.1. It is difficult to see how only the first emission band of a series could be depressed in this manner. The suggested interpretation offered here is that the band at 5157 Å is due to a separate centre. The first line of the edge emission series is at 5233 Å, corresponding to recombination through a level 0.16 eV from the band edge. The number of phonons associated with each band according to this assignment is indicated in Tables 10.1. and 10.3. The ratios of the intensities of the peaks at 5157 (I_o), 5233 (I_1) and 5314 Å, I_2 have been estimated for all the pure and doped crystals used in this work. The ratio I_1/I_o was found to vary between 74% and 120%, whereas I_2/I_1 only varied between 50% and 65%. The wide fluctuation in the relative intensities of the first two emission bands supports the argument that the first line of the edge emission series is at 5233 Å. The estimates of the intensities of the bands

are only approximate because of the severe overlapping

of peaks, and the different resolutions employed in the various

experiments. The discrepancies between the expected

relative intensities and those observed may be clarified

when more measurements are made at a lower temperature

(Table 10.1.).

The emission spectra of chlorine and silver doped

crystals did not show the broad band at 5800 Å nor any short

wavelength emission bands. The associated levels were either

not present in these crystals or the emission was too weak

to be detected.

10.6. Emission Spectrum of Indium Doped Crystals

The edge emission spectrum of indium doped cadmium

sulphide was almost completely masked by the strong emission

band centred at 5176 Å. This is probably due to recombination

through a shallow donor 0.14 eV below the band edge. (Fig.

8.9.1.). The emission does not appear to be coupled to

the lattice as is the normal edge emission. The short wave-

length band can be attributed to surface recombination.

10.7. Iodine Doped Cadmium Sulphide

The emission spectrum of iodine crystals did not show

any structure which has not already been discussed. (Fig.

8.10.1.) and is similar to that of a chlorine doped crystal.

The broad band at 5800 Å was present as were two short wavelength bands due to surface recombination. The intensities of the two most intense bands were very nearly equal. This suggests that iodine depresses the band at 5157 Å relative to that at 5233 Å in the same way as chlorine.

10.8. Electro-luminescent Emission of Pure Cadmium Sulphide

The electro-luminescent emission of pure cadmium sulphide has three components (Fig. 8.11.1.). (1) The weak band near 5800 Å is associated with recombination through a level at 0.41 eV. (2) A stronger series of four emission bands which can be related to ultra-violet stimulated emission forms the second component. The highest energy band of the four centred at 5147 Å (1. Fig. 8.11.1.) is probably not associated with the phonon assisted edge emission series (2.3.4.) but is identical with the band at 5157 Å found in all photo-luminescent spectra. The separation of the four bands was of the order of 300 /cm., but the resolution was not particularly good as only a small quantity of light entered the spectrophotometer. (3) The third and major region of emission was concentrated into two bands at 4981 and 5019 Å (y. x. Fig. 8.11.1.). The band at 5019 Å corresponds to the surface recombination observed in oxygen doped cadmium sulphide. (e. Fig. 8.4.1.). However the band at 4981 does not correspond to the second surface band at 4898. (f. Fig. 8.4.1.).

Thus, the band may correspond to recombination through
an impurity 0.03 eV from a band edge i.e. (ii) Fig. 8.3.1.
It has previously been suggested (5) that recombination
luminescence is associated with free holes recombining
with electrons trapped near the cathode. This suggestion
was based on the observation of a delay in the light output
with respect to the current after applying a voltage pulse
to a crystal. The level at 0.03 eV may therefore be
associated with a shallow level near the cathode contact
which would be especially active when electrons are injected.
Nicholas also found a trap approximately 0.05 eV below
the conduction band. Better resolution of this emission is
required before a distinction can be made between surface
and bulk recombination.

10.9. Long Wavelength and Infra-red Emission Measurements.

The curve of Fig. 8.12.1., showing emission at room
temperature and $77^{O}K$, indicates that the overall sensitivity
of the second measuring system was approximately 20 times
greater than that of the spectrophotometer (section 8.2.).
The room temperature spectrum shows a broad structureless
emission band attributable to edge emission and another band
at 0.66 microns. This latter band corresponds to recombination
through a level 0.65 eV from a band edge and may be the
0.61 eV level discussed in the last chapter. The increase

in emission above 3 microns is probably due to the large
error on the measurements in this spectral region as the
sensitivity of the detector is falling rapidly.

The emission spectrum at $77^{O}K$ has three interesting
regions apart from the edge emission, (i) the band at 0.66
microns, (ii) a series of bands near 1.3 microns (iii)
emission above 3 microns. (i) The emission at 0.66 microns is
unaffected by the decrease in temperature. This indicates
that the level near 0.65 eV is acting as a recombination
centre with a capture cross-section which is high relative
to other recombination mechanisms. This agrees with Nicholas'
conclusions that the 0.61 eV trap has a large capture cross
section. (ii) The series of bands near 1.3 microns were only
just resolved. The main band is at 1.3 microns and corresponds
to recombination through a level 0.95 eV from a band edge.
Other emission bands are tentatively put at 1.06, 1.14,
1.42 microns. They have associated photon energies which
indicate levels at 1.16, 1.08, and 0.87 eV from a band edge.
The first two of these levels and that at 0.95 eV may be
acceptor levels approximately 1 eV above the valence band
(section 4.7.). The level of 0.87 may be associated with
the level 0.83 eV below the conduction band discussed in the
last chapter. (iii) The increase in the emission above three
microns, which occurs when the crystal is cooled suggests that
more emission bands might be observed if the resolution and
detector sensitivity were improved. There is some indication

of an emission band near 3.1 microns which could be
associated with the level 0.4 eV below the conduction band
edge which would imply that the 3.1 micron and 5800 Å bands
are complementary. The quenching of the emission above
2.5 microns by radiation from a small lamp with a peak
output at 1.6 microns further indicates that the observed
signal was genuine.

10.10. Defect Centres Responsible for the Observed Effects

The edge emission series on the long wavelength side
of 5233 Å, the emission at 5157 Å and the broad band at
5800 Å are all observed with pure crystals. They are probably
associated with sulphur vacancies or interstitials (section
5.3.). In the neutral crystal, such defects would be
present in approximately equal numbers and would give rise
to the edge emission series and the band at 5157 Å. Cadmium
sulphide grown in hydrogen or oxygen is probably deficient
in sulphur (section 6.3.), leading to an excess of sulphur
vacancies and fewer sulphur interstitials. The edge emission
spectrum of such crystals was different from that of a pure
crystal whereas the band at 5157 Å was unaffected. It appears
therefore, that the edge emission series is associated with
sulphur interstitials and the band at 5157 Å with sulphur
vacancies. The strongest emission band at 5800 Å was observed
in a crystal grown in oxygen and consequently the level

at 0.41 eV is probably associated with sulphur vacancies. The observation of this emission in pure crystals indicates that these are also deficient in sulphur. The double structure, which may be associated with the split valence band, in the emission spectrum of a crystal grown in hydrogen supports the above interpretation. The structure was probably observed because the normal edge emission was very much reduced due to the decreased concentration of interstitial atoms of sulphur. The incorporation of chlorine or iodine would fill the sulphur vacancies substitutionally and reduce the emission at 5157 Å as observed experimentally. Better resolution is required before further conclusions can be drawn with regard to the short wavelength emission bands.

A similar interpretation of the emission spectra discussed in this chapter is possible in terms of cadmium vacancies rather than sulphur interstitials. However, since In^{+++} when substituted would lead to (Cd^{++}) vacancies an indium doped crystal should show intense edge emission bands. The edge emission structure of an indium doped crystal is not very intense and hence the balance of evidence is in favour of sulphur interstitials rather than cadmium vacancies forming the 0.16 eV level.

The separation of the band at 5157 Å from the absorption edge indicates that sulphur vacancies introduce levels approximately 0.13 eV below the conduction band edge.

Similarly, the first emission band of the edge emission series is due to recombination via a centre (probably a sulphur interstitial) with a level approximately 0.16 eV above the valence band, in which case the double structure would not be expected. The shallow trapping level introduced by sulphur vacancies is possibly the same level near the conduction band discussed in section 9.6.(b). Alternatively, the latter level may be due to indium donors levels 0.14 eV below the conduction band. In a pure crystal, diffusion at the contacts could introduce this level causing the observed increase in photocurrent of section 9.6.(b).

CHAPTER XI

Conclusions

Conduction processes in thin platelets of cadmium
sulphide are governed by the behaviour of complex defect
centres with levels in the forbidden gap. The measured
traps-filled-limit voltage is not directly related to the
total trap density due to the association and dissociation
of these defect centres. The steep rise in current is
associated with the filling of traps followed by the
removal of this trapped charge by an ionisation process
involving a complex defect. All the electrical phenomena
can be explained in terms of two complex defect centres
(0.41 eV - 0.61 eV; 0.25 eV - 0.83 eV). The observation
of both defects in the same crystal, in contradiction of
the work of Nicholas, may be due to the more sensitive
current measuring apparatus used in this work and the fact
that the 0.61 eV level is transformed into the 0.41 eV
complex by visible light. The interpretation of the behaviour
of crystal B should only be used as a broad framework on
which to base further work. In order to explore the dissoc-
iation of complex defects, it would be particularly useful
to study the spectral response of cadmium sulphide crystals
between 5000 $\overset{o}{A}$ and 3.5 microns at different temperatures

and after a variety of heat treatments.

The optical emission experiments show good correlation with all the defect levels proposed to explain the electrical measurements. The existence of an emission band close to the edge emission structure is probably due to recombination via a sulphur vacancy with a level approximately 0.13 eV below the conduction band edge. The edge emission series, on the other hand, is probably associated with recombination through a level 0.16 eV above the valence band which is due to sulphur interstitials. Emission bands on the high energy side of the main emission lines are probably due to surface and impurity recombination and perhaps band to band processes. This needs clarification in further work but two separate series are undoubtedly apparent. The injection of electrons and holes produces recombination again attributable to surface and impurity recombination as well as recombination at sulphur vacancies and interstitials. Further investigation is again required.

Measurements at lower temperatures with better resolution may distinguish the emission from chlorine and iodine doped crystals and may make possible some estimate of the stoichiometry of cadmium sulphide crystals.

REFERENCES

1. a) F. Seitz. A Modern Theory of Solids. McGraw-Hill.(1940).

   b) W. Shockley. Electrons and Holes in Semiconductors. Van Nostrand. (1950).

   c) C. Kittel. Introduction to Solid State Physics. Wiley 2nd Ed. (1956).

   d) N. Cusack. The Electrical and Magnetic Properties of Solids. Longmans (1958)

   e) R.A. Smith. Semiconductors. Cambridge University Press. (1959)

2. F. Herman. Rev. Mod. Phys. 30. 102.(1958)

3. M.S. Sodha. Progress in Semiconductors Vol. 3. Heywood.(1958)

4. F.J. Blatt. Solid State Physics. Vol. 4. Academic Press(1957)

5. G.A. Marlor. M.Sc. Thesis. Durham (1962)

6. T.S. Moss. Optical Properties of Semiconductors. Butterworths (1961)

   J. Strong. Concepts of Classical Optics. Freeman (1958)

7. B. Lax. Rev. Modern Phys. 30. 122. (1958)

8. Burstein, Picus and Gebbie. Phys. Rev. 103, 825, (1956)

9. Spitzer and Fan. Phys. Rev. 106, 882, (1951)

10. Smith and Moss. Proceedings of Brussels Conference (1958) Vol. 2.

11. Stephen and Lidiard. J. Phys. Chem. Solids. 9. 43. (1959).

12. Smith, Moss, Taylor. J. Phys. Chem. Solids. 11. 131. (1959).

13. Cardona. Phys. Rev. 121. 152. (1961).

14. Lax, Zwerdling. Progress in Semiconductors. Vol. 5. Heywood (1960).

15. Methods of Experimental Physics, Solid State Physics. Vol. 6. Part B. 256. (1959).

15. D. G. Avery. Proc. Phys. Soc. 65B, 425, (1952).

16. D. Curie. Progress in Semiconductors. Vol. 2. Heywood (1957).

17. D. Curie. Luminescence in Crystals. Methuen (1963).

18. R.H. Bube. Photoconductivity of Solids. Wiley (1960).

19. M.A. Lampert. J. Phys. Chem. Solids. 22. 189 (1961).

20. N.F. Mott and R.W. Gurney. Electronic Processes in Ionic Crystals. O.U.P. 2nd Ed. (1940). p.168-173.

21. M.A. Lampert. Phys. Rev. 103, 1648 (1956).

22. Parmenter and Ruppel. J.A.P. 30, 1548 (1959).

23. M.A. Lampert. R.C.A. Rev. 20, 682 (1959).

24. M.A. Lampert, A. Rose. Phys. Rev. 121, 26 (1960).

25. M.A. Lampert. Phys. Rev. 125, 1, 126 (1962).

26. E.S. Rittner and J.H. Schulman. J. Phys. Chem. 47. 537 (1943).

27. L. Pauling. Nature of the Chemical Bond. Cornell U.P. Ithaca (1945).

28. R. Frerichs. Phys. Rev. 72, 594 (1947).

29. Czyzak, Craig, McCain and Reynolds. J.A.P. 23, 932 (1952).

30. M.E. Bishop and S.H. Liebson. J.A.P. 24. 660. (1953).

31. W.W. Piper and S.J. Polich. J.A.P. 32. 1278 (1961).

32. Sommers, Berry and Sochard. Phys. Rev. 101, 987 (1956).

33. Balkanski, Des Chloizeaux. J. Phys. Rad. 21, 825; 22. 41. (1960)

34. D.G. Thomas and J.J. Hopfield. Phys. Rev. 116, 573, (1959).

35. D.G. Thomas and J.J. Hopfield. Phys. Rev. 122, 35, (1961).

36. F.A. Kroger, H.J. Vink and J. Volger. Physica 20, 1095 (1954)

37. J.D. Zook and R.N. Dexter. Phys. Rev. 129, 1980 (1962).

38. Piper and Marple. J.A.P. 32, 2237 (1961).

39. Sawamoto. J. Phys. Soc. Japan. 19, 318, (1964).

40. W.E. Spear, J. Mort. Proc. Phys. Soc. 81, 130,(1963.)

41. A.R. Hutson. J.A.P. 32, 2286 (1961).

42. Kroger, Vink and Volger. Phil. Res. Rep. 10. 39 (1955).

    R.H. Bube, J. Chem. Phys. 23, 18 (1955).

    R.H. Bube, S.M. Thomsen. J. Chem. Phys. 23, 15 (1955)

    R.H. Bube. J. Phys. Chem. Solids. 1. 234 (1957)

    R.H. Bube. Phys. Rev. 99, 1105 (1955).

43. Kroger, Vink and van der Boomgaard. Z. Phys. Chem. B203. 1. (1954).

44. D.A. Jenny and R.H. Bube. Phys. Rev. 96. 1190 (1954).

45. J. Woods and J.A. Champion. J. Elect. and Control. 7. 243. (1959).

46. K.H. Nicholas. Ph.D. Thesis. Durham (1963).

47. Balkanski and Waldron. Phys. Rev. 112. 123 (1958).

48. D. Dutton. Phys. Rev. 112, 785,(1958.)

49. R.H. Bube. Phys. Rev. 98. 431.(1955.)

50. D.G. Thomas, J. J. Hopfield. Phys. Rev. 128, 2135,(1962)

51. D.G. Thomas, J. J. Hopfield. Phys. Rev. 119, 570, (1960).

52. C.E. Bleil and I. Broser. J. Phys. Chem. Solids 25, 11, (1964).

53. R.J. Collins. J.A.P. 30, 1135, (1959)

54. Lyddane, Sachs and Teller. Phys. Rev. 59. 673,(1941)

55. Marshall, Mitra. Phys. Rev. 134, A1019, (1964).

56. S.Z. Czyzak et al. J. Opt. Soc. Am. 47, 209 (1957).

57. R.N. Dexter. J. Phys. Chem. Solids. 8, 39; 8, 216 (1959).

58. W. Shockley and W.T. Read. Phys. Rev. 87. 835 (1952)

59. P.N. Hall. Phys. Rev. 87. 387 (1952)

60. J. Lambe, C.C. Klick. Progress in Semiconductors Vol. 3. Heywood (1958.)

61. Lambe, Klick and Dexter. Phys. Rev. 103. 1715 (1956).

62. R.J. Collins and J.J. Hopfield. Phys. Rev. 120, 840 (1960).

63. B.A. Kulp and R.H. Kelley. J.A.P. 31, 1057 (1960).

64. R.W. Smith. Phys. Rev. 105. 900 (1957).

65. G.A. Marlor, J. Woods. Proc. Phys. Soc. 81, 1013, (1963).

66. R.H. Bube. J. Chem. Phys. 21, 1409 (1953).

    J. Lambe. Phys. Rev. 98. 985 (1955)

    S.H. Liebson. J. Electrochem. Soc. 101. 359 (1954).

67. Park, D.C. Reynolds. Phys. Rev. 132, 2450, (1963).

68. R.L. Kelly, W.J. Fredericks. Phys. Rev. Letters. 2, 389, (1959)

69. Balkanski and Besson. J.A.P. 32, 2292 (1961).

70. J.J. Hopfield. J. Phys. Chem. Solids. 10, 110. (1959.)

71. J.W. Allen. Nature 187, 403 (1960).

72. G.F.J. Garlick, A.F. Gibson. Proc. Phys. Soc. 78, A60, 574, (1948).

73. L.I. Grossweiner. J.A.P. 24, 1306 (1953).

74. Luschchik, Doklady. Akad. Nauk. S.S.S.R. 101, 641. (1955).

75. H. Dember. Physik. Z. 32, 554, 856, (1931); 33, 207 (1932).

76. W. Ludwig. Phys. Stat. Sol. 3, 1738. (1963).

77. Kroger, Diemer and Klasens. Phys. Rev. 103, 279 (1956)

78. Rose. Proc. I.R.E. 12, 1850 (1955).
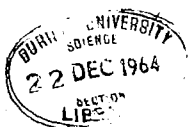
Space Charge Limited Currents in Cadmium Sulphide Crystals

By G. A. MARLOR and J. WOODS

Space Charge Limited Currents in Cadmium Sulphide Crystals

By G. A. MARLOR and J. WOODS

Department of Applied Physics, Durham Colleges in the University of Durham

Abstract. In order to test whether Lampert's theory (1956) of one carrier space-charge-limited currents can be applied to cadmium sulphide it is necessary to ensure that the electrical contacts to the crystals exclude the possibility of minority carriers entering the crystal. The use of many materials, including indium, can lead to hole injection at the anode at sufficiently high voltages. However, evaporated indium forms good electron injecting cathodes and hole blocking anodes, when it is deposited on surfaces previously subject to hydrogen ion bombardment. With these contacts current–voltage characteristics were measured over a range from −183 °c to 83 °c. Analysis of the results shows that a typical crystal contained $2 \cdot 5 \times 10^{14}$ traps per cm^3 at a distance of 0·61 ev below the conduction band. About 10^{12} cm^{-3} of these were filled with electrons which originated from shallow donors. According to Lampert's traps-filled theory the crystal contained $2 \cdot 5 \times 10^{13}$ traps per cm^3. It is concluded that the steep rise in current, attributed in Lampert's theory to the complete filling of traps, is in fact associated with trap emptying in this crystal.

§ 1. INTRODUCTION

IT is well known that currents considerably in excess of those predicted by Ohm's law can, under certain circumstances, be drawn through insulators when sufficiently large voltages are applied. Such currents are limited by the space charge of the free and trapped carriers. In order to obtain large space-charge-limited currents three conditions must be observed; (i) the insulator must be relatively free from traps, (ii) the anode–cathode separation must be small and (iii) one or both of the electrodes must provide a large reservoir of current carriers with easy access to the appropriate conduction band. It is usual to refer to an electrode with the required properties as an ohmic contact.

Mott and Gurney (1948) first discussed the problem of a metal–insulator contact. They showed that with a trap-free insulator the space-charge-limited current density j due to the passage of electrons from the metal to the insulator is

$$ j = \frac{9}{8} \frac{\epsilon \mu_e V^2}{d^3} \tag{1} $$

where V is the applied voltage, ϵ is the dielectric constant of the insulator, μ_e is the electron mobility and d is the electrode separation. The square law (1) is the solid state analogue of Child's three-halves power law in the vacuum diode.

Smith (1955) and Smith and Rose (1955) first showed that space-charge-limited currents could be obtained in thin, single crystal, plates of cadmium sulphide when indium was used as the material of the negative electrode. The requirements (ii) and (iii) for large space-charge-limited currents were met by using crystals between 10 and 100 μm thick, and by using indium, which is widely accepted to form ohmic contacts

on cadmium sulphide (Smith 1955, Kroger, Diemer and Klasens 1956). The question as to whether the condition (i) requiring a low trap density is met in cadmium sulphide, is one which has been widely debated recently. Some authors have suggested that measurements of space-charge-limited currents in some cadmium sulphide crystals indicate the presence of an effective trap density as low as 10^{12} per cm³. The present paper is chiefly concerned with methods of calculating trap densities from experimental space-charge-limited current–voltage characteristics.

§ 2. CURRENT–VOLTAGE CHARACTERISTIC OF AN INSULATOR WITH TRAPS

It was clear from Smith's work that his crystals contained an appreciable density of electron traps, so that the large currents predicted by equation (1) were not readily obtained. To account for this Lampert (1956) developed a theory of one-carrier space-charge-limited conduction in an insulator with traps. According to this theory the current–voltage characteristic shows several distinct regions. At low voltages, when the injection of excess charge carriers at the cathode is negligible, Ohm's law is obeyed, and the slope of the current–voltage curve defines the true resistivity ρ_0 of the crystal. $1/\rho_0 = n_0 e \mu_e$, where n_0 is the concentration of electrons in the conduction band in thermal equilibrium.

At some applied potential, V_1, the current begins to increase more rapidly than linearly with applied voltage. If the existence of traps were ignored this would occur when the charge injected equalled the carrier concentration already present. According to Lampert this happens when

$$V_1 = \frac{ed^2}{2\epsilon} n_0. \tag{2}$$

However with a real insulator some of the injected charge becomes localized in traps, where it contributes to the space charge, but not to the current flow. If there is one discrete set of electron traps of density N_t cm⁻³ at a depth E_t below the conduction band, and if the Fermi level lies below the trapping levels, the current will increase as V^2 for sufficiently large V. However, since most of the injected charge is trapped the current density will not be given by equation (1) but by

$$j = \frac{9}{8} \frac{\epsilon \mu_e V^2}{d_3} \theta \tag{3}$$

where θ is the ratio of free to trapped charge.

$$\theta = \frac{n}{n_t} = \frac{N_c}{N_t} \exp\left(-\frac{E_t}{kT}\right) \tag{4}$$

where n is the density of free electrons, n_t is the density of trapped electrons and $N_c = 2(2\pi m^* kT/h^2)^{3/2}$ is the effective density of states in the conduction band.

Since most of the injected charge is trapped, the transition voltage, V_1, given by equation (2) must be modified by the trapping factor θ, so that

$$V_1 = \frac{ed^2}{2\epsilon\theta} n_0. \tag{5}$$

Now according to Lampert at some still higher voltage, V_{TFL}, all the available traps become filled. When this happens the current which has been following the reduced square law (3) increases discontinuously by the large factor $1/\theta$ to the theoretical space-charge-limited current in a trap free insulator, given by equation (1). When this large

abrupt increase in current occurs the crystal is said to have reached the traps-filled limit. Lampert has shown that at this limit

$$V_{TFL} = \frac{ed^2}{2\epsilon} N_t.$$ (6)

Thus if Lampert's theory applies, a measure of V_{TFL} leads directly to an estimate of N_t, and if θ can be determined from the reduced square law characteristic, E_t can be calculated from (4).

Some recent workers have used these ideas to calculate N_t, and have concluded that their crystals contain surprisingly small numbers of traps. Thus Wright (1958, 1959) interpreted his data as indicating a trap density of 10^{12} cm^{-3}. Allen (1960) found similar low densities in semi-insulating gallium arsenide. Since these densities would appear to be improbably low, Allen explained his results by postulating a mechanism of almost complete compensation of traps by shallow donors. Recently Page, Kayali and Wright (1962) have invoked Allen's suggestion to explain the continued low values of N_t they obtain by applying equation (6).

One of the objects of the present work is to show that equation (6) must be used with extreme caution, since the steep increase in current may not be due to the complete filling of traps but rather to their emptying. Recent work by Ruppel (1961) and Bube (1962) suggests similar conclusions.

§3. ELECTRON INJECTING CONTACTS

Cadmium sulphide is essentially an n-type material with an electron mobility about twenty times as large as the hole mobility. It is necessary, therefore, in testing the applicability of Lampert's one carrier theory to cadmium sulphide crystals, to ensure that the cathode contact is ohmic, i.e. electron injecting, and that the anode does not permit the entry of holes into the crystal.

It is widely accepted that indium forms an ohmic contact on cadmium sulphide. Our results indicate that indium does indeed form an electron injecting contact, provided the indium is applied in the proper manner. If the indium is not properly applied, contacts with relatively large barrier heights $(\phi_m - \chi)$ are obtained. The significance of $(\phi_m - \chi)$ is evident in figure 1, where a contact between a metal with work function ϕ_m and an insulator with electron affinity χ, is illustrated. Our results also show that indium contacts with appreciable barrier heights become hole injecting when used as anodes. A satisfactory hole blocking electrode is one which would provide copious electron injection if it were used as a cathode.

Three methods of preparing indium contacts have been used. They were (i) soldering to the crystal in air at a temperature of about 170 °c, (ii) heating an indium bead in contact with the crystal surface to 300 °c for 3 min in an atmosphere of argon, and (iii) evaporating a layer of indium on to the crystal in a vacuum of 10^{-5} mmHg or better. When contacts were applied using the first two methods no pre-cleaning of the crystal was carried out. With method (iii) the crystal surfaces were bombarded, with either 2 kev electrons or hydrogen ions, prior to the deposition.

Contacts of type (i) were unsatisfactory and were soon discarded. They were noisy and it was impossible to obtain reproducible results with them. Furthermore the current decayed steadily for hours (with some samples for days) before a stationary value was reached. This lengthy decay was reduced to a few minutes simply by using contacts of type (ii) or (iii). The long decay appears to be associated with oxygen

impurity, since crystals grown in the presence of oxygen exhibit the slow decay no matter how the contacts are applied.

Contacts of type (ii), formed by melting indium on to crystals at 300 °c in argon, tend to saturate at high current densities. The broken curve in figure 2 is a current–voltage characteristic obtained for a crystal with both electrodes of this type. Region
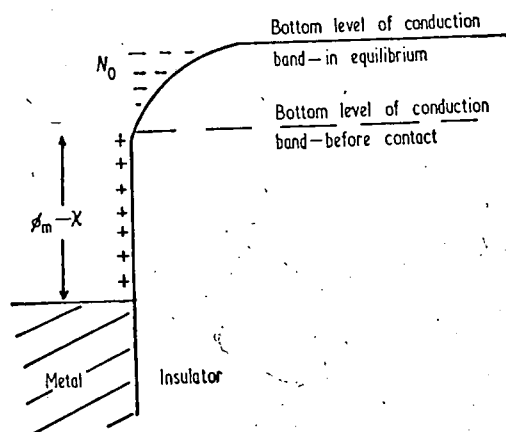

Figure 1. Energy band diagram of the contact between a metal with work function ϕ and an insulator with electron affinity χ. $\phi_{metal} < \phi_{insulator}$.
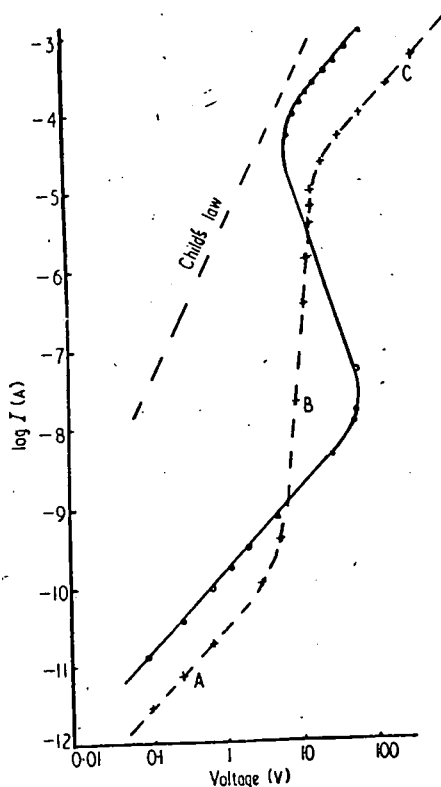

Figure 2. Current–voltage curves, at room temperature, for two crystals with melted indium contacts of type (ii). – – – –, area, 9×10^{-3} cm²; thickness, 8×10^{-3} cm; ———, area, 10^{-2} cm²; thickness, 5×10^{-3} cm. For explanation of lettering see text.

B is what would be ascribed to the 'traps-filled limit' according to Lampert's theory. With the higher applied voltages in region C the theoretical Child's square law for solids, equation (1), is not observed. Instead the current is proportional to the applied voltage. This is due to the fact that in region C the current is limited not by space charge but by the finite barrier height, $(\phi_m - \chi)$, at the cathode. Mott and Gurney (1948) showed that under conditions of contact limitation Ohm's law would be observed and

$$j = e\mu_e N_0 V/d \tag{7}$$

where N_0 is the concentration of free electrons just inside the insulator at the cathode. In fact

$$N_0 = N_C \exp\{-(\phi_m - \chi)/kT\}. \tag{8}$$

Assuming an electron mobility $\mu_e = 250$ cm² v⁻¹ sec⁻¹, the region C of the broken curve in figure 2 yields a value of N_0 of $9 \cdot 0 \times 10^{10}$ electrons cm⁻³, which corresponds, according to equation (8), to a barrier height of $0 \cdot 46$ ev.

No crystal with contacts of type (ii) has been observed to follow the space-charge-limited square law, predicted by equation (1). However, some crystals with two electrodes of type (ii) have produced characteristics similar to that of the solid curve in figure 2. The negative resistance régime is associated with the appearance of recombination luminescence at liquid nitrogen temperature, which clearly indicates the participation of free holes (this will be discussed below). It is concluded therefore that many anodes of type (ii) become hole injecting at sufficiently high voltages, and presumably have barrier heights greater than 0·46 ev.

In contrast with this behaviour, evaporated electrodes of type (iii) form good electron injecting cathodes and hole blocking anodes. At high current densities the current-voltage characteristic of crystals with two evaporated electrodes displays the square law dependence on voltage predicted by equation (1). No saturation effects have been observed up to the highest measurable currents, where the power dissipation sets the limitation. These results show that with this type of contact the cathode barrier height must be less than 0·3 ev. We have not found any evidence for hole injection with these electrodes and consequently they have been used exclusively in our study of single-carrier space-charge-limited currents.

§4. ELECTRON BLOCKING CONTACTS

Other types of contact have also been examined. These include painted colloidal dispersions of either silver or graphite, and evaporated layers of copper, silver or gold.
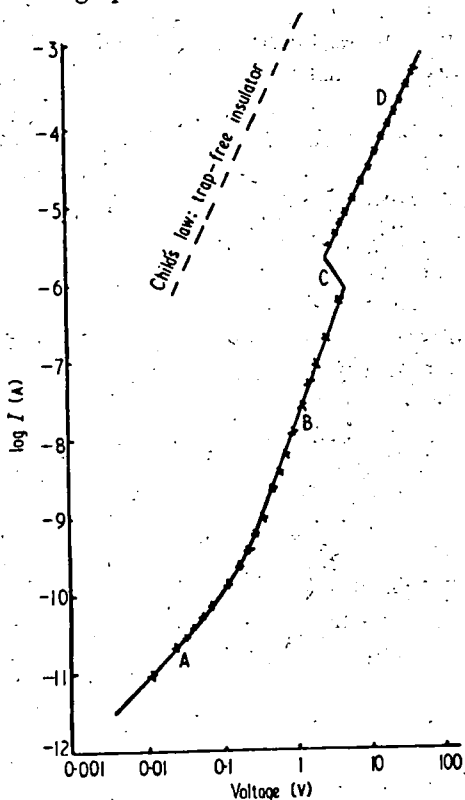

Figure 3. Current–voltage curves, at room temperature, for a crystal with an electron injecting cathode (indium contact of type (iii)), and a hole injecting anode (graphite). Area, 10^{-2} cm^2; thickness, $1·3 \times 10^{-3}$ cm. For explanation of lettering see text.

All these electrodes formed electron blocking contacts. Excellent rectification ratios of 10^5 for applied voltages up to 20 v were obtained with crystals with one evaporated indium electrode and one electron blocking contact.

Hole injection at the anode occurred with all the electron blocking electrodes listed above. This was demonstrated by the emission of recombination radiation at 77 °K, and by the region of negative resistance which was always observed when such anodes were used in conjunction with electron injecting cathodes. A typical characteristic is illustrated in figure 3. A square law variation at high voltages (D, figure 3) was usually found.

§5. DETERMINATION OF TRAP DENSITY

In order to determine the electron trap density in one of our typical plate-like crystals, evaporated indium contacts were used to ensure that the observed currents were due to the motion of electrons alone. The crystal was about 50 μm thick and had been grown by condensation, from a stream of argon carrying cadmium sulphide vapour. The argon flow had earlier been passed over a charge of purified cadmium sulphide at a temperature near 1100 °C. The crystal was mounted in a cryostat so that its temperature could be varied over the range 77–400 °K. A series of current–voltage curves was then taken with the crystal in the dark, and the results are shown in figure 4. At no stage of these measurements was a voltage applied which was sufficiently large to bring about the steep increase in current usually associated with the traps-filled limit. Results were accurately reproducible provided that before commencing measurements at any temperature the crystal was short-circuited and heated to 100 °C for several minutes. This treatment was sufficient to remove the excess charge which had become trapped in the crystal while previous measurements were being made.

At low voltages all the curves of figure 4 are ohmic, and all curves have a clearly defined kink, where the current begins to increase more rapidly than linearly with voltage. From the ohmic part of each curve we can calculate n_0, the density of free electrons, provided the electron mobility is known. It is not practicable to make Hall effect measurements on the highly insulating crystals used in these experiments. To calculate values of n_0, therefore, a value of mobility of 210 cm^2 v^{-1}sec^{-1} at 300 °K has been assumed, together with a variation with temperature as $T^{-3/2}$ (Kröger, Vink and Volger 1955).

We have analysed our results using a model in which one discrete set of traps N_A cm^{-3} at a depth E_A below the conduction band are partially filled with electrons from N_D cm^{-3} shallow donors. With such a model the free electron concentration is given by

$$n_0 = \frac{N_c N_D}{N_A} \exp\left(-\frac{E_A}{kT}\right). \tag{9}$$

A plot of $\log(n_0/T^{3/2})$ against $1/T$ should yield a straight line. The plot obtained using values of n_0 derived from figure 4 is shown by + in figure 5. The slope of the very good straight line gives $E_A = 0.61$ ev, while from the intercept a value of N_A/N_D equal to 240 is obtained.

The characteristics of figure 4 can be evaluated in a different way when it is appreciated that the deviation from Ohm's law occurs at a voltage determined by equation (5). Thus from the kink points of the curves in figure 4, values of θ, the ratio of free to trapped charge, can be deduced. According to equation (4)

$$\theta = \frac{N_c}{N_t} \exp\left(-\frac{E_t}{kT}\right). \tag{4}$$

To maintain conformity with the present notation N_t should be replaced by N_A and E_t by E_A. A plot of log $(\theta/T^{3/2})$ against $1/T$ should also yield a straight line. The experimental plot is shown by circles in figure 5. The slope of this line gives a value of trap depth of 0·61 ev, in complete agreement with the result obtained using equation (9) and the intercept leads to a value of $N_t = N_A = 2\cdot4 \times 10^{14}$ cm^{-3}. Since $N_A/N_D = 240$, it follows that $N_D = 10^{12}$ cm^{-3}.
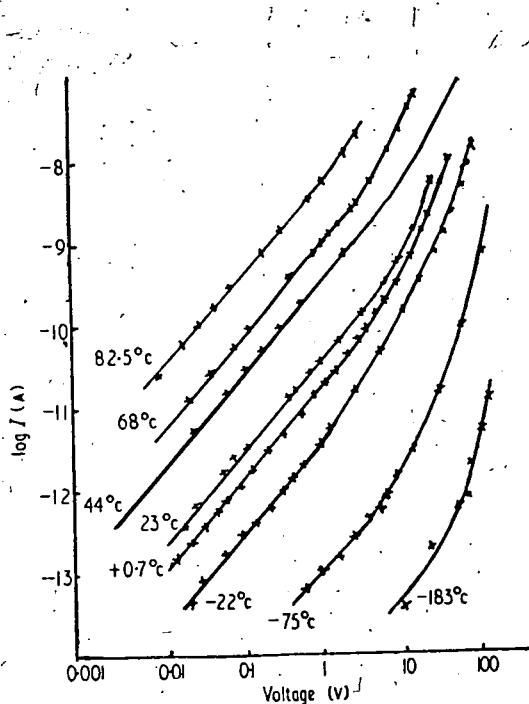

Figure 4. Current–voltage curves over a range of temperatures for a crystal with two evaporated indium contacts (no hole injection). Area, $5\cdot0 \times 10^{-3}$ cm^2; thickness, $5\cdot0 \times 10^{-3}$ cm.
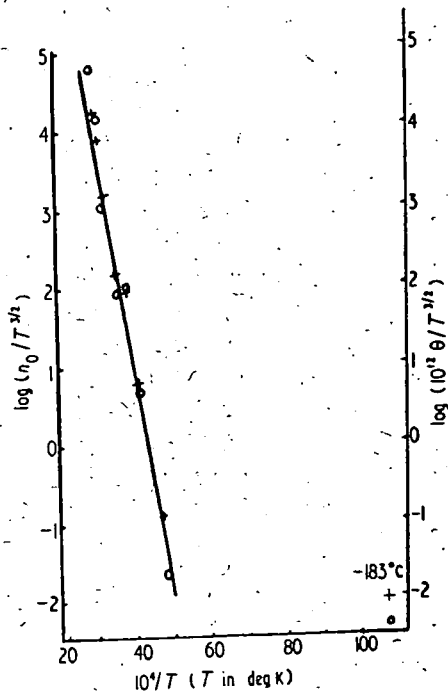
Figure 5. Line obtained by plotting: +, log $(n_0/T^{3/2})$ against $1/T$ (equation 9) and o, log$(\theta/T^{3/2})$ against $1/T$ (equation 4). Values of n_0 and θ obtained from figure 4.

The interpretation of the results of figures 4 and 5 therefore, is that the crystal contained $2\cdot4 \times 10^{14}$ acceptor-like electron traps per cm^3 at a depth of 0·61 ev below the conduction band. Of these 10^{12} cm^{-3} were filled with electrons which originated from that number of shallow donors.

After the series of curves shown in figure 4 had been determined, the applied voltage was increased so that the so-called traps-filled-limit voltage, V_{TFL}, could be measured. Then using equation (6) a trap density N_t of 3×10^{13} cm^{-3} was obtained. This is an order of magnitude smaller than the value deduced from the curves of figure 4. It would appear therefore that equation (6) does not apply, which means that the steep increase in current is not associated, in this crystal at least, with the complete filling of traps.

Values of n_0 and θ taken from the characteristic in figure 4 which was measured at −183 °c do not give points which lie on the straight line of figure 5. The currents measured at −183 °c were too high, and were probably associated with surface conduction which would cause significant leakage at such low temperatures.

§6. LUMINESCENT EFFECTS AND DOUBLE INJECTION

Crystals with suitable contacts emitted a green band of recombination radiation at 77 °K, centred near 2·4 ev, when constant currents of the order of 100 mA cm⁻² were passed. This luminescence was obtained using indium cathodes, and anodes of graphite, gold, copper, silver or indium heated in argon. No luminescence could be detected when evaporated indium anodes were used. The threshold voltage, at which the luminescent emission first appeared, was a function of crystal thickness. With most crystals the luminescence was first observed with mean fields of the order of 10³ v cm⁻¹, and since many crystals were only a few micrometres thick the applied voltage was then of the order of 3 v. The lowest threshold actually observed was 2·2 v for a crystal with a graphite anode. The lowest threshold voltages were obtained when graphite anodes were used. The luminescence was always associated with a current–voltage characteristic which displayed a region of negative resistance, and the light first appeared as the crystal entered this régime. The emission was too weak for any structure to be resolved with the apparatus available. However, it seems highly probable that the luminescence is of the same nature as the well-known phonon-assisted edge emission.

All these observations support the conclusion that hole injection occurs with all the anodes used here except those of evaporated indium. The injection of holes in appreciable quantities neutralizes the space charge of the free and trapped electrons. This process is responsible for the negative resistance régime. Whether the recombination takes place through a centre, which is close to the conduction band or the valence band, remains unresolved.

§7. DISCUSSION

The work described here shows that many electrode materials lead to the injection of holes when sufficiently large voltages are applied. This conclusion is supported by the observation of a negative resistance region, and the emission of recombination radiation at 77 °K. Alternative mechanisms by which the luminescent emission might have been produced seem very improbable. For example, luminescence could be initiated by a process of ionization of a luminescent centre by collision with an accelerated electron. However, the recombination radiation consists of photons of about 2·4 ev energy and has been observed with total applied voltages of 2·2 v. It is clearly unlikely that an accelerated electron could gain sufficient energy from the field to bring about the emission of a photon with greater energy. An alternative process, by which light might have been produced without the participation of free holes, is that of field ionization of luminescent centres. However, the fields required for such a mechanism are greater than 10⁷ v cm⁻¹. It is concluded therefore that it is much more probable that the recombination radiation is good evidence for the presence of free holes.

The negative resistance effect is the result of the annihilation of negative space charge by injected holes. According to Lampert (1961) the threshold voltage for the onset of negative resistance is

$$V_{\text{th}} = d^2/2\mu_{\text{p}}\tau_{\text{p}} \tag{10}$$

where μ_{p} is the hole mobility and τ_{p} is the hole lifetime at low injection levels. Inserting the experimental values from figures 2 (solid curve) and 3, $\mu_{\text{p}}\tau_{\text{p}} \sim 2\cdot5 \times 10^{-7}$ cm² v⁻¹ for both crystals. Assuming a hole mobility of 10 cm² v⁻¹ sec⁻¹ (Spear and Mort 1962), the corresponding hole lifetime is $2\cdot5 \times 10^{-8}$ sec.

According to Lampert and Rose (1961) the square law at high applied voltages in figure 3 is to be expected for space-charge neutralization by double injection. The

current density then becomes

$$j = e\tau\mu_e\mu_p n_0 V^2/d^3 \qquad (11)$$

where τ is now the common lifetime of electron and holes. Fitting region D of figure 3 to this equation and assuming $\mu_e \sim 210$ cm^2 v^{-1} sec^{-1} gives $\tau \sim 2.5 \times 10^{-5}$ sec.

This indicates that over the negative resistance region of the curve the hole lifetime increased by at least three orders of magnitude, which is in agreement with the general considerations put forward by Lampert (1961) to explain the negative resistance. The estimates of hole lifetime obtained here should be treated with reserve, since the application of equations (10) and (11) to our results implies a number of assumptions which may not all be valid. In particular since $\tau/\tau_p \sim 1000$ the negative resistance region should, according to Lampert's ideas, extend between two voltage limits which are in the ratio of τ/τ_p, i.e. 1000 : 1. This is obviously not true for the curve in figure 3.

The chief contribution of this work, however, is concerned with single carrier space-charge-limited currents. Using contacts which prevent the entry of holes, and making measurements over a range of temperature, it has proved possible to show that the steep increase in current at the so-called traps-filled-limit voltage is not associated with the complete filling of traps. A measure of that voltage, therefore, cannot be used to estimate the effective trap density. Whether the trap filling mechanism does occur in some crystals of cadmium sulphide, so that V_{TFL} gives an accurate estimate of the number of traps, can only be proved by making independent measurements of the trap density on crystals in which such a trap filling mechanism is suspected.

Since with our crystals at least the trap filling process does not occur, the large increase in current to the theoretical trap-free square law must be associated with a process of electron extraction from traps. Electron extraction would remove the trapped space charge and could occur either by ionization by collision or by field ionization. Recently Bube (1962) using independent methods of estimating trap densities, and Ruppel (1961) from measurements of charge stored in crystals, have come to similar conclusions.

REFERENCES

ALLEN, J. W., 1960, *Nature, Lond.*, **187**, 403.
BUBE, R. H., 1962, *J. Appl. Phys.*, **33**, 1733.
KROGER, F. A., DIEMER, G., and KLASENS, H. A., 1956, *Phys. Rev.*, **103**, 279.
KROGER, F. A., VINK, H. J., and VOLGER, J., 1955, *Philips Res. Rep.*, **10**, 39.
LAMPERT, M. A., 1956, *Phys. Rev.*, **103**, 1648.
—— 1961, *J. Phys. Chem. Solids*, **22**, 189.
LAMPERT, M. A., and ROSE, A., 1961, *Phys. Rev.*, **121**, 26.
MOTT, N. F., and GURNEY, R. W., 1948, *Electronic Processes in Ionic Crystals*, 2nd edition (London: Oxford University Press).
PAGE, D. J., KAYALI, A. A., and WRIGHT, G. T., 1962, *Proc. Phys. Soc.*, **80**, 1133.
RUPPEL, W., 1961, *J. Phys. Chem. Solids*, **22**, 199.
SMITH, R. W., 1955, *Phys. Rev.*, **97**, 1525.
SMITH, R. W., and ROSE, A., 1955, *Phys. Rev.*, **97**, 1531.
SPEAR, W. E., and MORT, J., 1962, *Phys. Rev. Letters*, **8**, 314.
WRIGHT, G. T., 1958, *Nature, Lond.*, **182**, 1296.
—— 1959, *Proc. Instn Elect. Engrs*, **106 B**, 915.